Società Geologica Italiana

ISPRA
Istituto Superiore per la Protezione e la Ricerca Ambientale
SERVIZIO GEOLOGICO D'ITALIA
Organo Cartografico dello Stato (legge N°68 del 2-2-1960)
Dipartimento Difesa del Suolo

Geological Field Trips

2015
Vol. 7 (2.1)

ISSN: 2038-4947

The variscan basement in Sardinia

29th Himalaya-Karakoram-Tibet Workshop – Lucca 2014

DOI: 10.3301/GFT.2015.03

GFT - *Geological Field Trips*

Periodico semestrale del Servizio Geologico d'Italia - ISPRA e della Società Geologica Italiana
Geol.F.Trips, Vol.**7** No.2.1 (2015), 118 pp., 82 figs. 3 tabs. (DOI 10.3301/GFT.2015.03)

The variscan basement in Sardinia

29th Himalaya-Karakoram-Tibet Workshop – Lucca, 5-8 September 2014

Rodolfo Carosi[1], Gabriele Cruciani[2], Marcello Franceschelli[2], Chiara Montomoli[3]

[1] Dipartimento di Scienze della Terra, via V. Caluso, 35 - 10125, Torino.
[2] Dipartimento di Scienze Chimiche e Geologiche, via Trentino, 51, Cagliari.
[3] Dipartimento di Scienze della Terra, via S. Maria, 53 - 56126, Pisa.

Corresponding Author e-mail address: rodolfo.carosi@unito.it

Responsible Director
Claudio Campobasso (ISPRA-Roma)

Editor in Chief
Gloria Ciarapica (SGI-Perugia)

Editorial Responsible
Maria Letizia Pampaloni (ISPRA-Roma)

Technical Editor
Mauro Roma (ISPRA-Roma)

Editorial Manager
Maria Luisa Vatovec (ISPRA-Roma)

Convention Responsible
Anna Rosa Scalise (ISPRA-Roma)
Alessandro Zuccari (SGI-Roma)

Editorial Board

M. Balini, G. Barrocu, C. Bartolini, D. Bernoulli, F. Calamita, B. Capaccioni, W. Cavazza, F.L. Chiocci, R. Compagnoni, D. Cosentino, S. Critelli, G.V. Dal Piaz, C. D'Ambrogi, P. Di Stefano, C. Doglioni, E. Erba, R. Fantoni, P. Gianolla, L. Guerrieri, M. Mellini, S. Milli, M. Pantaloni, V. Pascucci, L. Passeri, A. Peccerillo, L. Pomar, P. Ronchi, B.C. Schreiber, L. Simone, I. Spalla, L.H. Tanner, C. Venturini, G. Zuffa.

ISSN: 2038-4947 [online]

http://www.isprambiente.gov.it/it/pubblicazioni/periodici-tecnici/geological-field-trips

The Geological Survey of Italy, the Società Geologica Italiana and the Editorial group are not responsible for the ideas, opinions and contents of the guides published; the Authors of each paper are responsible for the ideas, opinions and contents published.

Il Servizio Geologico d'Italia, la Società Geologica Italiana e il Gruppo editoriale non sono responsabili delle opinioni espresse e delle affermazioni pubblicate nella guida; l'Autore/i è/sono il/i solo/i responsabile/i.

DOI: 10.3301/GFT.2015.03

INDEX

Information

Excursion notes

Itinerary

DOI: 10.3301/GFT.2015.03

DOI: 10.3301/GFT.2015.03

Riassunto

Dopo un breve e aggiornato inquadramento del lembo di catena Varisica affiorante in Sardegna viene descritto un itinerario geologico in Sardegna nord-orientale a partire dal basso grado metamorfico fino al complesso migmatitico con relative intrusioni. Sono state scelte le località più facilmente accessibili dove, nell'arco di quattro giorni, è possibile osservare i più classici affioramenti di rocce metamorfiche e magmatiche paleozoiche coinvolte nell'Orogenesi Varisica che hanno permesso di decifrare la complessa storia tettonica e metamorfica di questo settore di catena orogenica. Si parte dagli affioramenti più meridionali, con le metamorfiti di più basso grado, per proseguire verso Nord attraversando i complessi di medio ed alto grado, questi ultimi caratterizzati dalla presenza di corpi eclogitici. Lungo i vari Stops sono ben visibili gli effetti della tettonica polifasata che ha interessato questa porzione di basamento varisico e offre uno spettro completo di rocce deformate a diversi livelli strutturali con diverse impronte metamorfiche.

Parole chiave: *Basamento Varisico, Sardegna, tettonica, metamorfismo, escursione geologica.*

Abstract

After a short and up-to-date geological overview of the Variscan belt in Sardinia, we describe a field trip in the northeastern portion of the island that progresses from the low-grade metamorphic rocks to the Migmatite Complex and its related intrusions. The selected Stops are readily accessible and can be covered in four days. We include several exemplary outcrops that were instrumental in unravelling the tectono-metamorphic history of this sector of the Variscan belt. We start from the more southern outcrops, where the low-grade-metamorphic rocks crop out, moving further to the North towards the more metamorphic rocks characterized by the presence of eclogitic bodies. In the proposed outcrops we can observe clear examples of the polyphase tectonics of the Variscan basement with several nice examples of rocks deformed at different structural levels.

Keywords: *Variscan basement, Sardinia, tectonics, metamorphism, geological field trip.*

DOI: 10.3301/GFT.2015.03

Program

The geological field trip in the Variscan basement of Sardinia runs along the northeastern coast of the island, close to the Costa Smeralda touristic locality. The first outcrop near Lula can be reached from Cagliari with a journey of about 200 km (2 hours and a half) by the S.S. 131 until Abbasanta and then by its continuation (S.S. 131DCN) until the exit to Lula-Bitti-Dorgali. This outcrop can also be reached from the city of Olbia by driving southwards for approximately one hour along the S.S. 131DCN until Lula.
The first day excursion explores the metamorphic rocks of the low- to medium-grade metamorphic complex at the transition between the Nappe Zone and the Inner Zone of the Variscan chain. The progressive increase in metamorphic grade, and the relative metamorphic zonation of the Barrovian metamorphism can be observed towards north. Several types of phyllite, paragneiss, micaschist, metavolcanics, augen gneiss and orthogneiss are encountered. The spectacular landscape of the Mesozoic carbonatic sediments of the Monte Albo near Lula can also be observed.
The second day field trip starts with a walking path along the hills from the road between Lodè and Sant'Anna to Bruncu Nieddu, and continues with Punta Ainu and Porto Ottiolu-Punta de Li Tulchi. In these localities the field trip crosses the valley of the Posada river, giving the opportunity to observe the rock types cropping out in the Posada-Asinara shear zone. The second day eventually ends with the optional stop at Tamarispa were calc-silicate rocks contains spectacular coarse-grained garnet crystals.
The third day is spent in the proximity of Olbia, first along the coast between Pittolongu and Punta Sirenella-Punta Bados, were the participants can observe several types of migmatites and then in the inland at Monte Terrata and Montiggiu Nieddu were metabasite lenses preserving relics of eclogite and granulite facies assemblages crop out. The third day eventually ends with the optional stop at the mafic-silicic layered intrusion of Monte Plebi (Olbia).
The fourth day' morning is dedicated to the granitic rocks exposed in the abandoned quarry of Monte Mazzolu, near Arzachena. After a brief visit to the archaeological site of Nuraghe La Prisgiona, the field trip ends.

DOI: 10.3301/GFT.2015.03

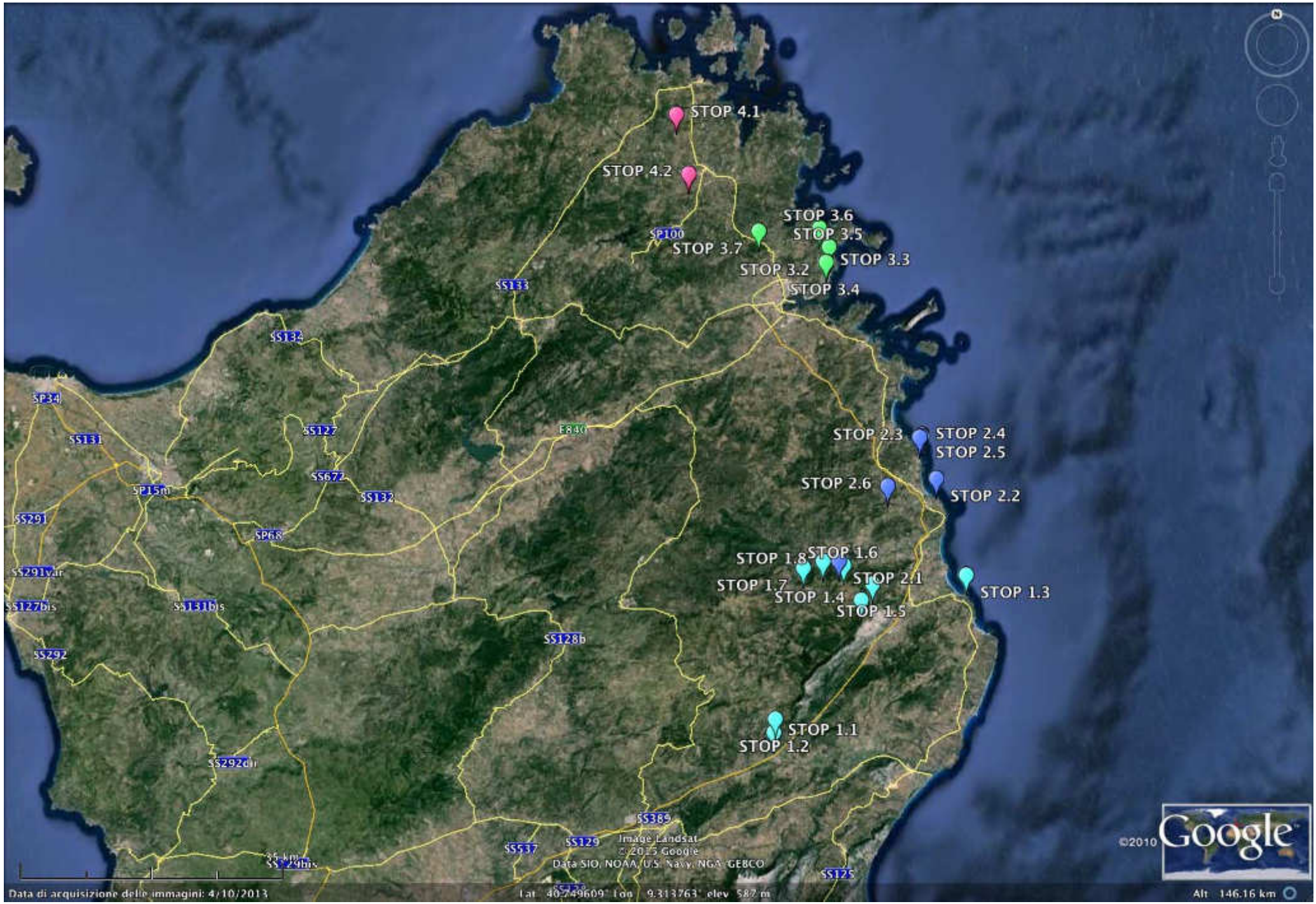

DOI: 10.3301/GFT.2015.03

Safety

No high altitudes are reached during the field trip and all the stops and outcrops are easily reached by car or by a few minutes walking from the cars. In summer hat, sunglasses, sun protection as well as trekking boots or shoes are recommended. In the second and third day lunch time is scheduled on the beach to give the possibility to swim before lunch.
Emergency contact numbers are: First aid 118, Carabinieri 113, Firefighters 115, Coast guard 1530. Hospitals: Ospedale San Francesco, via Mannironi, Nuoro, Tel. 0784 240237; Ospedale Giovanni Paolo II, via Bazzoni - Sircana località Tannaule, Olbia, Tel. 0789 552200.

Day 1: Altitude 0-600m a.s.l.
Day 2: Altitude 0-50m a.s.l.
Day 3: Altitude 0-300 a.s.l.
Day 4: Altitude 0-250 a.s.l.

Accommodation

The participants can easily find a comfortable accommodation in Olbia or in the villages of Posada, Siniscola, Budoni, Taunanella and surroundings, consulting the main search hotels and accommodation engines (e.g. www.trivago.it, www.venere.com, www.booking.com).

DOI: 10.3301/GFT.2015.03

Introduction

The Variscan basement in Corsica and Sardinia is an almost complete section across the South Variscan belt showing the transition from very low-grade up to medium-high-grade basement (Figs. 1, 2). The basement shows beautiful exposures of folded, sheared, and metamorphosed Paleozoic rocks that were only slightly affected by Alpine tectonics.

The aim of the field trip is to cover a section of the basement of Northern Sardinia to see the effects of progressive deformation and metamorphism along one of the classic geological transect in the Variscan belt in Northeastern Sardinia (Fig. 2). From south to north we observe clearly the effects of the D1 contractional

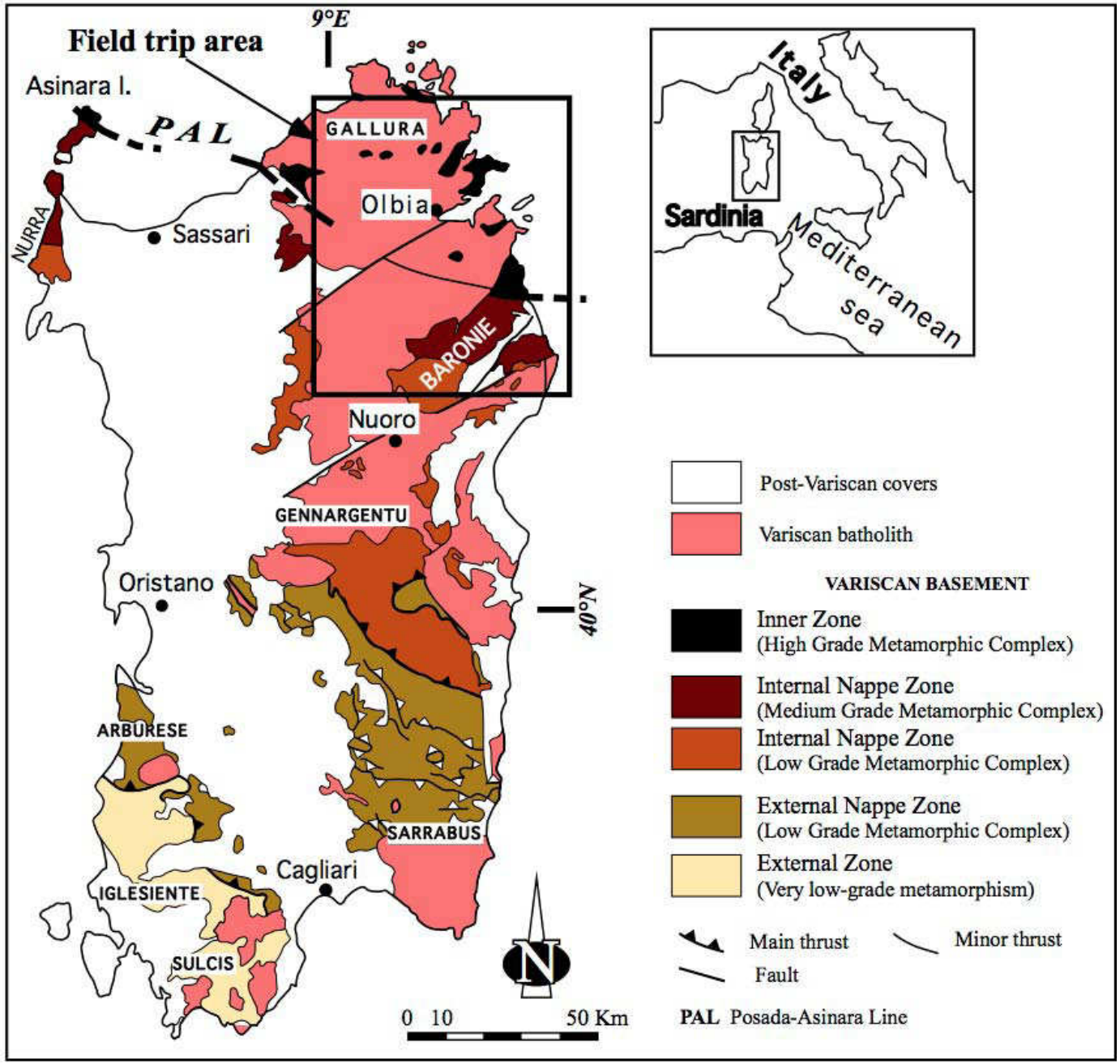

Fig. 1 - Tectonic sketch-map of the Variscan belt in Sardinia and location of the field trip area (from Carosi et al., 2005).

DOI: 10.3301/GFT.2015.03

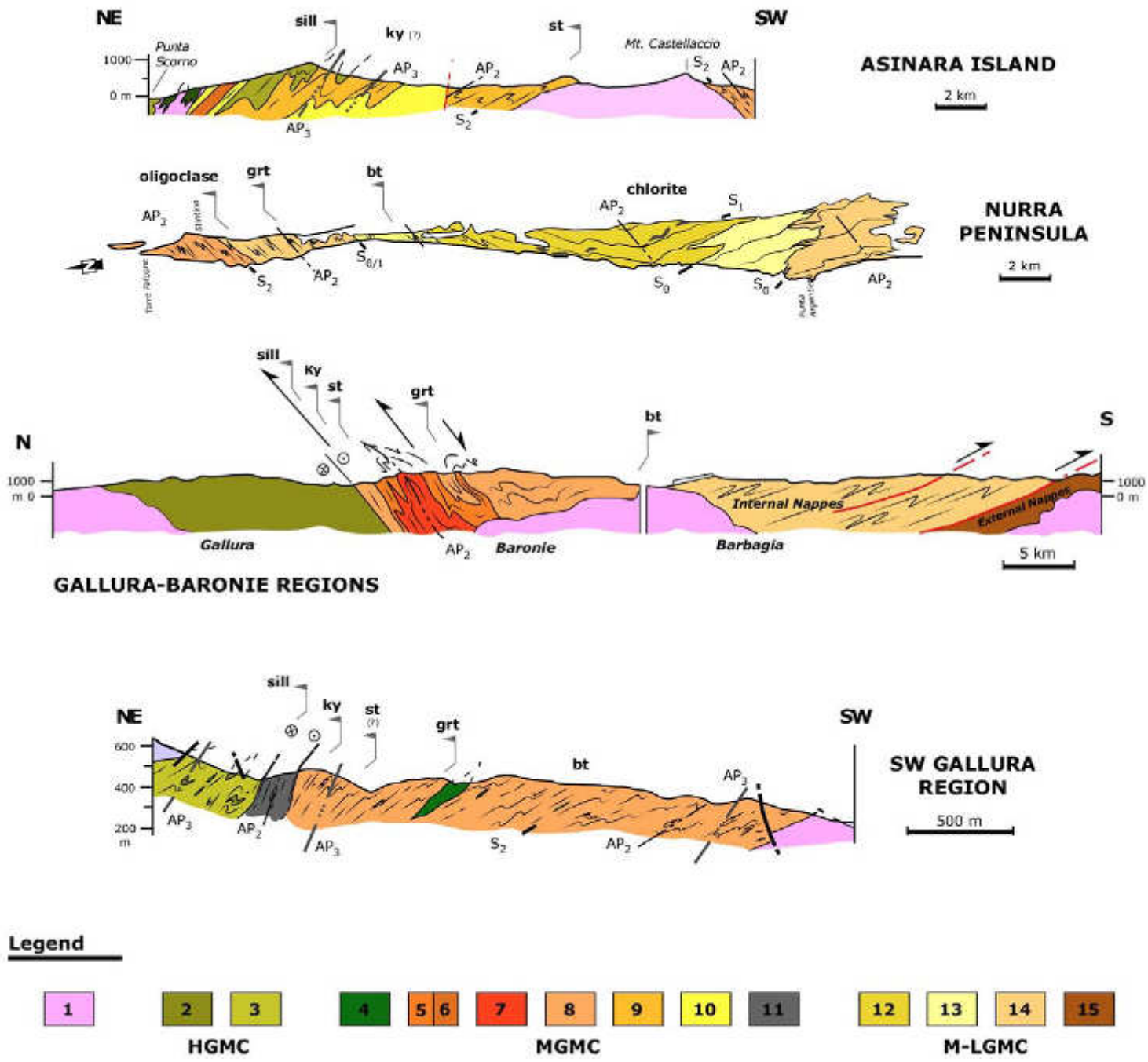

Fig. 2 - Geological cross sections (1-4) through the Variscan basement of Northern Sardinia along the NW, central, and NE sections of the island (see Geological map of Northern Sardinia, Carosi et al., 2005).
1- Variscan granitoids; HGMC: High-Grade Metamorphic Complex;
2- Migmatites;
3- High-grade mylonites; MGMC: Medium-Grade Metamorphic Complex;
4- Eclogites relics;
5- and **6-** Orthogneisses;
7- Augen gneisses;
8- Metasedimentary complex in amphibolite facies;
9- Metasedimentary complex with HT-LP metamorphic overprinting;
10- Mylonitic micaschists in amphibolite facies;
11- Phyllonite belt; L-MGMC: Low- to Medium-Grade Metamorphic Complex:
12-, **13**- and **14-** Internal Nappe;
15- External Nappe. (Modified after Carmignani et al., 1979; Oggiano & Di Pisa, 1992; Carosi & Oggiano, 2002; Carosi & Palmeri, 2002; Carosi et al., 2004a, b; 2005).

DOI: 10.3301/GFT.2015.03

deformation with south verging recumbent folds and ductile/brittle shear zones (thickening phase of the collision) affected by a D2 deformation, with strain increasing northward and tectonic transport parallel to the belt. The rocks, which are of Paleozoic age, underwent progressive Barrovian-type metamorphism increasing northward. The progression is beautifully exposed along the Baronie transect. In Asinara Island and Anglona we see the superposition of the high-grade metamorphic complex onto the medium-grade rocks. The effects of HT-LP metamorphism acting upon the Barrovian metamorphism are manifested at the microscopic-scale and at the outcrop scale, as well as by the growth of cm- to dm-size andalusite porphyroblasts. The relationships among late orogenic plutons, dykes, and metamorphics are clearly exposed in the transect followed in this field trip.

During the trip, results of the classic tectonic and metamorphic studies of the Variscan belt of Sardinia will be shown (Carmignani et al., 1994, 2001; Ricci et al., 2004; Carosi et al., 2005 and references therein) together with new results from research performed over the past decade by workers from Cagliari, Pisa, Torino, Genoa and Sassari Universities. Notable structures elucidated by new structural and geological mapping at 1:10.000 scale of key areas in Northern Sardinia (Nurra peninsula and Asinara island, Southern Gallura, Anglona and Baronie) include: the late D1 shear zones related to beginning of exhumation; the relationship between D2 transpressional deformation and the exhumation of the basement; the dating by $^{40}Ar/^{39}Ar$ of the D1 and D2 deformation events (Di Vincenzo et al., 2004) and in-situ U-Pb dating of zircon and monazite of the transpressional event (Carosi et al., 2012); the recognition, for the first time, of sinistral shear zones along the Posada-Asinara line; and the change in the classical zonation of Barrovian metamorphism in the Baronie due to the finding of staurolite+biotite appearance several kilometers southward with respect to the position of the classical isograd (Carosi et al., 2008). Other important discoveries include the first occurrence of HP metamorphism during D1 event recognized in chloritoid schist of the Low- to Medium-Grade Metamorphic Complex (L-MGMC) and the new petrological investigations by isochemical pseudosections (Cruciani et al., 2013; 2014a, b).

Despite these advances, several important aspects of the tectonic and metamorphic evolution of the Variscan belt in Corsica and Sardinia are still debated. These include: the localization of an oceanic suture; the pre-Variscan evolution and the presence of a pre-Variscan basement; the areal extent of the D1 high-pressure event; and the position of the Corsica-Sardinia microplate during the upper Paleozoic and its correlations with the other fragments of the Southern Variscan belt. In addition, the Permian differential rotation of blocks in Sardinia (Aubele et al., 2014) still needs to be reconciled with the lack of continuity in the earlier Variscan structures such rotation would cause.

DOI: 10.3301/GFT.2015.03

The Sardinian Variscan Belt

Sardinia and Corsica were brought into their present position by a 30° anticlockwise rotation of the Corsica-Sardinia block away from Europe caused by the opening of the Western Mediterranean Ligurian-Provençal basin. The rifting phase took place in the Oligocene (from 30 to 24 Ma) and was followed by a short Early Miocene oceanic accretion (ages ranging from 23 to 15 Ma, Ferrandini et al., 2000 and references therein). Thus the structural pre-drift directions, e.g., following the Variscan, must be restored by ~ 30° with respect to a stable Europe.

The largest part of Sardinia and Western Corsica comprises a Permo-Carboniferous batholith emplaced between ~ 340 and 280 Ma (Figs. 1, 3) into a Variscan basement.

In Northern Sardinia and Central and Southern Corsica the basement has been affected by Variscan tectono-metamorphic imprint.

The basement consists mainly of high-grade metamorphic rocks and was termed the "inner zone" by Carmignani et al. (1979; 1994; 2001) (Fig. 1), and, according to these Authors, it could be the result of a continental collision. The different structural Variscan zones were defined in Sardinia where Variscan metamorphic formations crop out widely and were extensively surveyed.

The Variscan belt in Sardinia developed from deformation and metamorphism of the northern margin of Gondwana and Gondwana-derived terranes during the Carboniferous, involving sedimentary and magmatic sequences ranging in age from Cambrian to Lower Carboniferous (Carmignani et al., 1994; 2001).

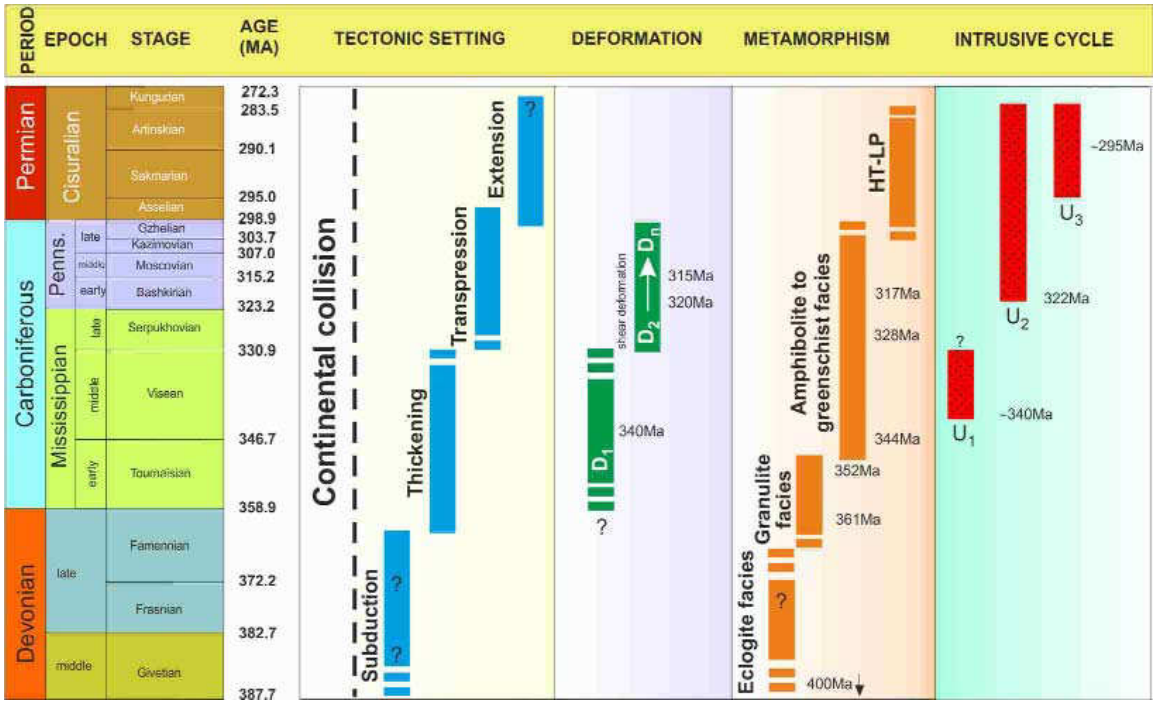

Fig. 3 - Synoptic table of the deformation, metamorphic and magmatic events in the Variscan basement of Sardinia.

DOI: 10.3301/GFT.2015.03

The terranes were affected by folds and thrusts indicating a SW tectonic transport (Carmignani & Pertusati, 1977; Carosi & Pertusati, 1990; Carmignani et al., 1994, 2001 and references therein; Montomoli, 2003; Carosi et al., 2005) and by prograde Barrovian metamorphism, from Anchizone in the external portion in the SW, to amphibolite facies in the inner zone in the NE with HP relics (Franceschelli et al., 1982a, 1989; Ricci et al., 2004 and references therein).
The Variscan basement in Sardinia shows a prominent NW-SE trend (Carmignani et al., 1979; 1986; 1994, 2001 and references therein) characterized by nappes, tectono-metamorphic zoning and shortening similar to those developed in continent-continent collision type orogens.
It is composed of Carboniferous-Permian magmatic rocks and a Cambrian – Lower Carboniferous igneous-sedimentary sequence with metamorphic grade increasing from south to north.
The collisional history results in three different major structural zones (Carmignani et al., 1982; 1994; 2001) (Fig. 1):
i) a foreland "thrusts-and-folds" belt consisting of a metasedimentary sequence ranging in age from upper (?) Vendian to lower Carboniferous, which crops out in the SW part of the island, with a very low-grade to greenschist facies metamorphic imprint;
ii) a SW-verging nappe building (central Sardinia) which equilibrated mainly under greenschist facies conditions, consisting of a Paleozoic sedimentary sequence bearing a thick continental arc-related volcanic suite of Ordovician age;
iii) an inner zone ("axial zone") (Northern Sardinia and Southern Corsica) characterized by medium- to high-grade metamorphic rocks with migmatites and abundant late-Variscan intrusions.

According to Carmignani et al. (1994, 2001) the inner zone consists of two different metamorphic complexes:
A) a High-Grade Metamorphic Complex (HGMC, or Migmatite Complex) made up of diatessite and metatexite hosting minor amphibolite bodies which equilibrated in HT-LP conditions that corresponds to the northernmost part of the island and extends to Corsica. In spite of this late re-equilibration, some granulite relic assemblages of high-intermediate P and unknown age are still detectable (Miller et al., 1976; Ghezzo et al. 1979; Franceschelli et al., 1982a; Di Pisa et al. 1993).
B) a medium-grade, chiefly metapelitic complex consisting of micaschist and paragneiss bearing kyanite±staurolite±garnet (Franceschelli *et al.*, 1982a) and including quartzite and N-MORB metabasalt boudins (Cappelli et al., 1992).

DOI: 10.3301/GFT.2015.03

The contact between these two complexes is well exposed along the Posada Valley, in Southern Gallura, and Asinara Island (Oggiano & Di Pisa, 1992; Carmignani & Oggiano, 1999; Carosi et al., 2005, 2009) and coincides with a wide transpressive shear belt (Carosi & Palmeri, 2002; Iacopini et al., 2008; Frassi et al., 2009) affected by late Variscan shear zones (Elter et al., 1990).
Thrusting of complex A onto complex B has been inferred in places where the contact has not been complicated by late Variscan retrograde dextral transpressional shear (Oggiano & Di Pisa, 1992; Carosi & Palmeri, 2002; Carosi et al., 2004a, b, 2005, 2008, 2009, 2012; Frassi et al., 2009).
Within the collisional framework, the high-grade migmatitic complex has been regarded as a crustal nappe comparable to the inner crystalline nappe of the French Massif Central and the highly strained complex B has been regarded by Cappelli et al., (1992) as the Sardinia segment of the south Variscan suture zone which re-equilibrated under intermediate pressure amphibolitic conditions. As a matter of fact some of the metabasalts embedded within the high-strain kyanite bearing micaschists and in the high-grade complex retain clear relics of eclogitic assemblages (Miller et al., 1976; Cappelli et al., 1992; Oggiano & Di Pisa, 1992; Cortesogno et al., 2004; Giacomini et al., 2005). However, the presence of a suture in Northern Sardinia separating the low- to medium-grade metamorphic rocks of Gondwanian origin from the high-grade metamorphic rocks belonging to the Armorica microplate, as proposed by Cappelli et al. (1992), has been questioned by several authors mainly on the basis of the absence of ophiolites and presence of similar Ordovician orthogneisses and similar evolution both south and north of the Posada-Asinara line (Helbing & Tiepolo, 2005; Giacomini et al., 2005, 2006; Franceschelli et al., 2005a). Schneider et al. (2014) identified a tectonically reworked and dismembered southern Variscan suture in the high-grade metamorphic complex of the Maures-Esterel Massif (Southern France) correlated to the HGMC in Northern Sardinia.
Several Authors have associated Sardinia with the "Hun Superterrane" (HS) (Stampfli et al., 2000, 2002; von Raumer, 1998; von Raumer *et* al., 2002, 2003; Franceschelli et al., 2005a; Giacomini et al., 2006), a ribbon-like continent detached from the northern margin of Gondwana during Silurian-Devonian times. According to this picture the main subduction of oceanic crust below the Gondwana continent happened at the northern margin of the HS (e.g., NW Iberia) during the Late Ordovician to Devonian producing eclogites during the period 440-360 Ma, whereas the southern margin (to which Corsica-Sardinia belonged) underwent extensional tectonics leading to the opening of the Paleo-Tethys. It was not until the Devonian/Carboniferous boundary that the southern passive margin of the HS became active with the subduction of the Paleo-Tethys crust northward below the southern margin of HS (Stampfli et al., 2002; Giacomini et al., 2006, 2008). During this stage continental crust in Sardinia underwent the main phase of southward migrating deformation and prograde Barrovian-type metamorphism.

DOI: 10.3301/GFT.2015.03

In places this collisional framework is complicated by the occurrence of a Neo-Variscan (300 Ma) HT-LP re-equilibration affecting both of the metamorphic complexes (Del Moro et al., 1991; Oggiano & Di Pisa 1992) (Fig. 3). This late HT-LP metamorphic evolution has been related by Oggiano & Di Pisa (1992) to the post-collisional gravitational collapse of the chain, chiefly on the basis of its age and of some meso- and micro-structural evidence. In an alternative interpretation, it could be related to late Variscan intrusions.

The geochronological data for the collisional stage in Nurra and in western Gallura are represented by Ar-Ar data on amphibole and muscovite and yield ages close to 350 Ma (Del Moro et al., 1991). In Northeastern Sardinia an upper limit to the collision-related metamorphism may be represented by the age of 344 ± 7 Ma (Rb-Sr age of isotopic exchange blocking among different compositional domains on a banded gneiss; Ferrara et al., 1978) (Fig. 3). More recent data yielded ~ 330 Ma (U-Pb zircon dating; Palmeri et al., 2004), 350-320 Ma (U-Pb zircon dating; Giacomini et al., 2006) and 330-340 Ma (Ar-Ar on white micas; Di Vincenzo et al., 2004) for the collision related metamorphism (Fig. 3). It is worth noting that U-Pb zircon dating (Palmeri et al., 2004; Cortesogno et al., 2004; Giacomini et al., 2005) suggests a HP event bracketed between the ~ 450 protolith age and the ~ 350 Ma age of the retrogressed eclogite of Northern Sardinia.

In the External zone and External nappe zone the younger formations that underwent thrusting, folding and Variscan metamorphism are Early-Carboniferous in age whereas the oldest ones not involved in deformation and metamorphism are those of the Late Carboniferous- Early Permian basins (Barca et al.,1995, Corradini et al., 2003). The subsequent D2 transpressional deformation has been constrained at 320-315 Ma (Ar-Ar on white micas on S2 foliation: Di Vincenzo et al., 2004; and U-Th-Pb on monazite and zircon in D2 mylonites: Carosi et al., 2012)(Fig. 3). The upper limit of the age of the deformation is constrained by the crosscutting Carboniferous granitoids at ~ 290-311 Ma (Rb-Sr whole rock isochron; Del Moro et al., 1975). Some syn-tectonic granites emplaced and deformed at ~ 310 Ma have recently been recognized in Northern Sardinia (Casini et al., 2012) (Fig. 3).

The structural and metamorphic evolution of the inner zone of the belt is well exposed along the transect provided in the field trip in Northeast Sardinia (Figs. 1 and 2).

The D1 collisional event is well-recorded in the southern part of the transect producing SW facing folds, top to the S and SW shear zones and the main fabric in the low-grade metamorphic rocks in southern part of the section (Carmignani et al., 1979, 1993, 1994, 2001; Simpson, 1989; Franceschelli et al., 1990; Carosi & Oggiano, 2002; Montomoli, 2003; Carosi et al., 2005). The collisional stage (D1 deformation phase) has been constrained at ~ 350 Ma by Ferrara et al. (1978) and at ~ 330 - 340 Ma by Di Vincenzo et al., 2004). However the best exposures of D1 folds and shear zones are in the southern part of the Nurra-Asinara section.

DOI: 10.3301/GFT.2015.03

Shear belts

A wide D2 shear belt is located at the boundary between the medium-grade (MGMC) and the high-grade metamorphic complexes (former Posada-Asinara line: PAL; Carmignani et al., 1994). The NW-SE-striking shear belt is affected by a major dextral shearing crosscutting the whole belt from West to East. Recent structural and kinematic studies by Carosi & Palmeri (2002), Iacopini et al. (2008), Carosi et al. (2005, 2009), Frassi et al. (2010), and Carosi et al. (2012) along the PAL documented:

(1) a sinistral top-to-the NW shear belt, developed during the initial D2 post-collisional deformation phase in the HGMC, readily observed in the southern Gallura section (central part of Northern Sardinia) (Carosi et al., 2012);

(2) a dextral top-to-the SE shear belt developing ductile and brittle-ductile D2 mylonites (within the MGMC and HGMC);

(3) high-strain phyllonites that mark the boundary between MGMC and HGMC; low-strain phyllonites developed in the HGMC that wrap lenses of sinistral mylonites and mm-thick cataclasites overprinting both earlier phyllonites and sinistral mylonites. Crosscutting relationships indicate that the D2 sinistral shearing began before the dextral kinematics. However U-Th-Pb analyses on zircon and monazite do not clearly distinguish the two events (Carosi et al., 2012).

At the same time we observed an increasing simple shear component from south to north approaching the Posada valley shear zone (Fig. 4) with mean vorticity number varying from 0.29 to 0.89. An increase in the pure shear component to the north of the high-strain zone has been observed in the Asinara section (Carosi et al., 2004b; Iacopini et al., 2008).

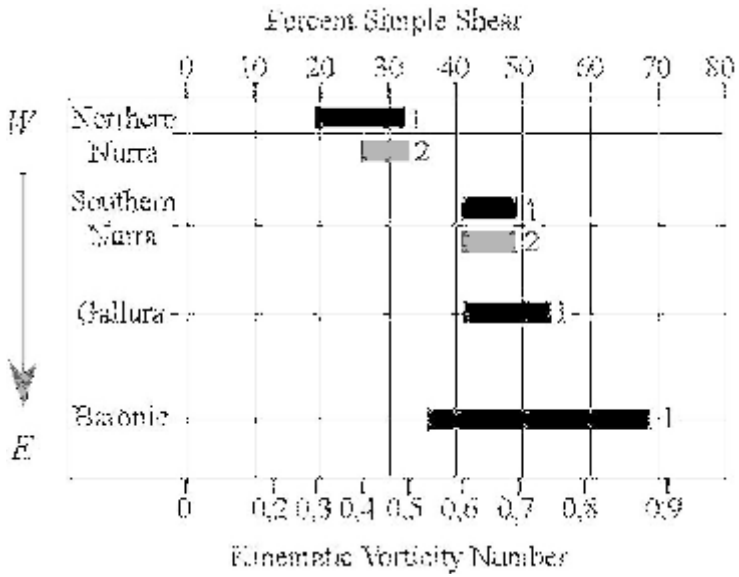

Fig. 4 - Chart showing the kinematic vorticity numbers and the corresponding percentage of simple shear along the three main cross sections shown in Fig. 1. For each area the bar represents the minimum and maximum values of the estimated vorticity kinematic numbers. Methods used: black line 1: stable porphyroclast analysis; grey line 2: syntectonic porphyroblasts with internal helicitic foliation. Modified after Carosi & Palmeri (2002) and Carosi et al. (2006). The highest vorticity values are recorded approaching the Posada-Asinara line.

DOI: 10.3301/GFT.2015.03

The D2 sinistral shear belt developed within fine-grained gneiss, metric-size sillimanite-bearing migmatite, pegmatite, and almandine + plagioclase + kyanite sillimanite micaschist and gneiss (HGMC), whereas the D2 dextral shear belt developed within garnet-plagioclase kyanite staurolite-bearing metasedimentary sequences (MGMC) (Carosi et al., 2012). Dextral and sinistral mylonites overprint prograde Barrovian index minerals (garnet, plagioclase, staurolite and kyanite) formed during the collisional stage (Ricci et al., 2004) whereas sillimanite that grew parallel to or obliquely to the sinistral shear planes indicate growth along a decompression path during the exhumation (Carosi et al., 2009; 2012).
Deformation within both the sinistral and dextral shear zones involved general non-coaxial flow with simultaneous contribution of pure and simple shear (Carosi & Palmeri, 2002; Iacopini et al., 2008, 2011; Frassi et al., 2009). Transpressional deformation initially produced sinistral mylonites under a simple-shear-dominated regime and subsequently dextral mylonites during a pure-shear-dominated regime (Frassi et al., 2009). Using vorticity analysis methods (stable porphyroclasts, quartz fabric, and foliation in porphyroblasts) we detected an important component of pure shear during D2 non-coaxial deformation (Fig. 4).
Microstructural and quartz petrofabric results also constrain the non-coaxial shearing activity under deformation temperatures ranging from 350-550° to 450-600°C for the dextral and sinistral shear belt respectively (Frassi et al., 2009).

The D2 transpressional deformation is related both to NNE-SSW direction of compression and to a NW-SE shear displacement (Carosi & Oggiano, 2002; Carosi & Palmeri, 2002; Carosi et al., 2004a, 2005, 2009; Iacopini et al., 2008). The D2 deformation is continuous and heterogeneous and is characterized by northeast verging F2 folds (Fig. 5) that become tighter from south to north approaching the Posada-Asinara line and by dextral shearing that becomes prominent in the high-strain zone.
D2 transpression is characterized by the presence of a crustal-scale shear deformation overprinting previous D1 structures, related to nappe stacking and top-to-the S and SW "thrusting". The prominent L2 object lineation points to an orogen-parallel extension (Fig. 5) and to a change in the tectonic transport from D1 to D2. Orogen-parallel extension could be attributed to the position of Sardinia close to the NE part of the Cantabrian indenter during the progressive evolution of the Ibero-Armorican arc (Carosi et al., 1999; Conti et al., 2001; Carosi & Oggiano, 2002; Carosi & Palmeri, 2002) or to a general progressive curvature of the belt, as well as to the presence of an irregular collided margin. It has been suggested that the D1 phase developed

DOI: 10.3301/GFT.2015.03

during initial frontal collision whereas the D2 deformation characterized the progressive effect of horizontal displacement during the increasing curvature of the belt. The Nurra-Asinara transect is a clear example of heterogeneous transpressional deformation of Northern Sardinia that is partitioned across the region (Carosi et al., 2004a; Iacopini et al., 2008). A switching in the attitude of L2 object lineation along the north-south direction has been detected. Trending of L2 lineations varies from nearly sub-horizontal and parallel to A2 fold axes in the South, to down-dip in the northern part of the Asinara Island, according to theoretical models of transpression proposed by Tikoff & Teyssier (1994).

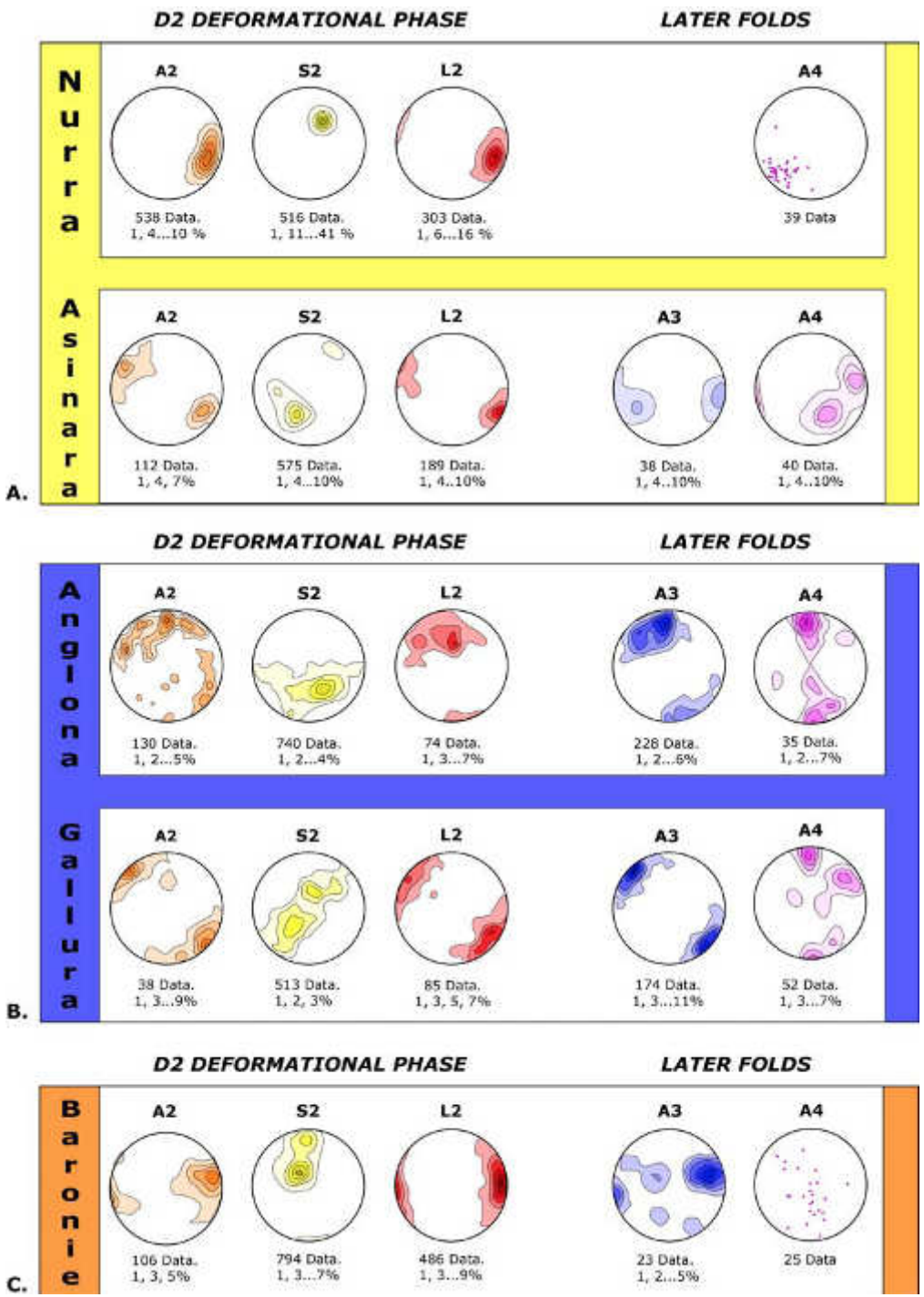

Fig. 5 - Stereographic projections (Schmidt equal area projection, lower hemisphere) of the main structural elements (D2-D4 deformation phases) in Northern Sardinia (from Carosi et al., 2005, 2006). **A.** Nurra-Asinara zone; **B.** Anglona–SW Gallura zones; **C.** Baronie zone. A2: axes of F2 folds; S2: second phase schistosity; L2: object and mineral lineation. A3 and A4 refer to later fold axes.

DOI: 10.3301/GFT.2015.03

Timing of D2 deformation

In situ $^{40}Ar/^{39}Ar$ laser probe analysis on white mica allowed Di Vincenzo et al. (2004) to constrain the age of the S1 and S2 foliation in the Grt + Bt zone of the Baronie area and to better constrain the age of the collisional (D1) and transpressional (D2) deformation phases. Using microstructural relationships, microchemical composition, and age they characterized deformed celadonite-rich mica flakes that define the D1 phase (both inside garnet and plagioclase porphyroblasts and in the core of large white micas in the matrix) and a celadonite-poor white mica aligned along the S2 foliation. The resulting ages range from 345 Ma to 300-310 Ma for the interval spanning D1 and D2 (Di Vincenzo et al., 2004) (Fig. 3). D1 ages concentrate around 330-340 Ma whereas D2 ages were constrained between 315 and 320 Ma (Fig. 3). These results, as well as the absence of a postulated deformed unconformity, do not support the existence of a pre-Variscan metamorphic basement represented by the micaschist and gneiss of the L-MGMC of Baronie, as proposed by Helbing & Tiepolo (2005). This hypothesis has also been questioned by Franceschelli et al. (2005a).
Zircons and monazites were collected in sinistral and dextral shear zones in SW Gallura for in situ U-Th-Pb ages; results indicate that the shear zones were active at *c.* 320 Ma (Carosi et al., 2012). The superposition relationships indicate that the sinistral shear zones started earlier than the dextral ones within the D2 transpressional event, causing the early exhumation of the HGMC and its oblique thrusting onto the MGMC (Carosi et al., 2012). Even though the sinistral shear zones appear to be slightly older than the dextral shear zone, U-Th-Pb geochronology, with its associated analytical errors, do not yet enable us to distinguish them.
The occurrence of a system of shear zones that was active at *c.* 310-320 Ma, first recognized by Carosi & Palmeri (2002) in a transpressive setting, is now recognized as a common feature of the Southern European Variscan belt (Schneider et al., 2014 with references). The age of the dextral shear zones in the high-grade metamorphic complex of southern Corsica of just under 320 Ma is in line with the age of D_2 in Northern Sardinia (Giacomini et al., 2008; Carosi et al., 2012), pointing to a consistent geological, structural, and geochronological framework in Northern Sardinia and Southern Corsica.
Corsini & Rolland (2009), Carosi et al. (2012), and Schneider et al. (2014) recognized a wide correlation among tectonic, metamorphic, and geochronological evolution between Corsica-Sardinia and the Maures-Tanneron massifs connected to the East Variscan Shear Zone (Corsini & Rolland, 2009).

DOI: 10.3301/GFT.2015.03

Metamorphism

Franceschelli et al. (1982a) and Ricci et al. (2004) distinguished the following main lithological complexes moving from south to north:
a) phyllite and metasandstone of the biotite zone, b) micaschist and paragneiss of the garnet + albite and garnet + oligoclase zone, c) granodioritic orthogneiss and augen gneiss, d) micaschist and gneiss of the staurolite + biotite and kyanite + biotite zones, mylonite and subordinate amphibolite lenses, e) migmatite and gneiss of the sillimanite + muscovite and sillimanite + K-feldspar zones with retrogressed eclogite lenses and calc-silicate nodules.
A Barrovian-type metamorphism related to the thickening stage of the belt has been recognized since the seventies (Carmignani et al., 1979; Franceschelli et al., 1982a,b, 1989; Ricci et al., 2004).
Based on the mineralogy of pelitic and psammitic schist, seven metamorphic zones with increasing metamorphic grade from south to north have been recognized in NE Sardinia (Figs. 1, 7):
i) biotite zone; ii) garnet + albite zone; iii) garnet + albite + oligoclase zone; iv) staurolite + biotite zone; v) kyanite + biotite zone; vi) sillimanite + muscovite zone; and vii) sillimanite + K-feldspar zone (Franceschelli et al., 1982a,b, 2005a). The P–T paths of the metamorphic zones of NE Sardinia have been described by several Authors (Carosi & Palmeri, 2002; Di Vincenzo et al., 2004; Franceschelli et al., 1989, 2005a; Ricci et al., 2004). The isograds run parallel to the lithological contacts deformed by the D2 orogen-parallel deformation event and are telescoped approaching the Posada-Asinara line (Carosi & Palmeri, 2002).
Within these zones, all metamorphic rocks display clockwise P–T paths characterized by a prograde stage, with peak pressure diachronous with peak temperature, followed by a stage of decreasing temperature and pressure (Fig. 6). Based on theoretical expectations (Thompson & England, 1984) this P–T evolution (Fig. 6) may reflect homogeneous thickening (Franceschelli et al., 1989).
The L-MGMC contains eclogite-facies metabasite and amphibolite lenses in the Posada Valley (Cruciani et al., 2011) (Figs. 3, 7). However, omphacite has not been found in the amphibolites of the Posada Valley. A granulite or upper amphibolite stage was followed by an amphibolite stage leading to the formation of plagioclase + amphibole coronas around garnet rims (Franceschelli et al., 2007). The age of the sedimentary protolith of the pelitic–psammitic sequences is unknown.

DOI: 10.3301/GFT.2015.03

Regarding the igneous-derived metamorphic rocks, Helbing & Tiepolo (2005) provided magmatic U/Pb ages of 474 ± 13 Ma for the Lula porphyroid, 456 ± 14 Ma for the Lodé orthogneiss, and 458 ± 7 Ma for the Tanaunella orthogneiss.

From granulitized eclogites embedded within the migmatite complex of Punta de li Tulchi (Fig. 7), Palmeri et al. (2004) obtained three main U–Pb zircon ages of 453 ± 14, 400 ± 10, and 327 ± 7 Ma.

The first age was interpreted as the protolith age, the second was interpreted either as the age of the HP metamorphism or the result of Pb loss during the main Variscan event, and the third age was attributed to amphibolite facies retrogression.

For one eclogite sample embedded in anatectic migmatites, an age of 457 ± 2 Ma of magmatic zircon was interpreted by Cortesogno et al. (2004) as a minimum protolith age. A second group of zircon grains gave an age of 403 ± 4 Ma, which has been interpreted as dating zircon crystallization during the high-grade event. Giacomini et al. (2005) dated zircons from the Golfo Aranci (NE Sardinia) eclogites. Magmatic zircon yielded a mean age of 460 ± 5 Ma, interpreted as the protolith age, while a second group of zircon grains gave a weighted average of 352 ± 3 Ma. From zircon in eclogite embedded within the HGM Complex, Giacomini et al. (2005) obtained metamorphic ages clustering around Early Visean and between Late Visean and 300 Ma.

These authors attributed the first and second cluster to the HP metamorphic overprint and post-HP amphibolitic equilibration, respectively.

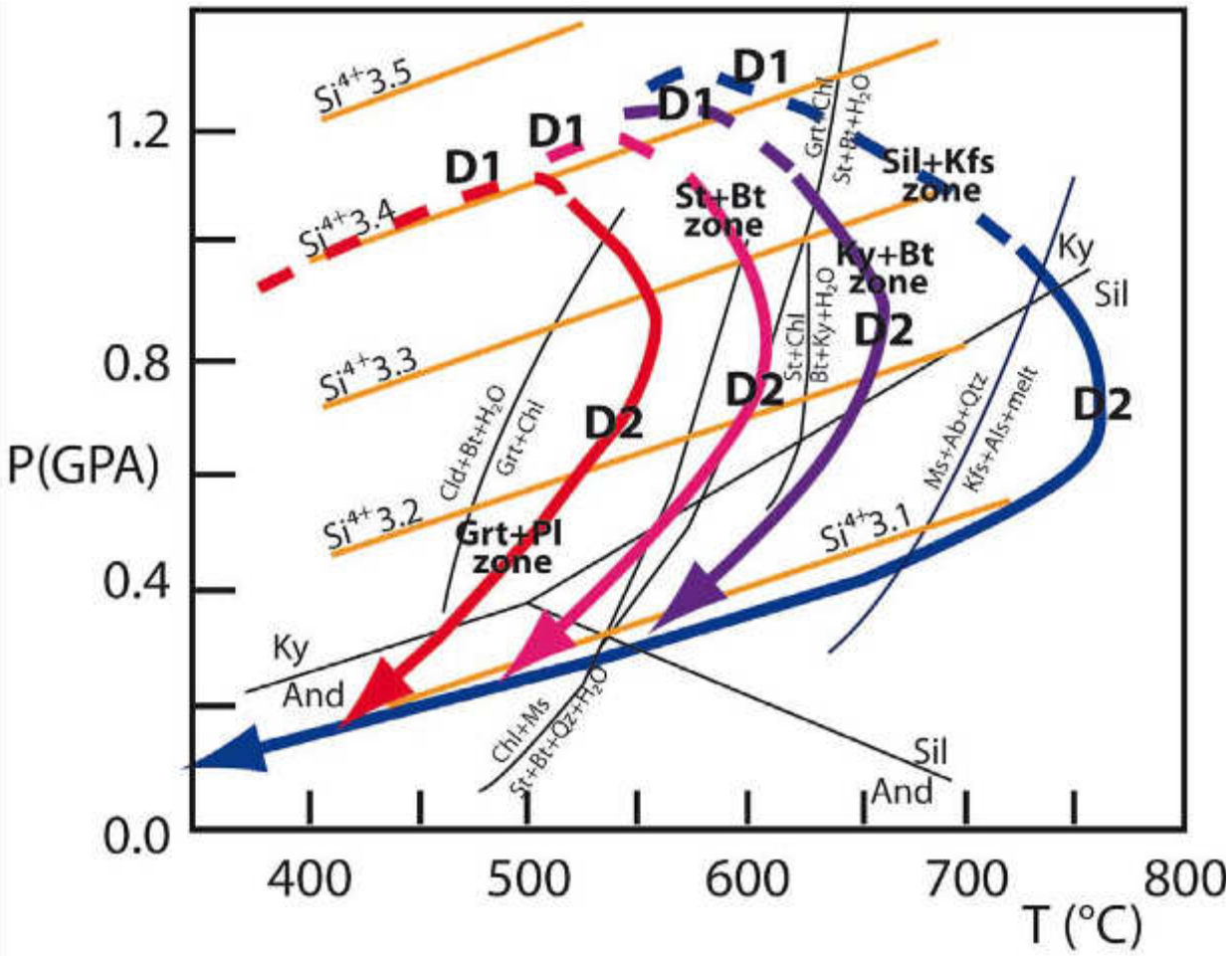

Fig. 6 - P-T-t paths for the various metamorphic zones of NE Sardinia (modified after Di Vincenzo et al., 2004).

DOI: 10.3301/GFT.2015.03

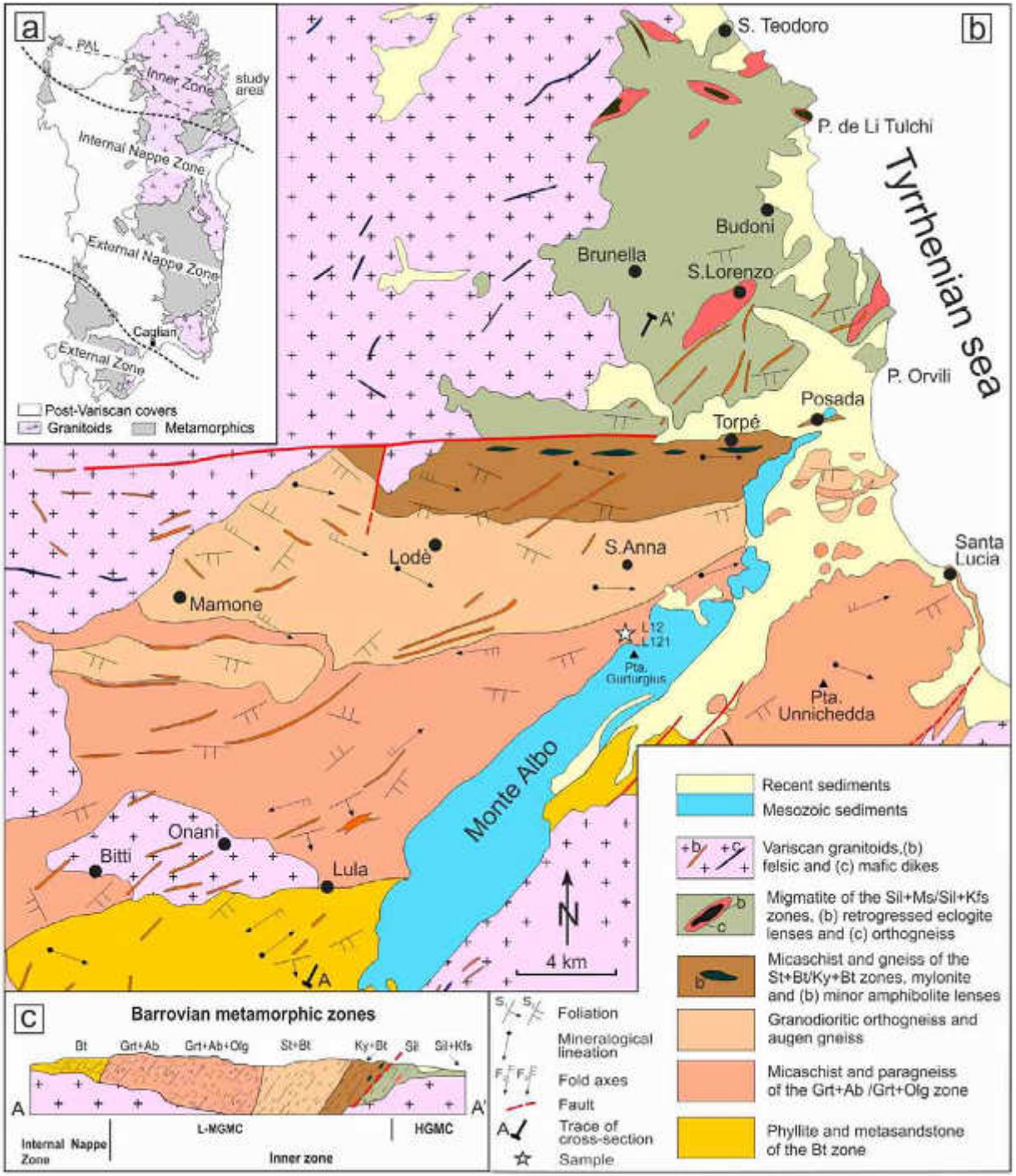

Fig. 7 - Geological and structural map of the Baronie area (from Cruciani et al., 2013). **a)** Simplified tectonic sketch map of the Variscan belt in Sardinia; PAL: Posada–Asinara line; **b)** Geological sketch map of NE Sardinia modified from the 1:200000 geological map of Sardinia northern sheet (modified from Carmignani et al., 2001); **c)** Geological cross-section through the Variscan basement of Sardinia from south of Lula to south of Brunella (mineral abbreviations according to Fettes & Desmons, 2007). Olg.:oligoclase.

Sheared and folded isograds

The geometry of the Barrovian isograds shows a complex pattern, appearing inverted in the central and northwestern parts of the island and normal in the Baronie, (Carmignani et al., 1994, 2001; Carosi et al., 2005) (Fig. 2).

New mapping, rock sampling, and structural analysis led to the identification of staurolite + biotite assemblage dozens of kilometers further south (Carosi et al., 2008) than the previously proposed Posada valley isograd. This finding cannot be explained by a simple increase of metamorphism towards the north; the repetition of the staurolite-biotite isograd demands a tectonic explanation.

This new finding is in line with the microstructural observation that the

DOI: 10.3301/GFT.2015.03

Barrovian index minerals are pre- to syn-D_2 (Franceschelli et al., 1982a; Carosi & Palmeri, 2002; Carosi et al., 2012) so that we expect to find Barrovian "isograds" folded by F_2 folds and sheared by dextral shear zones. Detailed geological mapping at the scale of 1:10.000 and structural analysis have shown that the staurolite + biotite isograd in the Posada valley corresponds to the isograd in the Mamone synform having been displaced by two km-scale northeastern-verging F_2 antiforms and synforms. Unfolding northeast-verging F_2 folds, the isograds show an inverted pattern with increasing metamorphism upward toward the overlying HGMC. It can be argued that the southward overthrusting of the HGMC onto the MGMC could have caused the inversion of the isograds from biotite to kyanite and initiated the exhumation of the HGMC. An inversion of the metamorphic isograds has also been described in the southwest Gallura region and Asinara Island (Carosi et al., 2004a, 2005) (Fig. 2).
In the classical view of the Barrovian metamorphism in Northern Sardinia the appearance of sillimanite is placed after kyanite in a prograde metamorphic sequence (Franceschelli et al., 1982a, 1986, 1989, and Ricci et al., 2004 with references therein). This may be true for temperature but not for pressure, which shows a decrease of at least 0.3-0.4 GPa passing from the kyanite to the sillimanite+muscovite zone (see Carosi & Palmeri, 2002 and Ricci et al., 2004). In Northern Sardinia (Carosi et al., 2004a, b, 2005), the sillimanite starts to grow along the S2 foliation, whereas porphyroblastic staurolite and kyanite grew mainly before the formation of the S2 foliation. We therefore suggest that the prograde metamorphism reached HP in the kyanite stability field and, starting from the medium pressure metamorphic rocks and migmatites associated with the D2 deformation, underwent decompression (isothermal decompression in the migmatites according to Carosi et al., 2004a and Giacomini et al., 2005), eventually reaching the sillimanite stability field.
The recent finding of HP during D1 in the chloritoid schist of the L-MGMC by Cruciani et al. (2013) shed new light on the metamorphic framework described above, suggesting previously unrecognized true HP conditions during the D1 deformation (Fig. 3).
Thus, the basement of Northern Sardinia has a complex metamorphic history characterized by an early prograde HP metamorphism acquired during the underthrusting of continental crust (D1) reaching higher pressures, followed by a nearly isothermal decompression from D1 to D2 reaching the sillimanite stability field, and followed in some places (e.g. SW Gallura and Asinara island) by a further (local ?) HT-LP metamorphic event (Fig. 3). The occurrence of HP relics in metapelites in the L-MGMC suggests the presence of crustal slices that, at a minimum have been reworked, or even been subjected to a true high-pressure nappe in the Sardinian Variscides, larger than previously thought and extending south of the HGMC. However, the areal extent of HP metamorphism during D1 in the L-MGMC needs further investigation.

DOI: 10.3301/GFT.2015.03

Corsica-Sardinia batholith

The Sardinia-Corsica batholith, one of the largest European Variscan batholiths, was emplaced during the Middle Carboniferous to Permian post collisional phase of the Variscan orogeny (Fig. 3). Based on field relations, composition, and geochemical affinity, three main suites (U_1, U_2, U_3) have ben distinguished by Rossi & Cocherie (1991) (Fig. 3). The early U_1 suite (magnesian- potassic intrusion) developed only in Western and North-western Corsica at 340-320 Ma during a N-S directed shortening. The U_1 suite consists mainly of quartz-monzonite and monzonite-containing stocks and enclaves of comagmatic, ultrapotassic mafic rocks that emplaced at depth from mid-crustal levels to close to the surface.
The U_2 suite, which spans in age from 321 to 280 Ma and forms the largest part of the Sardinian batholith, consists of a composite plutonic-volcanic association volumetrically dominated by large granodiorite and monzogranite plutons. Minor peraluminous intrusions and mafic bodies are also present. The early U_2 plutons were emplaced within narrow strike-slip shear zones. The basic rock association of the U_2 suite has a tholeiitic affinity and derives from mantle magmatism that also gives rise to andesitic volcanic rocks and layered mafic intrusions (Rossi & Faure, 2012). The proportions of gabbro-diorite, tonalite-granodiorite, and granite in the U_2 suite are 5:15:82 (Orsini, 1980).
The batholith construction in North Sardinia started around 320 Ma with the emplacement of small granodiorites that accumulated within the narrow dilatational sites developed along E-W and NW-SE strike slip shear zones inferred to be the equivalent to the Posada-Asinara line (Casini et al., 2012).
The U_3 suite consists of large pink biotite-leucogranite plutons, a subalkaline gabbroic sequence, metaluminous to slightly peraluminous A-type biotite granite, and peralkaline granitoids. The age spans 290 -280 Ma. A-type granites only occur in Corsica.
The batholith is crosscut by localized dense networks of acidic and basic dykes. According to Poli et al. (1989) the Sardinian batholith resulted from a two stage process. In the first stage a sub-crustal magma interacted with a monzogranitic melt produced by crustal anatexis. The formation of tonalite and granodiorite intrusions is related to this stage. During the second stage, the leucogranites were formed by low degrees (15-25%) of crustal melting. According to this interpretation, crustal anatexis played a dominant role in the petrogenesis of the batholith.

DOI: 10.3301/GFT.2015.03

Tectonic evolution

Taking into account the new data, the following tectono-metamorphic history is tentatively proposed (Figs. 3, 8):
- stages a, b: Early D1 deformation phase. During the collisional event or during the north-directed subduction of the Sardinian continental crust belonging to northern Gondwana or peri-Gondwanan derived terranes, both the L-MGMC and HGMC underwent HP metamorphism, with the HP metapelites reaching pressures of nearly 1.7 GPa (Cruciani et al., 2013), followed by Barrovian metamorphism with T and P increasing to the northeast (Ricci et al., 2004);
- stage c: Late D1 deformation phase. Exhumation of the HGMC starts by activation of NW-SE striking and top-to-the south and southwest shear zones and faults with a major dip-slip component of movement. These caused the tectonic repetition of the metamorphic sequences and the building up of the nappe pile;

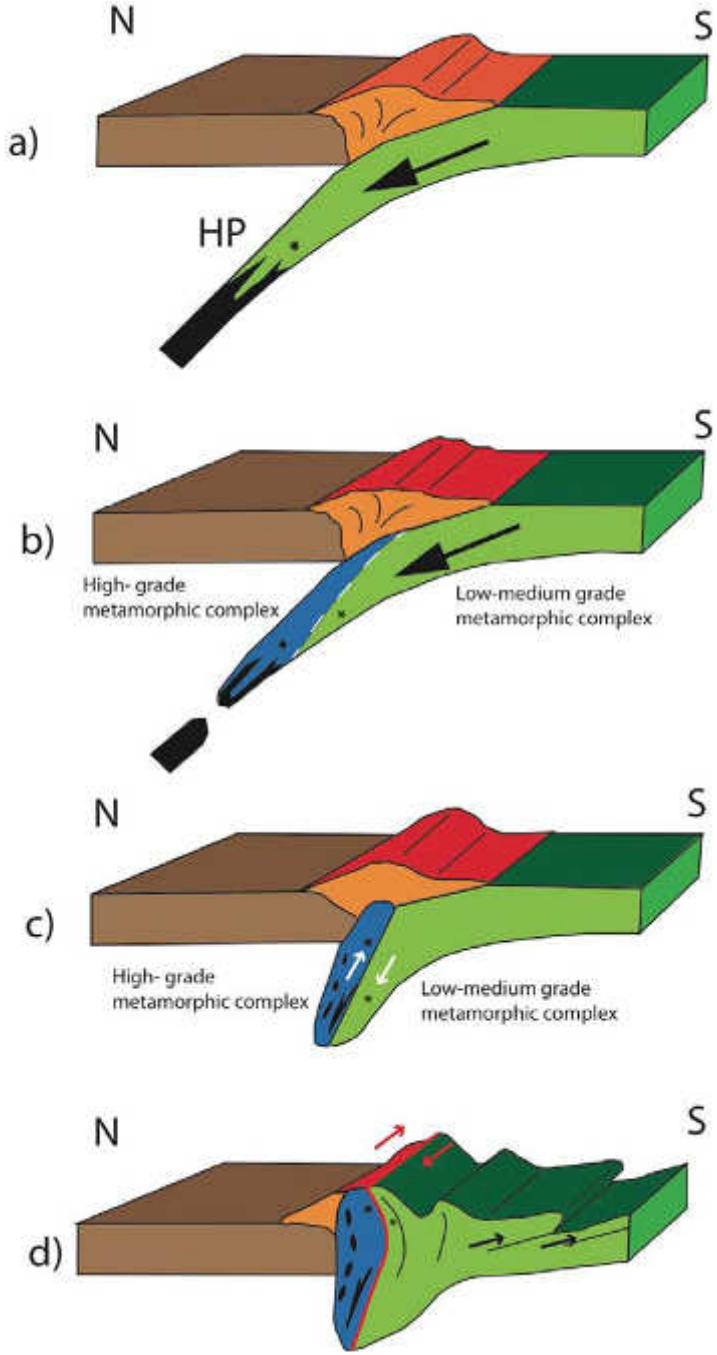

Fig. 8 - Sketch of the proposed tectonic evolution of the Sardinian Variscides. Stage **a)** Collision stage at 360-340 Ma; start of the D1 tectonic phase and HP metamorphism in the oceanic and continental crust; Stage **b)** D1 tectonic phase; HP metamorphism in the future HGMC and in the deeper part of the L-MGMC; Stage **c)** Late D1 tectonic phase: thrusting of the HGMC over the L-MGMC; exhumation of the HGMC starts while the L-MGMC continues to be underthrust; Stage **d)** D2 tectonic phase during transpressional deformation between HGMC and LMGMC. Overall exhumation with an oblique component (initial sinistral and later dextral shear sense). Green and blue: Gondwana continental crust; blue: deeper portion of the crust undergoing HP metamorphism in the future HGMC; black: oceanic crust; orange and red: upper crustal level of the rising Variscan belt; brown: hinterland; asterisks: HP metamorphism.

DOI: 10.3301/GFT.2015.03

- stage d: D2 deformation phase. With P-T conditions at 470-560°C and 03-0.6 GPa (Carosi et al., 2009), an initial sinistral shearing occurred at ~ 325-320 Ma (U-Th-Pb on monazite and zircon, Carosi et al., 2012). This was followed by a generalized top-to-the SE shearing along the PAL (NW-SE trending) with a major dextral orogen-parallel displacement (Carosi & Palmeri, 2002; Iacopini et al., 2008; Carosi et al., 2009). The HGMC was exhumed as the hanging-wall of the PAL, whereas the MGMC, as the footwall of the PAL, continued to be underthrust to the north. The D2 deformation phase is partitioned into two components: an orogen-parallel shearing developed along the PAL, and an F2 back-folding with a N and NE vergence (Carosi & Palmeri, 2002; Iacopini et al., 2008), mainly developed south of the PAL.
Some of the oldest U_2 granitoids at ~ 320-310 Ma emplaced during the overall transpressional regime (Casini et al., 2012).

During the final stages of exhumation, a HT-LP metamorphism developed in some portions of Northern Sardinia (e.g., Asinara Island: Carosi et al., 2004a and Anglona: Carosi et al., 2009) (Fig. 3). Two later phases of deformation caused re-folding of the nappe pile, and affected the basement by forming open folds with orogen-parallel (NW-SE trend) and orogen-perpendicular fold axes (NE-SW trend) (Fig. 5), still in a contractional regime, but without significantly changing of the overall geometry of the belt.
Later extensional tectonics affected the nappe pile at higher crustal levels by forming "collapse folds" and low- to high-angle faults.

DOI: 10.3301/GFT.2015.03

Remarks on the itinerary

The itinerary mostly follows the Variscan basement as it crops out along the northeastern coast of Sardinia. We start from the L-MGMC, travelling northwards to the HGMC with its migmatites and Carboniferous-Permian intrusions.
Starting from the lowest metamorphic grade (biotite zone) and moving north, we observe the regional metamorphic grade increase from biotite, garnet, staurolite, kyanite, up to the sillimanite zone. The degree of deformation also increases from south to north, with the D2 deformation progressively transposing the D1 folds and foliation. In addition, a component of dextral shear becomes more pronounced as we move toward the Posada-Asinara shear zone.
In the Migmatite Complex we see melted protoliths and its associated metamorphism and deformation. Melting in high-grade crustal rocks increases in the northern part of the island, which is mainly composed of the Carboniferous-Permian intrusions of the large Corsica-Sardinia batholith. The Migmatite Complex contains boudins with relicts of HP rocks.
On the last day we see features of the Carboniferous-Permian granitoids that crop out around the village of Arzachena.

The stops feature some of the finest and most readily accessed outcrops of the northeastern Sardinia basement. The locations are well-described in the literature. The trip provides an overview of the essential aspects of the tectonometamorphic history of the Variscan basement and takes just under four days. Some stops are indicated as optional and can be skipped without omitting important material. The chosen localities lie within a few minutes' walk from the road, or are situated directly on the road cuts.
The description of each stop includes both field photographs and photomicrograph that point out significant microstructural features of the outcrops and the key relationships between the deformation, minerals, and metamorphism. Geological sketch maps help connect the observations to the overall geology of the island. GPS coordinates (WSG84 reference) help users of the guide to locate the outcrops.

DOI: 10.3301/GFT.2015.03

First day

Olbia, Posada, Lula, Lodè, Posada

From Olbia, take highway SS131 to Nuoro until the cross road to Lula and Bitti villages, after Siniscola. Take the new road and after few hundred meters, stop on the right side of the road. Carefully cross the road. On the left we observe a wide and long road cut with phyllites showing many small-scale folds.

Fig. 1.1 - Location of the first day stops

STOP 1.1: Road to Lula

(N 40° 24’ 05.96”, E 9°29’ 04,84”)

We enter in the L-MGMC, mainly made up of phyllite, paragneiss, metasandstone, quartzite and minor levels of metavolcanics (Fig. 1.2). Sedimentary bedding is still clearly recognizable, both at the meso- and micro-scale.

The S1 foliation is fine and continuous in the more pelitic levels, while it is a spaced foliation in the more arenitic ones. It is defined by the orientation of white mica, biotite, and quartz, and is deformed by tight to isoclinal F2 folds with steeply dipping axial planes (Fig. 1.3) and NE vergence. The S2 foliation, developed parallel to F2 axial planes, is a discrete crenulation cleavage (classification according to Passchier & Trouw, 2005). D2 axial planes and S2 foliation strike NW-SE and

DOI: 10.3301/GFT.2015.03

Fig. 1.2 - Geological sketch map of Northern Sardinia showing the Stops (modified after Carosi et al., 2005).

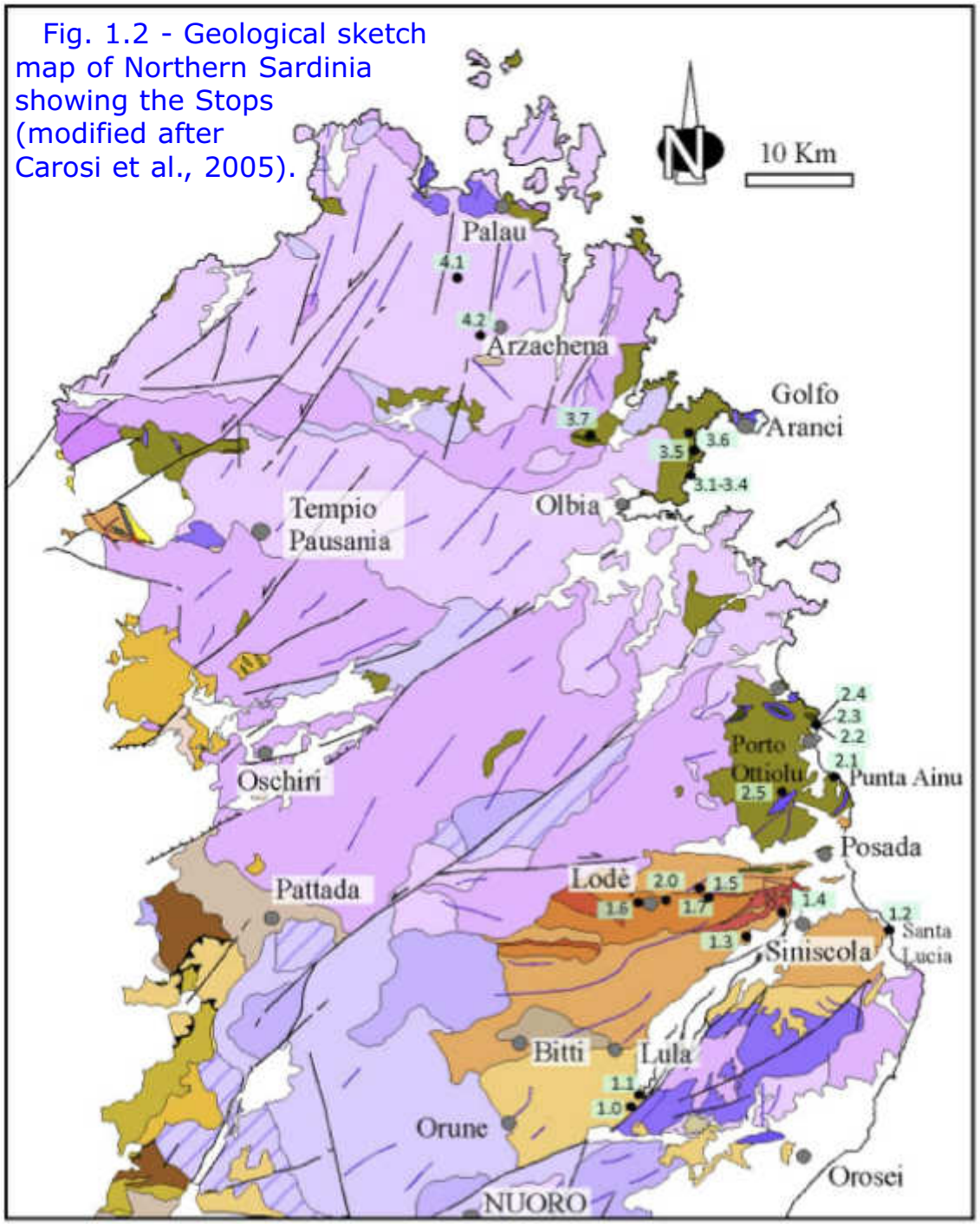

Post-Carboniferous covers

Intrusive complex ***(Upper Carb.- Perm.)***

Main dykes

Equigranular leucogranites; Grt-bearig leucogranites.

a b — Bt-monzogranites and sodic sienites (a) and monzogranitic granodiorites (b).

a b — Tonalitic granodiorites (a) and tonalites, gabbroes and gabbro-tonalite bodies (b).

a b — Crd-bearing (a) and foliated granitoids (b).

Variscan metamorphic complex

Migmatites with calc-silicate lenses. ***Carb.***

Granodioritic and monzogranitic orthogneisses. ***Ord.-Middle Sil.***

Amphibolites and ultramafic amphibolites with granulites relics. ***?Precamb.***

Amphibolites with eclogites relics. ***Ord.***

a b — a- Granodioritic orthogneiss. ***Ord.***
b- Punta Scorno orthogneiss (Asinara I.).

Augen gneiss. ***? Middle Ord.***

Metasediments of amphibolites facies (Grt±Ky±St) and Grt±Olig, Grt±Ab micaschists and paragneisses. ***Paleozoic.***

Metasediments of amphibolites facies metamorphism with a HT overprinting (And±Sill±Crd). ***Paleozoic.***

a — Amphibolites- to greenschist-facies mylonites and phyllonite (a).

Internal Nappe

Graphitic dark phyllites, metasiltstones, black quartzites and marble. ***Silurian.***

Metavolcanic and meta-epiclastic rocks. ***Middle Ord.***

Metasandstones, quartzites, phyllites. ***Cambrian-Upper Ord p.p.***

External Nappe

Black shales, dark quarzites and pelagic metalimestones. ***Lower Sil.-Lower Dev.***

Metavolcanic rocks metaconglomerates. ***Middle Ord.***

Micaceous metasandstones, quartzites and phyllites. ***Middle Camb.-Lower Ord.***

DOI: 10.3301/GFT.2015.03

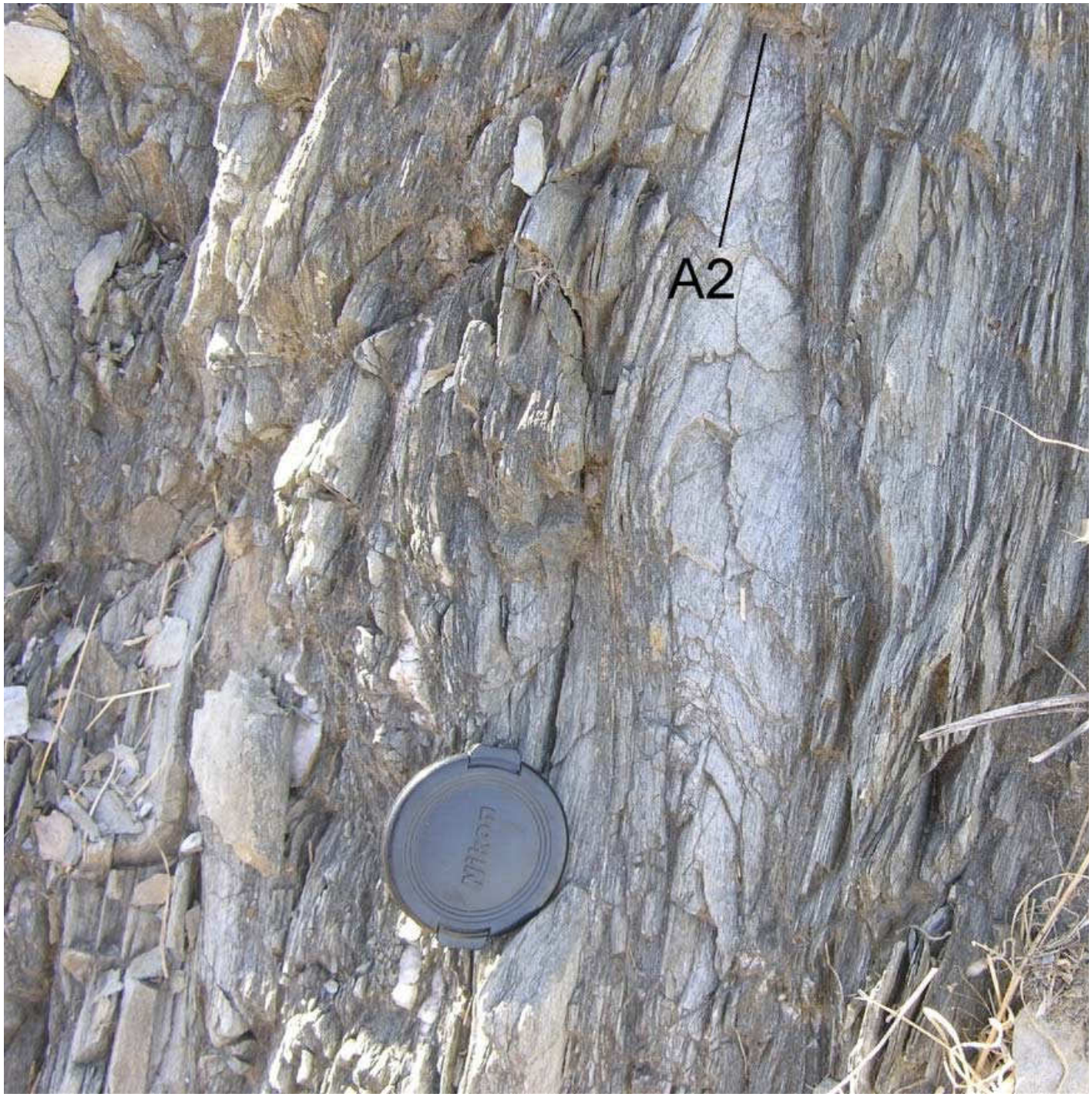

dip 40-50° to the SE. A2 fold axes trend NE-SW with variable plunge. Here, S1 is still well-preserved in D2 microlithons, whereas further north, as the D2 deformation intensity increases, the S1 foliation is progressively transposed by D2.

Fig. 1.3 - F2 tight folds with steeply plunging A2 axes in biotite-bearing phillyte south of Lula. The S1 foliation is folded but it is still clearly observable.

DOI: 10.3301/GFT.2015.03

STOP 1.2: Old road to Lula - Folds in the Variscan basement (N 40° 25' 02.66, E 9° 29' 13.05").

Return to the crossroads and drive along the old road to Lula for a few kilometers. Here,decametric F2 folds in the L-MGMC are well-exposed in the road cut (Fig. 1.4). The sedimentary sequence is represented by metasandstone, paragneiss, and micaschist (Figs. 1.5a, b).

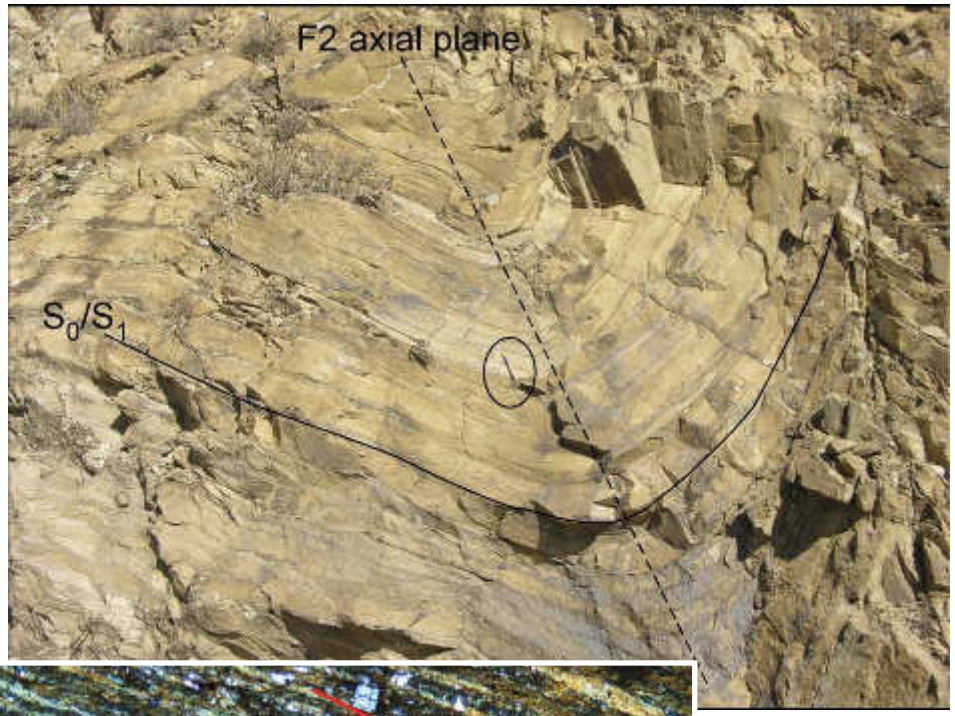

Fig. 1.4 - Sedimentary bedding in metasandstone with a nearly parallel S1 foliation folded by F2 folds. Pencil (circled) for scale.

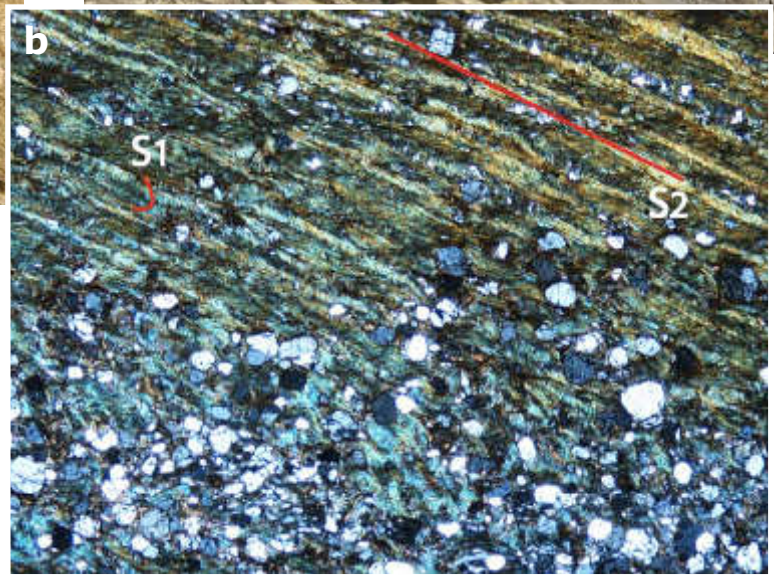

Fig. 1.5 - **a)** Albite-rich layers in reworked metavulcanite folded by upright F2 folds. **b)** Photomicrograph showing the relationships between sedimentary bedding (sub-horizontal and marked by a change in composition of the layers), folded S1 foliation in the microlithons, and S2 crenulation cleavage axial plane of the metric F2 fold observed at the outcrop scale. The lower part is mainly composed of albite porphyroblasts. Crossed polars (CPL), 20x.

DOI: 10.3301/GFT.2015.03

The prominent foliation is S0/S1 folded by north-verging F2 folds (Figs. 1.4, 1.5, 1.6) with A2 axes trending N050E. Albite-rich layers are frequently found in the sequence (Figs. 1.5a, b).

Geothermobarometry with pseudosection modelling on a metasandstone sample from the biotite zone gives T = 430-470°C and P = 0.65-0.95 GPa (Costamagna et al., 2012).

Looking to the east-north-east we see the Jurassic and Cretaceous carbonate rocks of Monte Albo dipping to the South East. They unconformably cover the Variscan basement and are affected by oblique thrusts along the NE-SW striking Nuoro fault that developed during Tertiary transpressional tectonics.

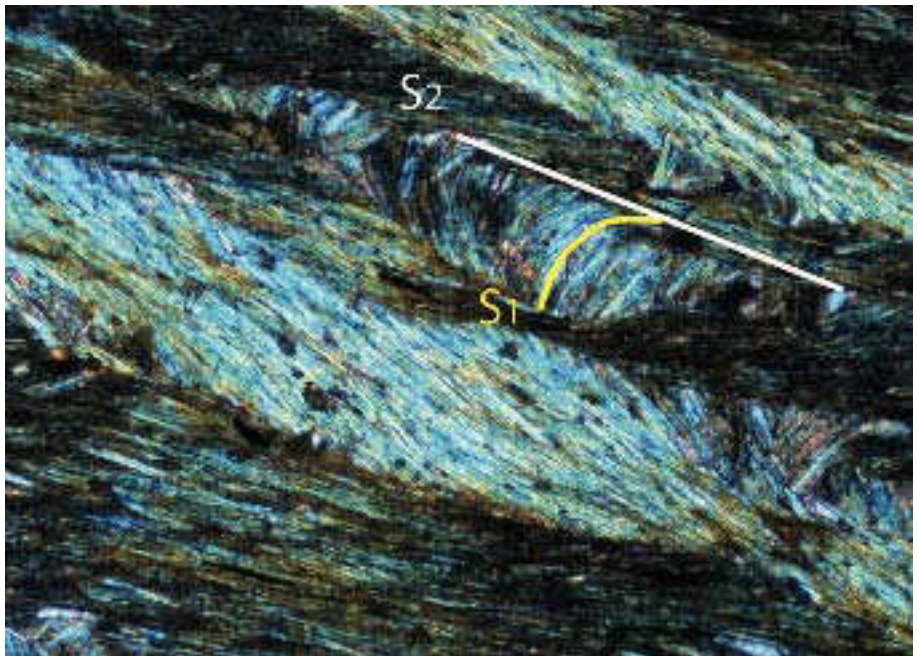

Fig. 1.6 - Detail of the relationship between S1 foliation in the microlithons and S2 crenulation cleavage in pelite-rich layers. (CPL), 60x.

Fig. 1.7 - Centimetre-sized garnet in garnet micaschist (garnet zone) at S. Lucia. Garnets are pre-D2 to syn-D2 and show helicitic inclusions.

STOP 1.3 (optional): S. Lucia village - Garnet micaschist (N 40° 34′ 51.1″, E 9° 46′ 50.6″).

Return to SS131 to Siniscola and go past the exit to S. Lucia village to the SE. At the seaside, park in a small parking area just few meters beyond the old tower. Along the outcrops on the shore we see mm- to cm-size red garnets in micaschists (Fig. 1.7).

DOI: 10.3301/GFT.2015.03

We are now in the classic Barrovian metamorphic garnet zone, starting form Lula and striking ~ E-W.
Many folded and transposed quartz veins and layers showing a prominent mineral lineation and scattered fold axes are visible, including some folds that resemble sheath-folds. On the XZ sections of the garnet micaschist, a dextral sense of shear is visible marked by C-S fabrics and asymmetric rotated garnets (Fig. 1.8).

Fig. 1.8 - C-S fabric with a top-to-the NW sense of shear in garnet schist within the garnet zone at S. Lucia.

To the south we see decimetric-thick brittle shear zones, striking nearly E-W, with cataclasites and breccias showing a dextral sense of shear.
A thin basic dike (generally placed in the Late-Carboniferous-Permian) intrudes both the micaschist and the cataclasites so that the dike post-dates the brittle dextral shearing.
Other N-S striking brittle shear zones with breccias and cataclasites are the most recent deformation seen in the outcrop since they crosscut all the other structures present.

DOI: 10.3301/GFT.2015.03

Siniscola: *Altitude: 40m a.s.l.; Surface Area: 199,96 km²; Population: 11519.*

Panoramic view of Siniscola;
from: http://www.siniscolacomunitaospitale.it

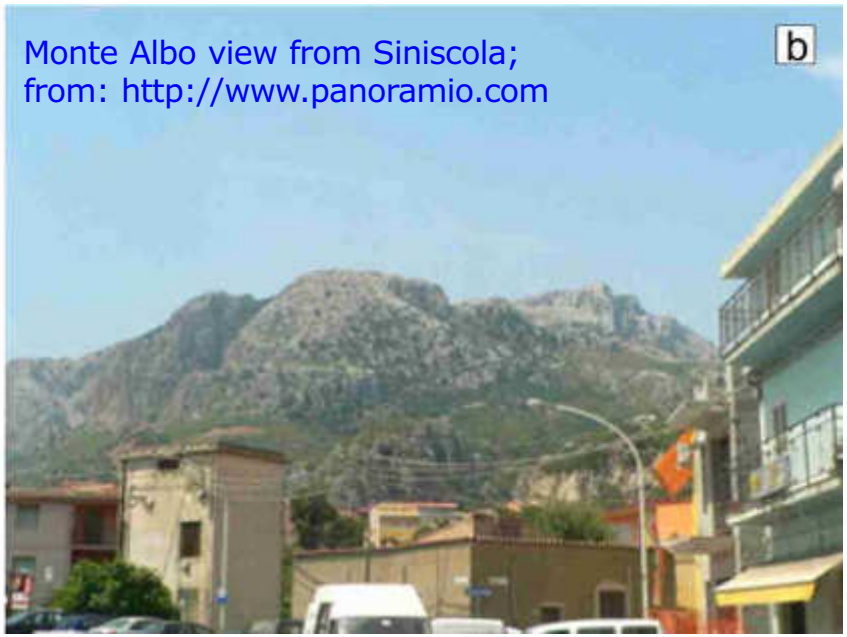

Monte Albo view from Siniscola;
from: http://www.panoramio.com

Siniscola town (Thiniscòle in Sardinian language), is located in the eastern coast of Sardinia, inside the historical region of Baronie, which is the most important center. This town is located on the slopes of Mont'Albo in the north-east and is facing the sea. The main activities carried out in Siniscola are breeding, farming, the processing of dairy products, mining, crafting and fishing. The leading activity is represented by terracotta crafting, made possible since ancient times thanks to a particularly red clay subsoil. Is it also very important the tourism sector, because Siniscola has many monuments and places of interest such as religious buildings, archaeological sites (dating back to nuragic and pre-nuragic period). The natural attractions are the beautiful beaches, such as Saint Lucia, Berchidda and Capo Comino, and the cave of "Gana e Gortoe", located under the residential settlement, inside which there is a small stream. The origin of this stream is unknown, since the cave is partially unexplored.

DOI: 10.3301/GFT.2015.03

Lula - *Altitude: 521m a.s.l.; Surface Area: 148,56 km²; Population: 1582.*

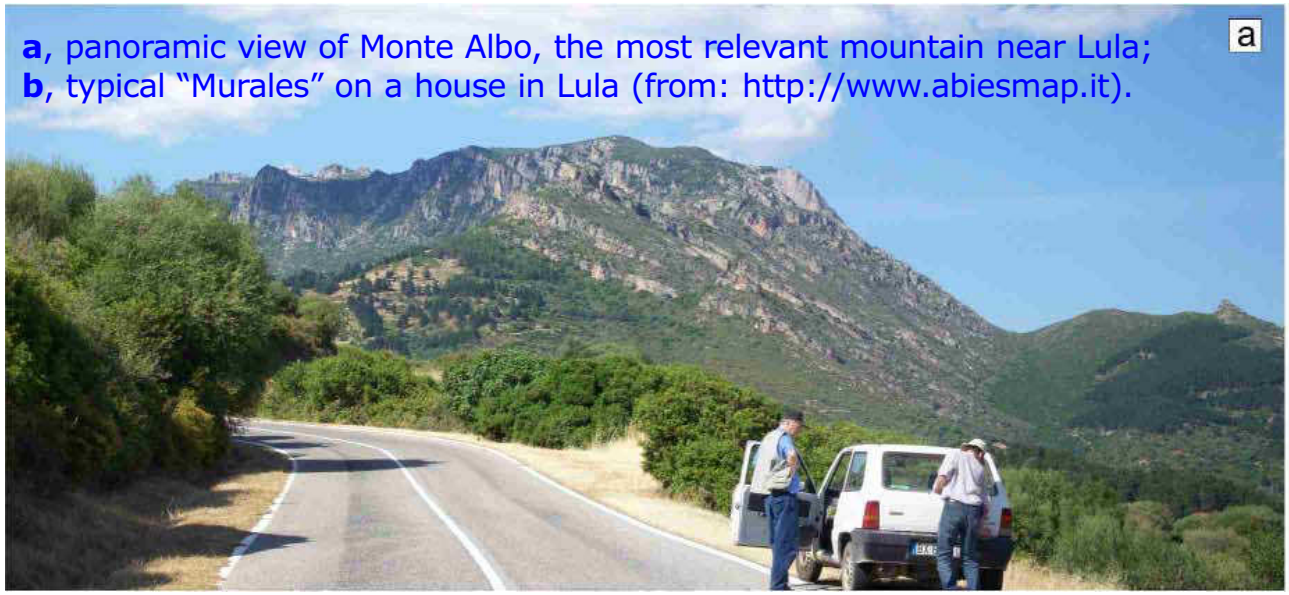

a, panoramic view of Monte Albo, the most relevant mountain near Lula;
b, typical "Murales" on a house in Lula (from: http://www.abiesmap.it).

The village of Lula is located at the foot of the western slope of a limestone chain called "Mont'Albo", and was recently cited by the European Union a SIC (Site of Community Importance). The thick vegetation on the mountain provides a habitat for several species of animals and birds including mouflon, foxes, and eagles. The mining history of the village is linked to the mines of Sos Enattos, S'Arghentaria and Guzzurra, now part of the Historical and Environmental Geominerary park of Sardinia. Lula is also the destination of pilgrimages to the rural sanctuary of S. Francesco. Notable local traditions include "Su ballu e sa vaglia" and the mask of "Su Batiledhu", the star of the Lula carnival.

STOP 1.4: North slope of Mt. Albo - road from Lula to Lodè - Chloritoid schist with relics of HP metamorphism (N 40° 33' 14.2", E 9° 37' 08.1").

Continuing from Stop 1.2 along the same road to Lula, we see chloritoid schists cropping out in the L-MGMC (Carmignani et al., 1994). The schists include mm-size reddish garnet and small dark green flakes which are chloritoid crystals (Fig. 1.9).

DOI: 10.3301/GFT.2015.03

Fig. 1.9 - Field aspect of the garnet-chloritoid schist. Garnet is the red mm-size mineral. Small dark flakes are chloritoid crystals.

A polyphase deformation is characterized by two penetrative foliations: S1 and S2. They are defined by the orientation of muscovite, paragonite, and chloritoid (Fig. 1.10a, b). Chlorite is an additional mineral oriented along S2. Late margarite grew at the expense of chloritoid + garnet (Fig. 1.11). Garnet porphyroblasts, enclosing quartz, chloritoid, rutile, Fe-oxide, apatite and paragonite, show a progressive decrease of spessartine component from 17 to 7 mol.% and an increase of pyrope component from 4 to 6 mol.% from core to rim. The grossular content first increases from the inner (Grs~21) to the outer core (Grs~27) and then decreases towards the outermost rim (Grs~15) (Fig. 1.12). Compositional mapping of white mica also revealed zoning and a wide range in Si content (from 3.0 to 3.3 a.p.f.u.). The highest Si content is related to the highest Fe and Mg content and the lowest Na content. P-T pseudosections were calculated in the system Na_2O-K_2O-CaO-FeO-MnO-MgO-Al_2O_3-TiO_2-SiO_2-H_2O for compositions of chloritoid schists. The highest Si contents of potassic white mica and the garnet core composition suggest pressures close to 1.7 GPa and temperatures of 470-500°C (Fig. 1.13) (Cruciani et al., 2013).

The garnet rim composition and low Si content in potassic white mica are compatible with re-equilibration at 540-570°C and 0.7-1.0 GPa. These results suggest an HP-metamorphic imprint during the D1 deformation phase which occurred before the Barrovian amphibolite-facies metamorphism of NE Sardinia.

DOI: 10.3301/GFT.2015.03

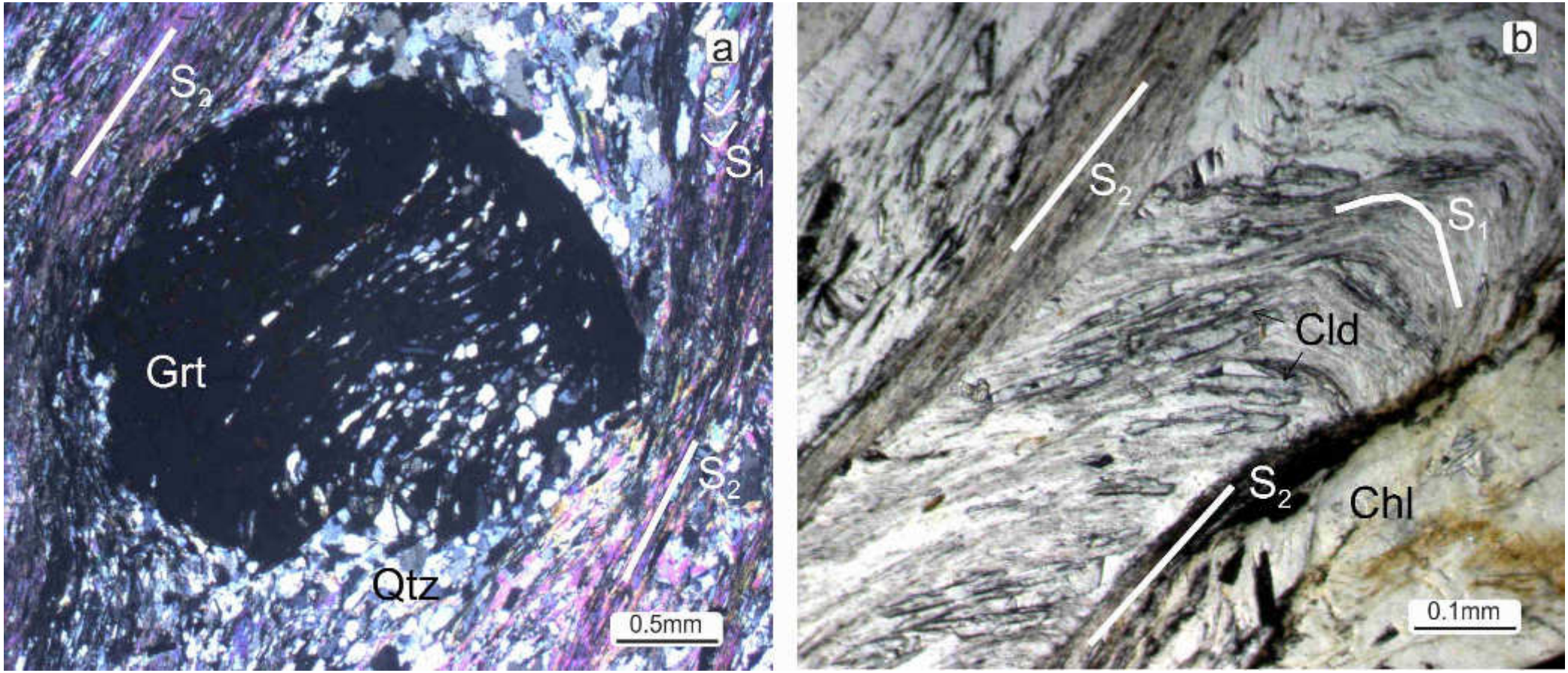

Fig. 1.10 - Microstructural features of the chloritoid schists. On the left **(a)** garnet porphyroblast rich in quartz inclusions enveloped by phyllosilicates oriented along S2 foliation (CPL). On the right **(b)** elongated chloritoid in microlithon-type structure, plane polarized light (PPL) (from Cruciani et al., 2013).

P-T conditions recorded in the metapelites are in keeping with the ones recorded in the eclogite boudins in the HGMC to the North. D2 folding and dextral orogen-parallel shearing in a transpressional tectonic setting occurred at decreasing P-T conditions during the exhumation of the metamorphic complex (Carosi & Palmeri, 2002; Iacopini et al., 2008). As a consequence, the classic Barrovian metamorphism of NE Sardinia was not recorded during increasing P and T conditions but developed later during the exhumation of the metamorphic complex after the HP stage (Carosi & Palmeri, 2002; Cruciani et al., 2013).

DOI: 10.3301/GFT.2015.03

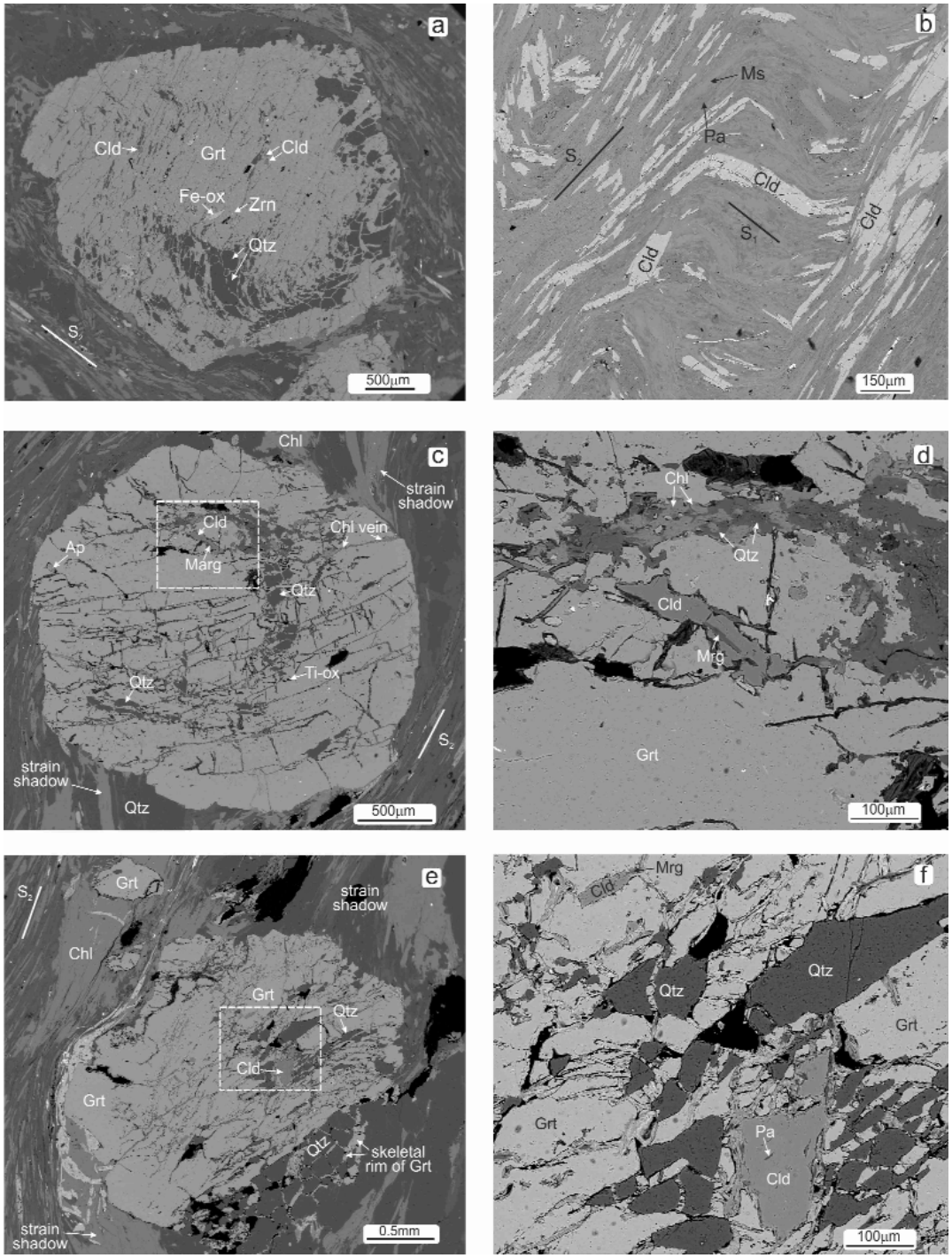

The recent discovery of HP in metapelites in the L-MGMC suggests the presence of reworked crustal slices, at a minimum, or even a true high-pressure nappe in the Sardinian Variscides. However, the areal extent of HP metamorphism during D1 in the L-MGMC needs further investigation.

Fig. 1.11 - SEM images showing microstructural features of the chloritoid schists: **a)** inclusions in garnet; **b)** relationships between minerals and foliations; **c)** garnet with inclusions and strain shadows; **d)** margarite growth on chloritoid included in garnet; **e)** garnet with strain shadows of chlorite and skeletal quartz at garnet boundary; **f)** quartz and chloritoid inclusions in garnet (from Cruciani et al., 2013).

DOI: 10.3301/GFT.2015.03

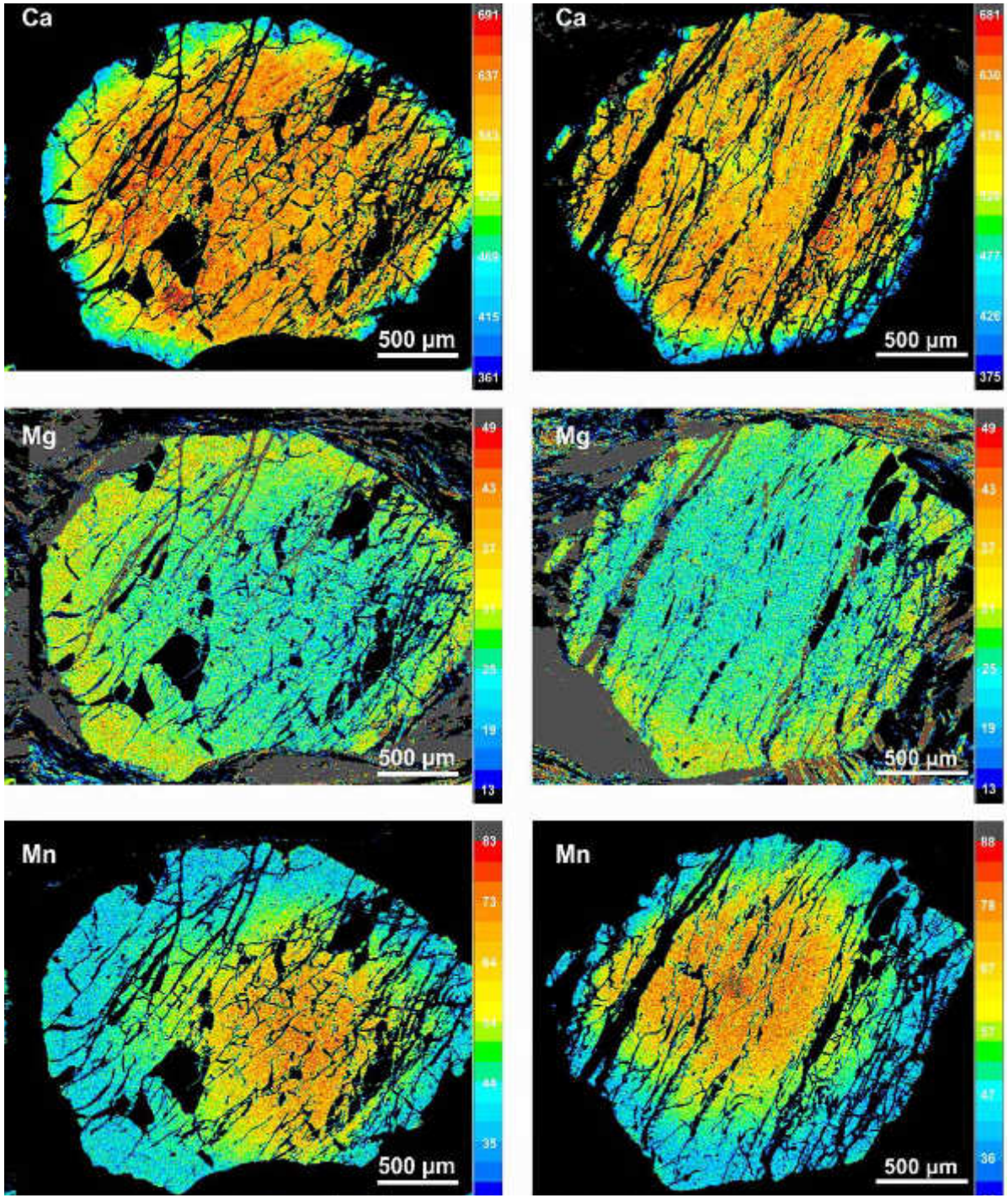

Fig. 1.12 - Ca, Mg and Mn concentration maps of two selected garnets. Color code on the right hand side of the images corresponds to counts per second (from Cruciani et al., 2013).

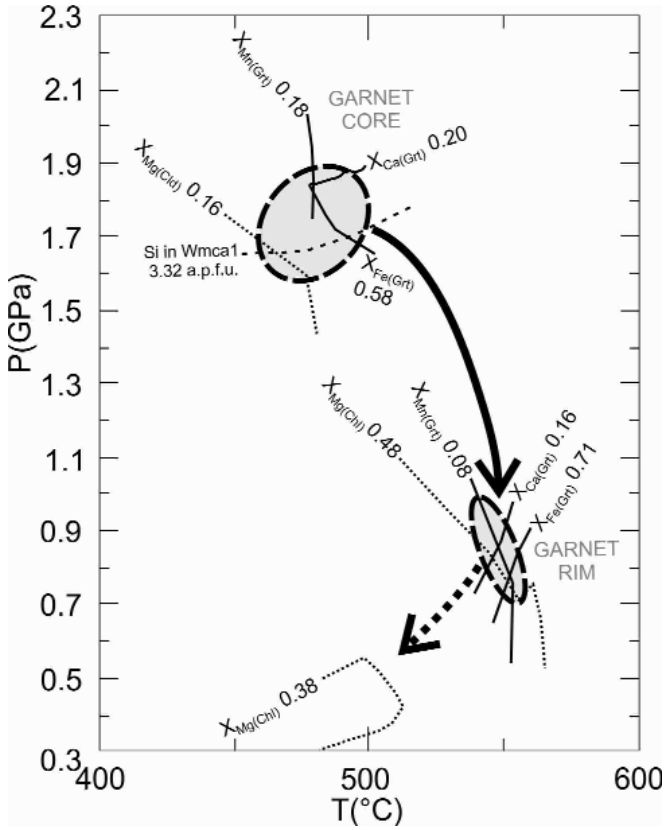

Fig. 1.13 - P-T path of the chloritoid schists reconstructed using the P-T pseudosection and compositional isopleths. Dotted ellipses represent P-T conditions inferred from the comparison of modeled isopleths with garnet core and rim composition (from Cruciani et al., 2013).

DOI: 10.3301/GFT.2015.03

STOP 1.5: Road from Siniscola to Cantoniera di S. Anna and Lodè - Contact between porphyroblastic paragneiss and granitic augen gneiss (N 40° 04' 20.0''; E 9° 38' 11.6'').

Fig. 1.14 - Albite-oligoclase rich layers and micaschist with shear band cleavage showing a top-to-the NW sense of shear.

Following the main road to the Cantoniera di S. Anna locality, continuing along the northeastern slope of Mt. Albo (made up of mesozoic limestones, dipping to the SE), we see metamorphic rocks of the garnet + albite + oligoclase zone: micaschist, porphyroblastic paragneiss (Figs. 1.14 and 1.15) and granitic augen gneiss (Fig. 1.16).

The contact between the basal levels of the porphyroblastic paragneisses and the granitic

Fig. 1.15 - Albite-oligoclase bearing paragneiss with ribbon quartz and shear band cleavage showing a top-to-the NW sense of shear.

DOI: 10.3301/GFT.2015.03

Fig. 1.16 - Sheared augen gneiss with kinematic indicators showing a dextral sense of shear (top-to-the NW). Strain increases from the bottom to the top as highlighted by decreasing grain-size of the feldspar porphyroclasts.

augen gneisses is visible on the road cut. It is the southern limb of the Mamone-Siniscola D2 antiform (Figs. 1.17 and 1.18), and shows a nearly E-W trending axis, plunging to the east (Carosi & Palmeri, 2002). Elongation lineation (L2) trends nearly N80E and plunges 10-20° to the SE (Fig. 1.17). Kinematic indicators both in schist and augen-gneiss (C-S fabric and sigma type porhyroclasts) indicate a top-to-the NW sense of shear (Figs. 1.14, 1.15, 1.16). During a short walk along the road we observe sheared augen gneiss with heterogeneous deformation and development of cm-thick ultramylonites and ribbon quartz. The porphyroblastic paragneisses are characterized by the occurrence of millimetric plagioclase porphyroblasts with albite cores and oligoclase rims (Franceschelli et al. 1982a,b) showing evidence of post-D1 and pre-D2 growth. The porphyroblasts include an internal foliation (S1) (Fig. 1.20) defined by inclusion trails of white mica, quartz, garnet and minor biotite (Figs. 1.20a, b). Syn-D1 white micas are invariably celadonite-rich and paragonite-poor, whereas D2 micas usually show low-celadonite and high-paragonite composition. The external foliation envelops porphyroblasts and forms an advanced S2 crenulation cleavage dominated by white mica and minor chlorite and biotite. Garnet, oligoclase and opaque minerals are also found along S2. Microlithon relics of the S1 foliation and F1 fold hinges are preserved within S2.

DOI: 10.3301/GFT.2015.03

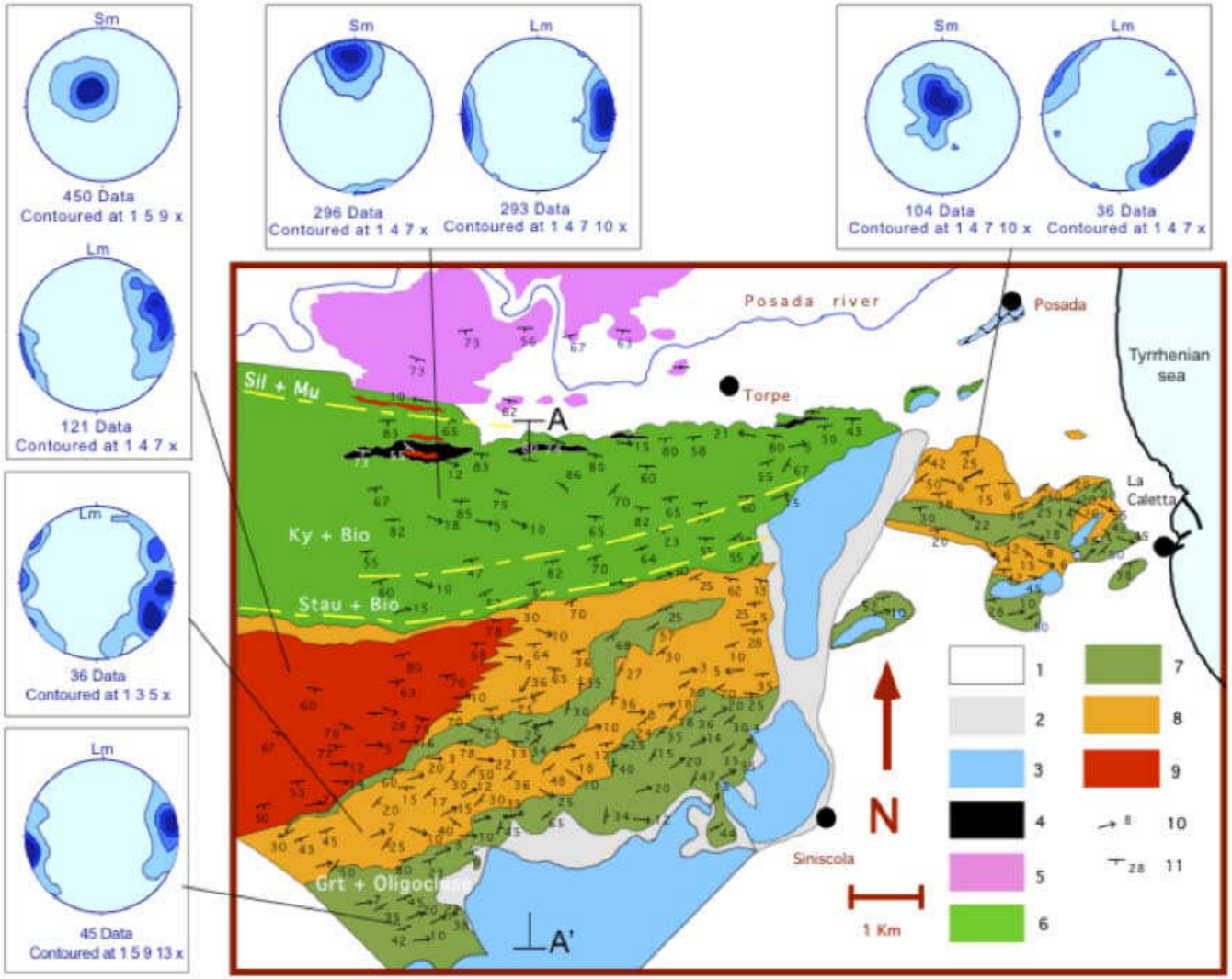

Fig. 1.17 - Geological and structural map of the Baronie area south of Posada Valley (modified after Carosi & Palmeri, 2002). **1**: Continental beach deposits (Pliocene-Quaternary); **2**: Slope debris (Quaternary); **3**: Carbonate platform sediments, continental and evaporites (Triassic - Jurassic - Cretaceous); **4**: Amphibolites with relics of granulite facies paragenesis; **5**: Migmatitic complex of Sil + Mu and Sil + K-feldspar zones (344+/-7 Ma); **6**: Micaschists and porphyroblastic paragneisses of St + Bt and Ky + Bt zones; **7**: Phyllites and metasandstones of Bt zone; micaschists and paragneisses of Grt + Ab and Grt + (Albite+Oligoclase) zones; **8**: Granitic augen gneisses (441+/-33Ma); **9**: Granodioritc orthogneisses (458+/-31 Ma); **10**: Trend and plunge of L2 stretching lineation; **11**: Strike and dip of mylonitic foliation (S2). A-A': trace of the geological cross-section of Fig. 1.18.

In situ Ar-Ar laser analyses of white micas yelded ages of ~ 340-315 Ma (Di Vincenzo et al., 2004) (Fig. 1.21). It is worth noting that the oldest ages (335-340 Ma) were detected in syn-D1 white mica not texturally and chemically re-equilibrated at upper crustal levels. Syn-D2 white mica ages cluster at 315-320 Ma.

The estimated temperatures for the garnet-albite-oligoclase zone range from 453°C to 521°C moving from the upper to the deeper part of this zone. The pressure obtained from Grt-Bt-Ms was around 0.7-0.8 GPa (Franceschelli et al., 1989). Carosi & Palmeri, (2002) and Di Vincenzo et al. (2004) reported temperatures of

DOI: 10.3301/GFT.2015.03

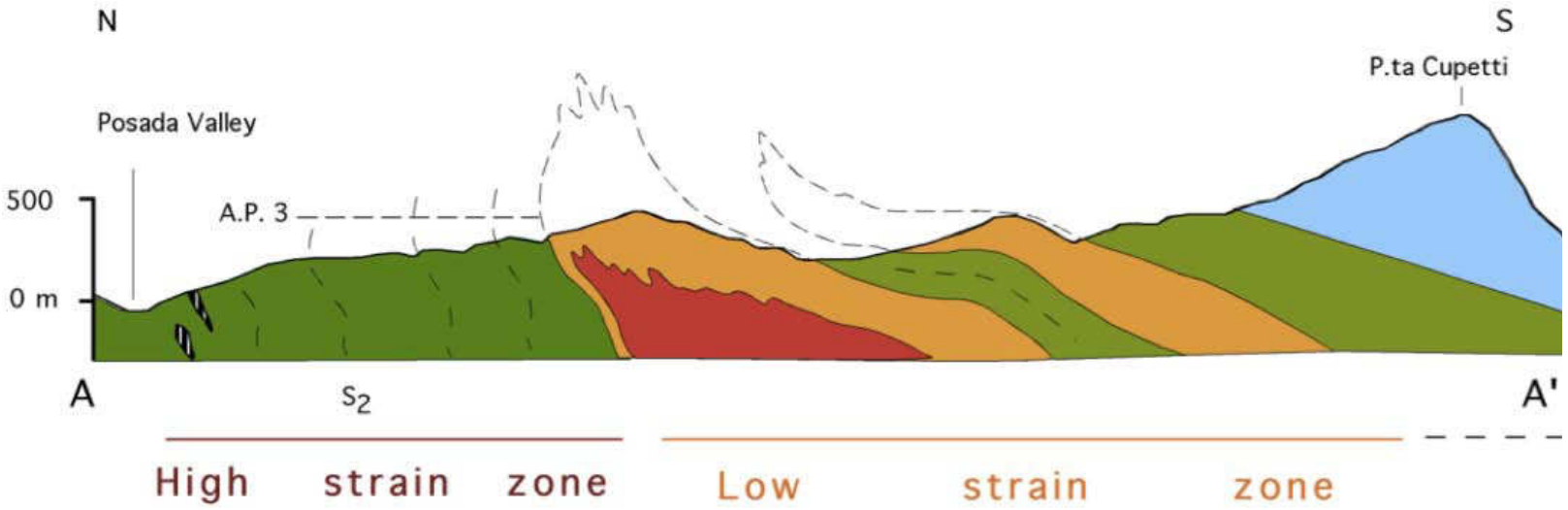

Fig. 1.18 - N-S geological cross section in the Posada Valley. See the geological map (Fig. 1.17) for explanations of the colours (modified after Carosi & Palmeri, 2002).

TECTONIC SETTING	DEFORMATION	Qz Pl Grt Stau Ky Bt Ms Chl Ilm	Grt + Bt zone		Stau + Bt zone		Ky + Bt zone	
			T °C	P Kbar	T °C	P Kbar	T °C	P Kbar
CRUSTAL THICKENING	D1 S1 foliation		500-570	10-11	< 590	> 8	< 675	> 9
DEXTRAL TRANS-PRESSION	D2 S2 foliation + D3 F3 later folds ?		570	6-7	590-620	9-5	675	11-6
EXTENSIONAL COLLAPSE	D4 S4 foliation							

Fig. 1.19 - Synoptic table of the deformation phases and related estimates of pressures and temperatures (Carosi & Palmeri, 2002).

DOI: 10.3301/GFT.2015.03

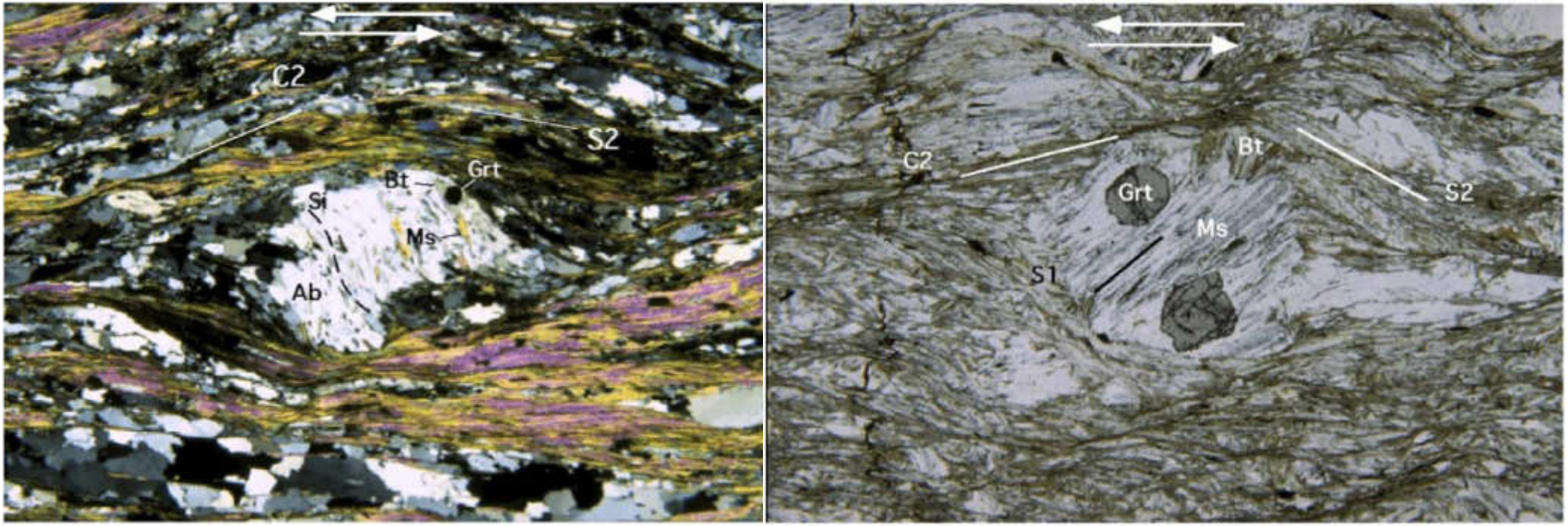

Fig. 1.20 - **a)** Albite porhyroblast with a sigmoidal inclusion pattern (Si) marked by quartz, garnet, biotite, muscovite and graphite (Stop 1.4). Si is nearly continuous with S2 foliation. S2-C2 fabric point to a top-to NW sense of shear (micaschist of the garnet + albite+oligoclase zone, CPL, 52x) (Carosi & Palmeri, 2002). **b)** Albite porhyroblast including a straight inclusion pattern (S1 foliation), marked by garnet, biotite, muscovite and graphite (Stop 1.4). S2-C2 fabric points to a top-to NW sense of shear (micaschist of the garnet + albite+oligoclase zone, PPL, 52 x).

500-550°C and pressures of 0.8-1.1 GPa during D1, and temperatures of 550-600°C and pressures of 0.7-0.9 GPa for the D2 phase (Fig. 6).

Walking few hundred meters toward Cantoniera di S. Anna we observe granitic augen gneiss below the micaschist in the core of a tight F2 north-verging antiform. Augen gneiss is deformed by the D2 shearing phase and shows rotated porhyroclasts and shear bands (Fig. 1.16). The granitic augen gneiss is mainly made up of layered bodies of augen gneiss alternating with thinner micaschist layers. The rocks were originally considered to be the product of Variscan metamorphism of rhyolite and arkosic sandstone (Ferrara et al., 1978) but in fact they represent an intrusive facies of Ordovician granitoids. The age has been constrained at 441±33 Ma (Rb-Sr whole rock; Ferrara et al., 1978; Helbing & Tiepolo, 2005). Augen gneiss crops out at the contact

DOI: 10.3301/GFT.2015.03

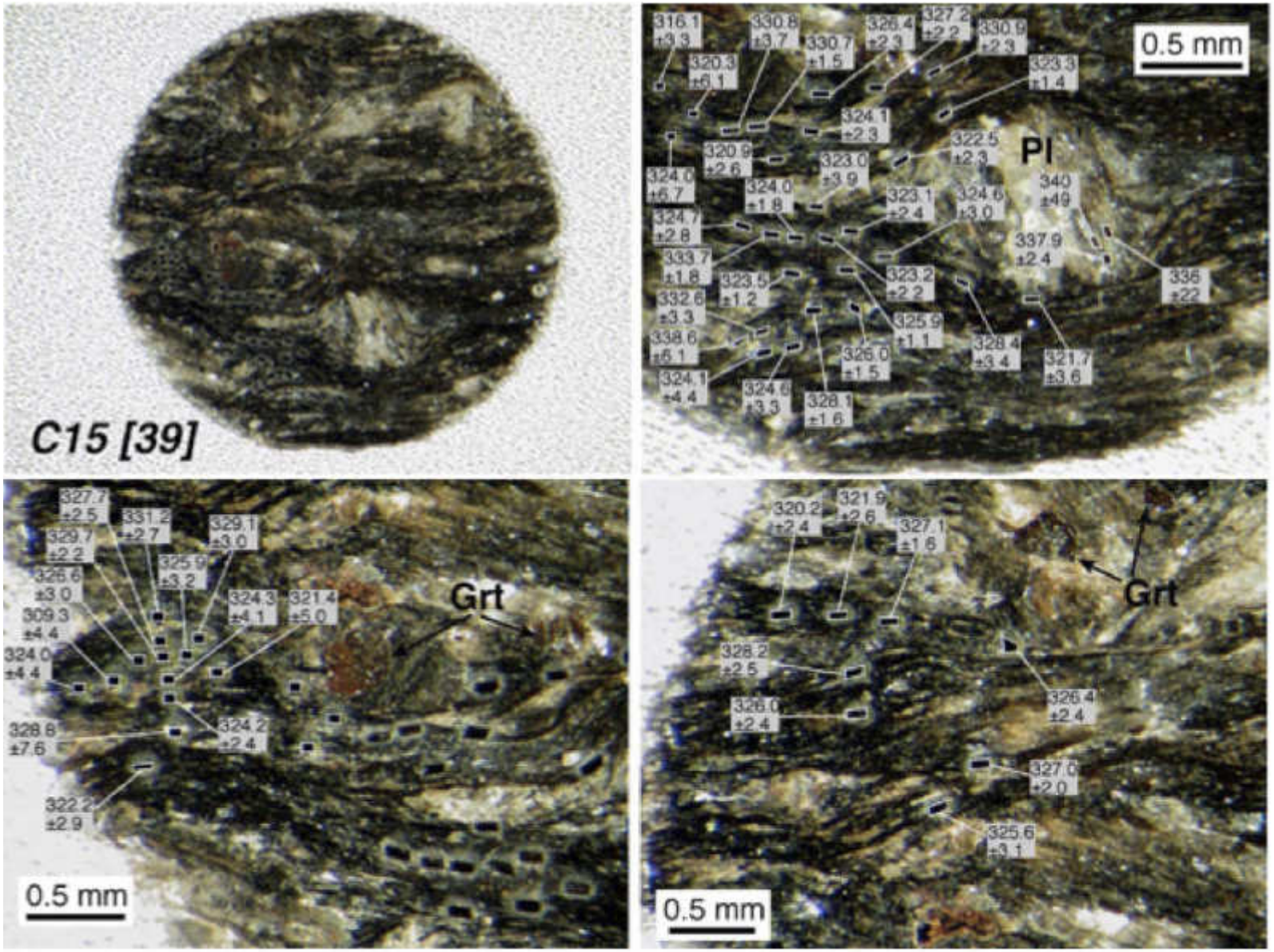

Fig. 1.21 - Example of in-situ $^{40}Ar/^{39}Ar$ laser probe analysis on white mica from sample C15 (albite micaschist). Error is 2σ. Oldest ages are obtained from phengitic micas inside albite porphyroclasts whereas the younger ages are from D2 S-C fabric (modified from Di Vincenzo et al., 2004).

between granitic orthogneiss and micaschist. According to Perugini (2003) the augen gneiss represents the result of fractional crystallization processes acting in the peripheral portions of the magma chamber whereas granodioritic orthogneiss is thought to be produced by mixing plus fractional crystallization processes in the core of the magma chamber.

DOI: 10.3301/GFT.2015.03

STOP 1.6: «Cantoniera» Mt. Tundu - Granodioritic orthogneiss with C-S fabric

(N 40° 35’ 40.4”; E 9° 35’ 34.0”).

Road from Siniscola to Lodè. A few kilometers after Cantoniera di S. Anna we stop on the right at Cantoniera Mt. Tundu. We park on the right side of the old building of «Cantoniera Mt. Tundu», then follow the main road to the NW, and in about 100 m we take a dirt road to the north. On the road we start to see flat outcrops with prominent C-S fabric (Fig. 1.22).

A few dozen meters north of the Cantoniera house we can observe granodioritic orthogneiss with a prominent C-S fabric and C’ structures pointing to a top-to-the NW sense of shear (“dextral”)(Figs. 1.22, 1.23, 1.24, 1.25). The main foliation (S2) is nearly vertical, striking nearly E-W, and preserves a large number of melanocratic inclusions which are flattened along the S2 foliation (Fig. 1.26).

Fig. 1.22 - C-S fabric in the granodioritic orthogneiss (top-to-the NW sense of shear).

Fig. 1.23 - Photomicrograph of biotite fish in mylonitic granodioritic orthogneiss (top-to-the SE sense of shear. PPL; field of view (fov) is nearly 3 mm).

DOI: 10.3301/GFT.2015.03

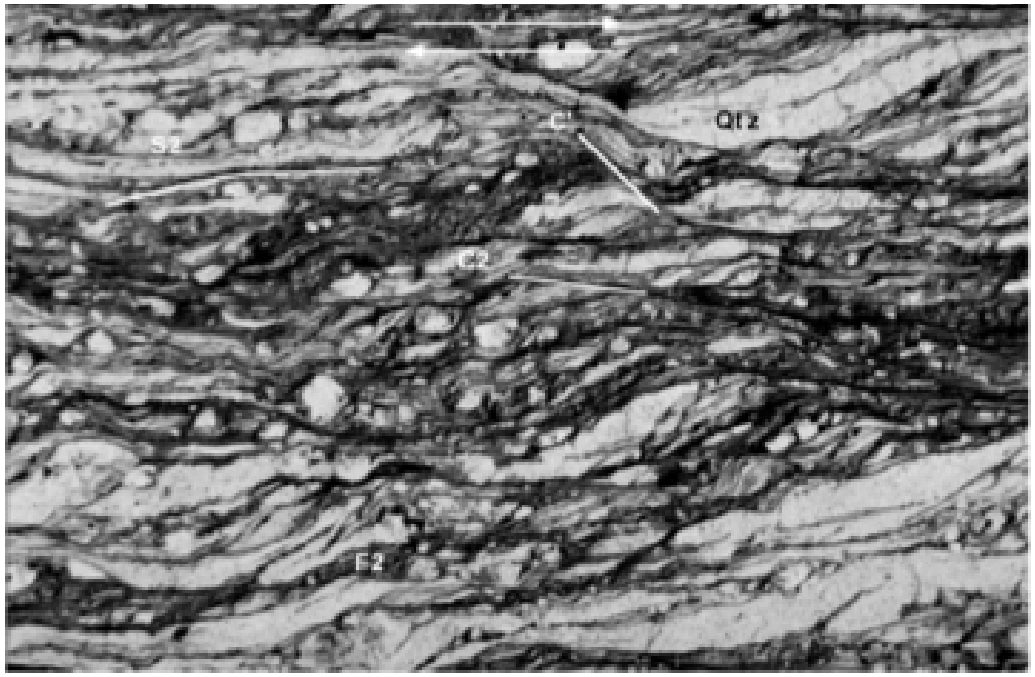

Fig. 1.24 - Shear band cleavage in mylonites from gneiss in the high-strain zone in the Posada Valley (top-to-the NW sense of shear, PPL; fov is ~ 8 mm).

Fig. 1.25 - C-S fabric in mylonite from gneiss (PPL; fov is 7 mm).

Thin layers of cataclasites occur in the mylonites. The orthogneiss originated as intrusive rocks of granodioritic composition with a radiometric ages of 458±31 Ma (Rb-Sr whole rock; Ferrara et al., 1978) and 456±33 Ma (U-Pb on zircons; Helbing & Tiepolo, 2005) that underwent a Variscan amphibolite facies metamorphism (age of isotopic closure of muscovite and biotite 289-319 Ma; Ferrara et al., 1978). This Ordovician magmatism is widespread from the HGMC to the north to the External Zone (Capo Spartivento) to the south (Carmignani et al., 1994). In the southernmost portion of the Island, close to Capo Spartivento, an Ordovician contact metamorphism, due to the intrusion of the Mt. Filau gneiss, is suggested by andalusite porphyroblasts deformed by the main Variscan deformation (Carosi et al., 1995; 1998). Contact metamorphism in the country rocks around the Lodè-Mamone orthogneiss is not evident due to the intense shearing and metamorphic overprint.

DOI: 10.3301/GFT.2015.03

STOP 1.7 (optional): Lodè village - Granodioritic orthogneiss and augen gneiss (N 40° 35′ 30.9″, E 9° 31′ 52.5″).

Drive to Lodè and at the end of the village (road to Mamone) we can observe a quite homogeneous granodioritic orthogneiss. It is sheared with a well-developed stepply dipping C-S fabric indicating a top-to-the NW sense of shear (dextral shearing).
Coming back to the beginning of the village (close to painted murales) an augen gneiss with feldspar augens and often without biotite crops out. It is sheared with asymmetric augens indicating a top-to-the NW sense of shear. In places cm-size kinks or chevron folds (D3 phase) affect the main foliation (Fig. 1.27).

Fig. 1.26 - Deformed mafic microgranular enclave in the sheared granodioritic orthogneiss.

Fig. 1.27 - Kinked augen gneiss (F3 fold). Kinks affect the S2 mylonitic foliation. Lodè.

DOI: 10.3301/GFT.2015.03

Lodè: *Altitude: 345m a.s.l.; Surface Area: 120,87 km²; Population: 1898.*

Panoramic views of Lodè

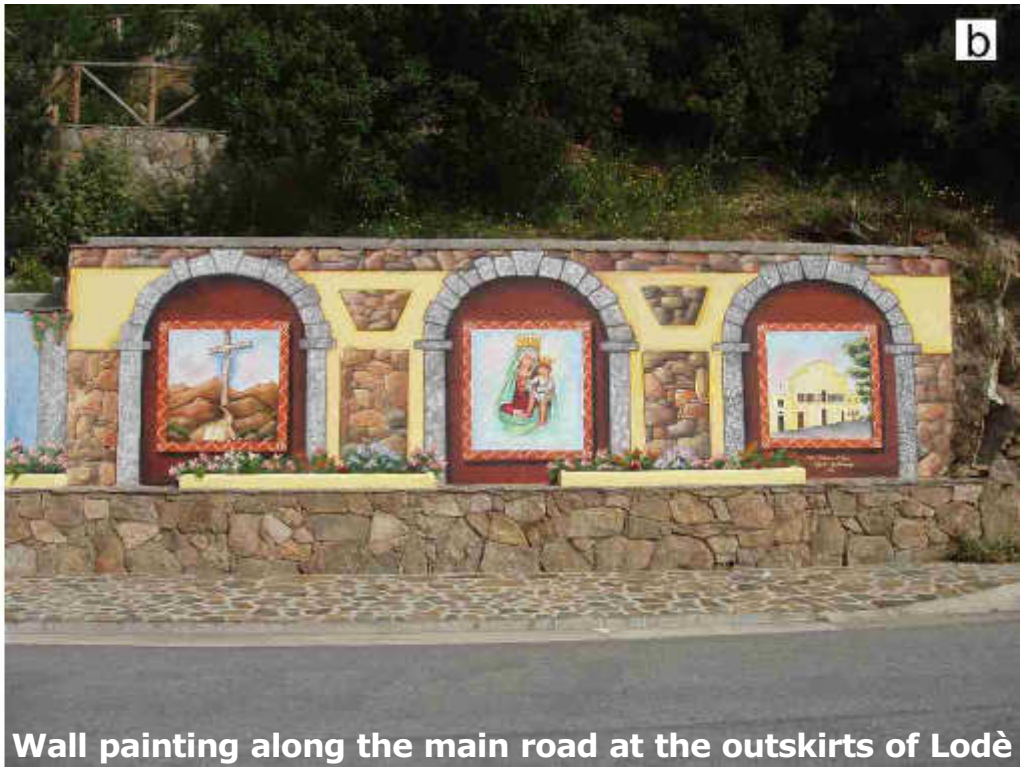

Wall painting along the main road at the outskirts of Lodè

The village of Lodè is located at the foot of Mt. Calvario and its largely hilly territory is part of the Baronie region, half way between the sea and mountains. In the Middle Ages, Lodè was at the western border of the Giudicato di Gallura and was obliged to defend itself with a contingent of a hundred soldiers. In the village, which developed on the ridge of a hill called Su Inucragliu, some buildings of the old town are still well preserved. The Sant'Anna wood, the whitish carbonatic rocks of Monte Albo and the Usinavà Forest (also known as "Sa Ghiniperaglia") are also worth seeing.

DOI: 10.3301/GFT.2015.03

STOP 1.8: Road from Siniscola to Lodè and deviation to Torpè - Sheared granitic augen gneiss (N 40° 35′ 57.50″; E 9° 33′ 40.00″).

From Stop 1.6 we return to the cars and continue, following the main road to Lodè. Stop after the hairpin bends of the road and park at the crossroads to Torpè. Walk few meters toward Lodè and see granitic augen gneiss, highly deformed by the D2 shearing phase showing cm-size shear bands and rotated porphyroclasts (Fig. 1.28). According to Perugini (2003) the augen-gneisses are interpreted as being formed by fractional crystallization processes acting in the peripheral regions of the magma chamber. Granodioritic orthogneiss is thought to be produced by mixing and fractional crystallization processes in the core region of the magma chamber from magma batches that evolved into different degrees of hybridization, bearing mafic microgranular enclaves (observed in Stop 1.6).

Fig. 1.28 - C-S fabric and sigma-type porphyroclast showing a top-to-the NW sense of shear in the augen gneiss.

Descending to Torpè and Posada, we cross the mylonitic foliation with a sub-horizontal prominent mineral lineation. On the road cut, open folds are visible, with sub-horizontal axial planes that are probably related to a later phase of extensional deformation at upper crustal levels.

At the bottom of the Rio Posada Valley (Figs. 1.17 and 1.18) the classic sillimanite-muscovite isograd appears, roughly coinciding south of the first appearance of migmatitic rocks. Franceschelli et al. (1989) estimated a temperature of 605 °C and pressure of 0.4 GPa for this zone.

Crossing into the migmatites we enter the sillimanite+K-feldspar zone. The oldest structure observed in the migmatites is a gneissic layering, pre-dating the most pervasive (S2) foliation. Mesosomes are medium-grained, with a fabric defined by the alignment of biotite parallel to the S2 schistosity. Mesosomes consist of quartz,

DOI: 10.3301/GFT.2015.03

plagioclase, biotite, garnet, fibrolite, minor kyanite, muscovite and K-feldspar. Kyanite occurs sporadically as relic minerals. Retrograde white mica occurs in both the mesosome and the leucosome on sillimanite and K-feldspar. Leucosomes are coarse-grained, poorly-foliated rocks, tonalitic to granitic and rarely trondhjemitic in composition.
Temperatures up to 750 °C under which anatexis processes developed, and pressures of 0.6-0.8 GPa have been reported for the migmatite (Palmeri, 1992; Cruciani et al., 2001). According to Giacomini et al. (2005), migmatization started in the kyanite stability field at about 750-800°C and pressures above 1.0 GPa.
Ar/Ar ages on muscovites from both migmatitic orthogneiss and metasedimentary stromatic migmatite from Punta de li Tulchi yielded comparable results of ~300 Ma to ~320 Ma (Di Vincenzo et al., 2004).

Torpè: *Altitude: 24m a.s.l.; Surface Area: 92,30 km²; Population: 2912.*

Panoramic view of Torpè

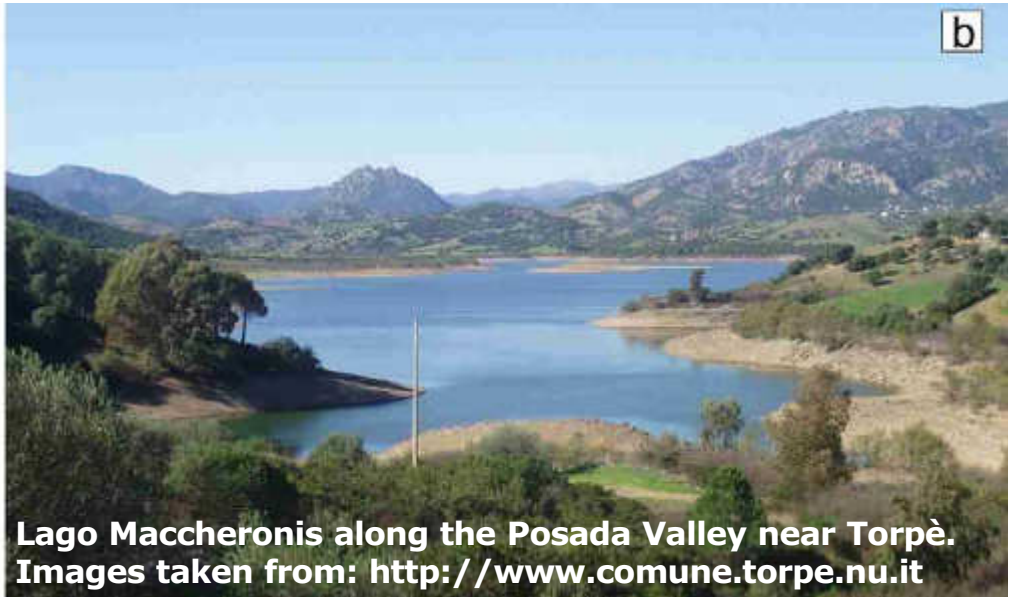

Lago Maccheronis along the Posada Valley near Torpè.
Images taken from: http://www.comune.torpe.nu.it

The territory of Torpè village is mostly mountainous and had been largely sold to the "Ente Foreste Demaniali" that takes care of the woods. One of the most beautiful places that one can visit here is the Mt. Nurres, from where you can admire a breathtaking view, the Posada sea in the horizon and his wonderful landscape characterized by the fortress called "Castello della Fava". Can also be admired the famous pine forest of "Sa Dea",

DOI: 10.3301/GFT.2015.03

near the artificial lake Maccheronis. This lake is a valuable reserve of water supplies for the towns of Posada, Budoni and San Teodoro. There are also other important steps for the visitor of Torpè, like the beautiful parish church dedicated to "La Madonna degli Angeli", the typical old narrow streets of the old town and some archaeological finds, such as the Nuraghe "San Pietro" and the ''Domus De Janas'' in the locality "Predas ruias''.

Posada: *Altitude: 37m a.s.l.; Surface Area: 33,52 km²; Population: 3015.*

Castello della Fava at the top of the hill above Posada

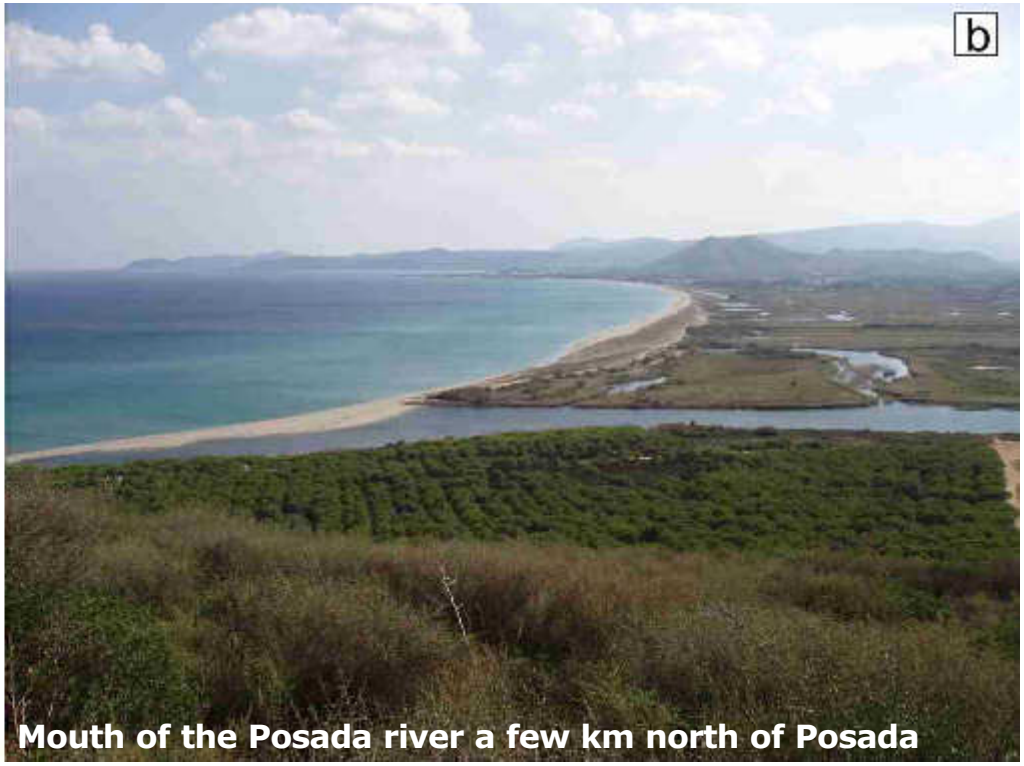

Mouth of the Posada river a few km north of Posada

Posada, the most important village of the Baronie region, is built on the foot of a limestone hill on the top of which stands the tower called 'Casteddu de sa Fae' or "Castello della Fava". From the tower there is an amazing view of the Posada Valley and of the eponymous river. At the foot of the castle, the old town consists of well-preserved ancient buildings. To the east are the green pinewood of 'Orvile', the white sandy beaches, the ancient San Giovanni tower built to protect the village from the Saracens, and the small harbour. Towards west the limestone hill on which Posada is built continues towards the Monte Albo dolostones and dolomitic limestones of Jurassic age.

DOI: 10.3301/GFT.2015.03

Budoni: *Altitude: 16m a.s.l.; Surface Area: 55,90 km²; Population: 4812.*

The village of Budoni, located on the northeastern coast of Sardinia, lies close to small coves and long beaches with crystal-clear sea, and is developing into an important tourist destination. At the village center is the San Giovanni Battista Church, built in 1969. There are also some interesting archaeological remains such as the nuraghe "Su Entosu". A few km to the north, the Ottiolu touristic port, with more than 400 berths, very well organized.

DOI: 10.3301/GFT.2015.03

Second day

Posada, Bruncu Nieddu, Punta Ainu, Porto Ottiolu, Punta de li Tulchi

From Posada we return to the mylonites of the Posada Valley shear zone to see how deformation and metamorphism increases towards the Posada Valley, crossing from the st+bt zone to the ky+bt zone.

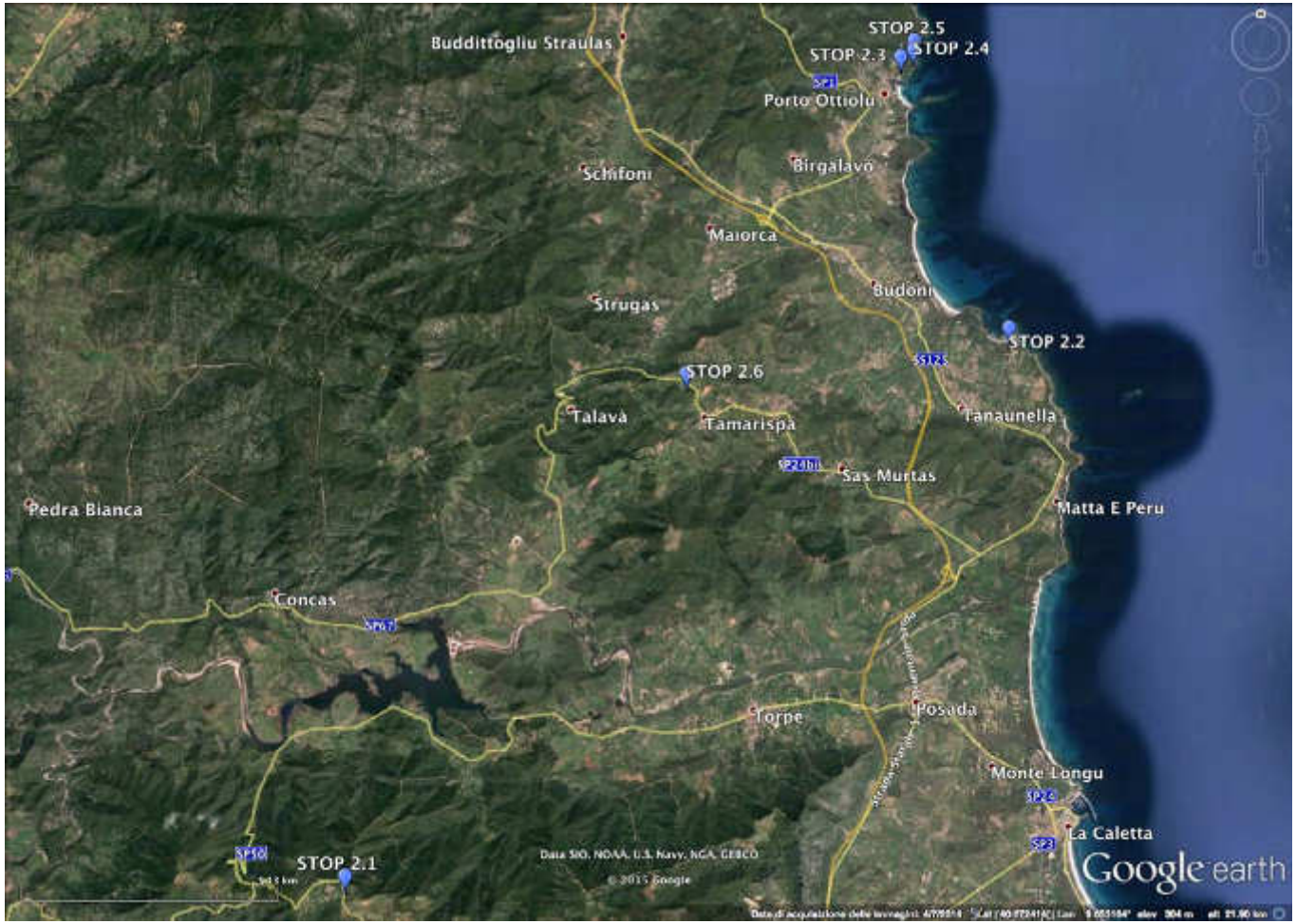

STOP 2.1 – Road from Torpè village to Lodè - S. Anna villages; Mt. Bruncu Nieddu - Staurolite and garnet bearing micaschist; kyanite bearing micaschist; mylonite of the Posada Valley shear zone (N 40° 36’ 0.6”, E 9° 34’ 56.6”).

Stop a few hundred meters to the north of the contact between the orthogneiss and micaschist. Walk for few hundred meters, crossing the staurolite + biotite zone and the kyanite + biotite zone up to a small tower with a panoramic view of the Posada valley and Carboniferous granite to the north. The micaschists are affected by a mylonitic deformation with a prominent C-S and C’ fabric showing a top-to-the NW sense of shear (dextral shear being the C-S fabric nearly vertical) (Fig. 2.2).

DOI: 10.3301/GFT.2015.03

Fig. 2.2 - S-C-C' fabric in staurolite and garnet bearing micaschists. Top-to-the NW sense of shear.

Near the gate at the entrance of a small forest track, we see cm-size staurolite and garnet porphyroclasts on the S2 foliation of the micaschist (Fig. 2.3). The porphyroclasts of garnet, staurolite and plagioclase grew between the D1 and D2 deformation events (Fig. 2.4), and are therefore flattened, rotated, and sometimes reduced in grain size during the D2 event (Figs. 2.3, 2.4, 2.5, 2.6, 2.7 and 2.8). This is classically regarded as the first appearence of

Fig. 2.3 - Cm-size staurolite porphyroclasts (brown-reddish crystals) developed on the S2 foliation in schists at the beginning of the road to Bruncu Niedddu St+Bt zone.

Fig. 2.4 - Thin section from micaschist of the St+Bt zone (staurolite is the brown-yellowish mineral) with shear bands developed during D2 shearing (top-to-the NW sense of shear, PPL; fov 30 mm).

DOI: 10.3301/GFT.2015.03

Fig. 2.5 - Mm to cm-size kyanite crystals aligned along the mylonitic foliation in the micaschist at Bruncu Nieddu from the Ky + Bt zone.

staurolite in northeastern Sardinia (Franceschelli et al., 1982a, 1986, 1989; Carmignani et al., 1982, 1994; Ricci et al., 2004 with references).
The D1 fabric is transposed by D2 and only the S2 foliation that strikes W-E and WNW-ESE and dips moderately to strongly toward the S and the SW can be identified. It bears an oblique sub-horizontal stretching lineation (L2) marked by the alignment of chlorite, muscovite, quartz, and biotite and by the stretched and fractured porphyroclasts of K-feldspar, kyanite, staurolite (Figs. 2.6 and 2.7), and garnet.
The rocks of the staurolite+biotite zone consist of staurolite, garnet and plagioclase porphyroblasts (up to ~ 1 cm in size) often in a mylonitic matrix made up of phyllosilicates and quartz. Garnet is anhedral and rounded with quartz, biotite, and chlorite inclusions. Garnet shows a bell-shaped zoning from core to rim for Mn (Carosi & Palmeri, 2002). Towards the rim Mg and Fe gradually increase and Ca decreases. Staurolite occurs as elongated prisms with several phyllosilicates, quartz, and graphite inclusions. Staurolite is chemically homogeneous and Fe-rich. Mg-content is up to 0.30 a.p.f.u. and X_{Mg} ratio ~ 0.17. X_{Mg} of biotite is 0.35. Muscovite is celadonite-poor (Mg+Fe up to 0.42 a.p.f.u.).
Temperatures and pressures in the range of 570-625 °C and 0.7-1.0 GPa have been reported by Franceschelli et al. (1989) and Di Vincenzo et al. (2004) for the thermal peak (Fig. 6). In situ argon ages on muscovite along the S2 foliation are mainly within 310-320 Ma (Di Vincenzo et al., 2004).
About 0.5 km further north along the track we reach the kyanite+biotite isograd with mm- to cm-size bluish kyanite crystals in the matrix of the mylonites and in quartz-rich veins (Fig. 2.5).
The kyanite+biotite isograd is marked by the first appearance of kyanite crystals. The rocks consist of porphyroblasts of staurolite, kyanite, and plagioclase enveloped in a mylonitic matrix of muscovite, biotite, chlorite, and ilmenite. Garnet often occurs as euhedral clear or cloudy inclusions in staurolite, plagioclase, and occasionally in kyanite porphyroblasts. The clear garnet contains calc-silicate micro-inclusions of idiomorphic

DOI: 10.3301/GFT.2015.03

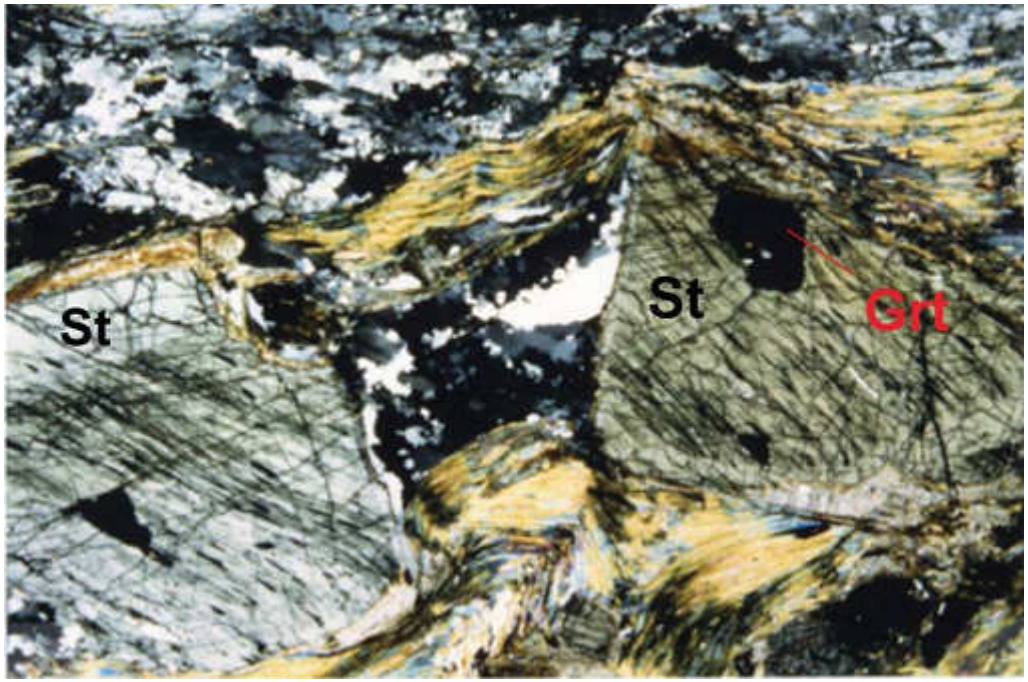

Fig. 2.6 - Photomicrograph showing stretched staurolite porphyroblasts during D2 shearing. The gap between boudins is filled by white mica and recrystallized quartz. (CPL; fov is ~ 2 mm).

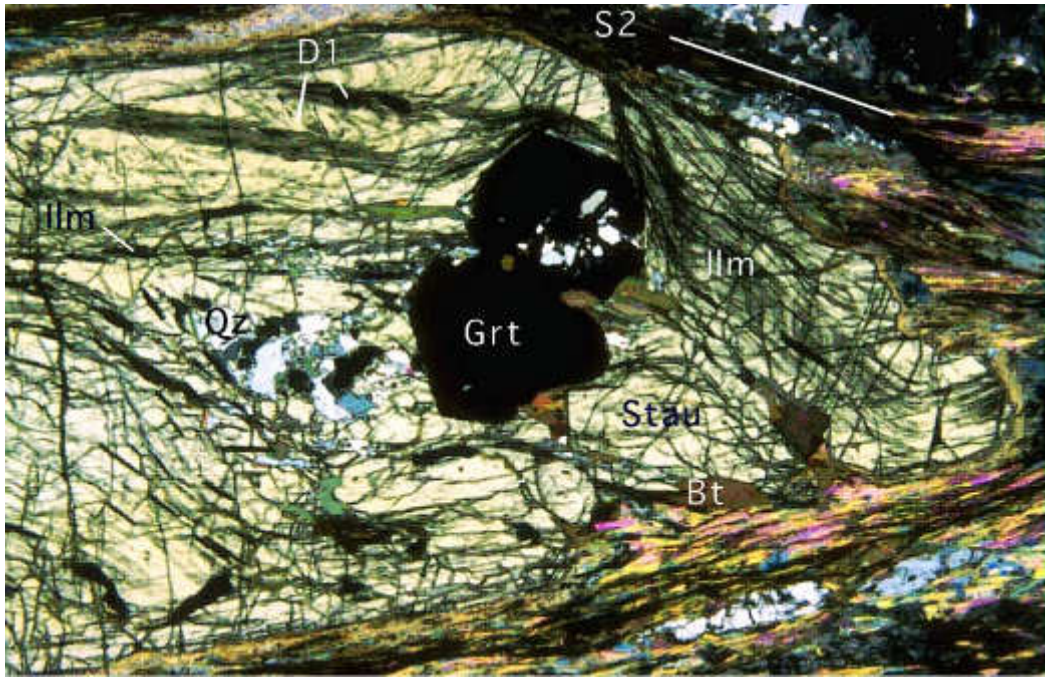

Fig. 2.7 - Photomicrograph showing a stretched staurolite (Stau) porphyroblast that grew post-D1 and pre-D2, including D1 related minerals (Grt, Ilm, Bt, Qtz) (CPL; fov is ~ 1.8 mm).

anorthite, epidote, and margarite (Connoly et al., 1994). Garnet from the matrix or the cloudy inclusions have a similar composition, with a slight increase in spessartine content from core to rim, and a concomitant decrease in the other garnet components. Plagioclase included in garnet is extremely calcic (An= 99-67) while the plagioclase enclosed in cloudy garnet has a compositional range of An=22-59. X_{Mg} of biotite ranges from 0.8 to 1.2 and TiO_2 is up to 2.3% wt. %. Muscovite is Na- and celadonite poor (Ricci et al., 2004).
Temperatures up to 595 °C and pressures up to 0.67 GPa have been reported by Franceschelli et al. (1989), and pressures over 0.9 GPa by Carosi & Palmeri (2002) for the metamorphic peak (Fig. 6).
The micaschists are intruded by an undeformed Permo-Triassic dyke of camptonite (K-Ar age: 228±3 Ma; Baldelli et al., 1987). It has mineralogical and textural features of a lamprophyre, and is porphyritic with biotite and amphibole euhedral phenocrystals.

DOI: 10.3301/GFT.2015.03

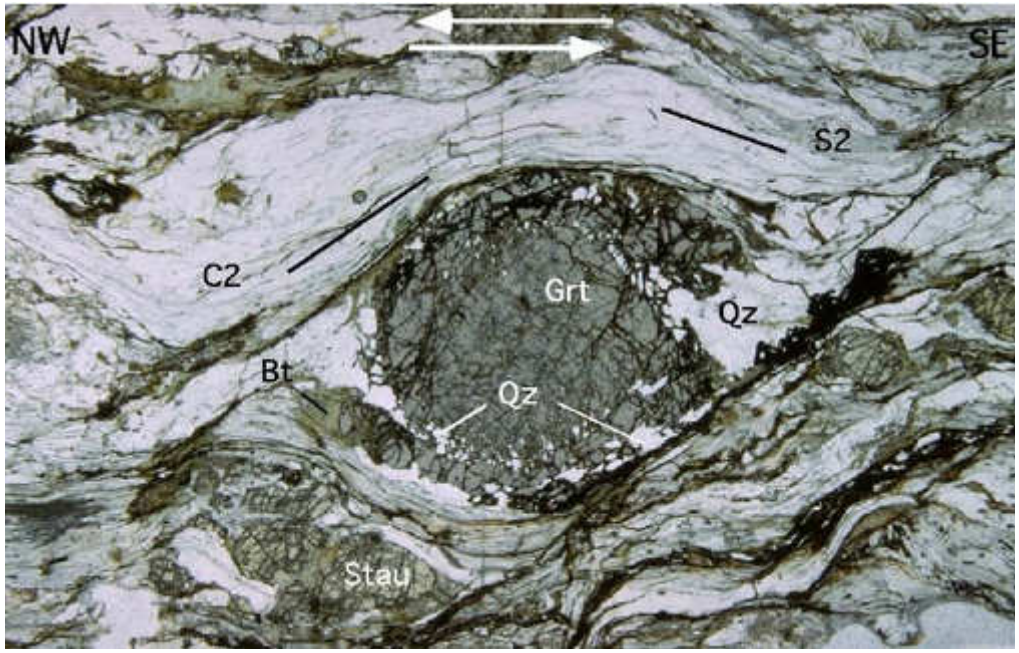

Fig. 2.8 - Syn-D2 rotated garnet and relic staurolite (Stau): top-to-the NW sense of shear (micaschist from the St+Bt zone, PPL; fov is 4.5 mm) (from Carosi & Palmeri, 2002).

Walk few hundred meters further to reach a small tower with a panoramic view of the Posada Valley (Fig. 2.9). Recent detailed mapping led to the discovery of outcrops characterized by cm-size porphyroblasts of staurolite+biotite in the core of the F2 Mamone synform, nearly a dozen km to the south of the accepted staurolite+biotite isograd running on the southern flank of the Posada Valley (Carosi et al., 2008).

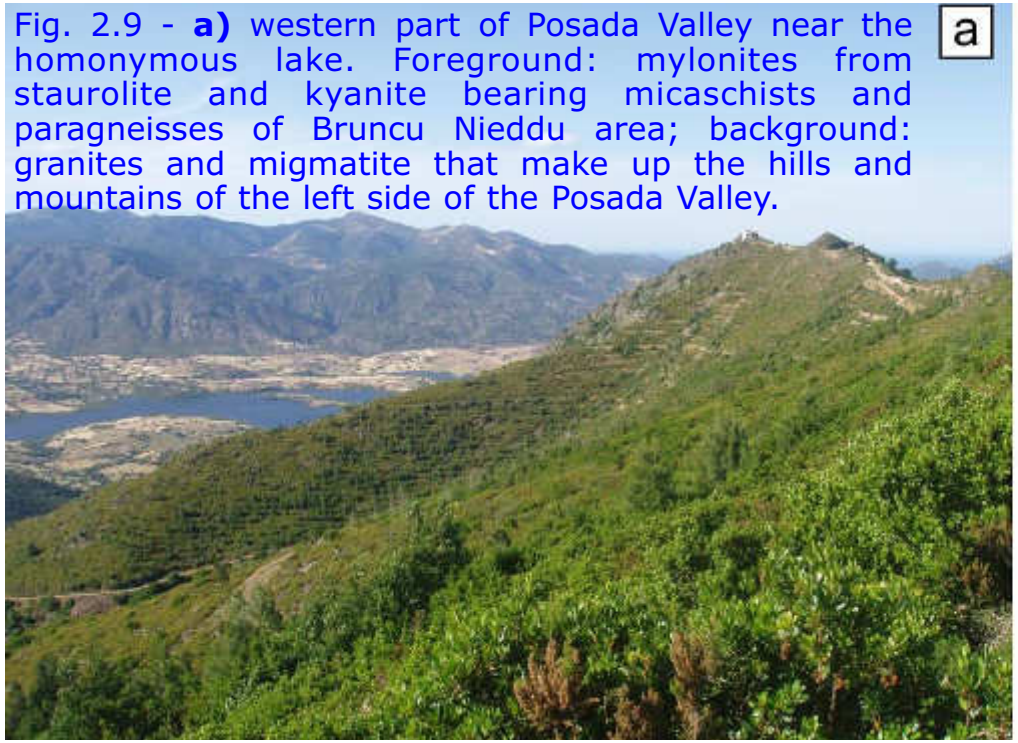

Fig. 2.9 - **a)** western part of Posada Valley near the homonymous lake. Foreground: mylonites from staurolite and kyanite bearing micaschists and paragneisses of Bruncu Nieddu area; background: granites and migmatite that make up the hills and mountains of the left side of the Posada Valley.

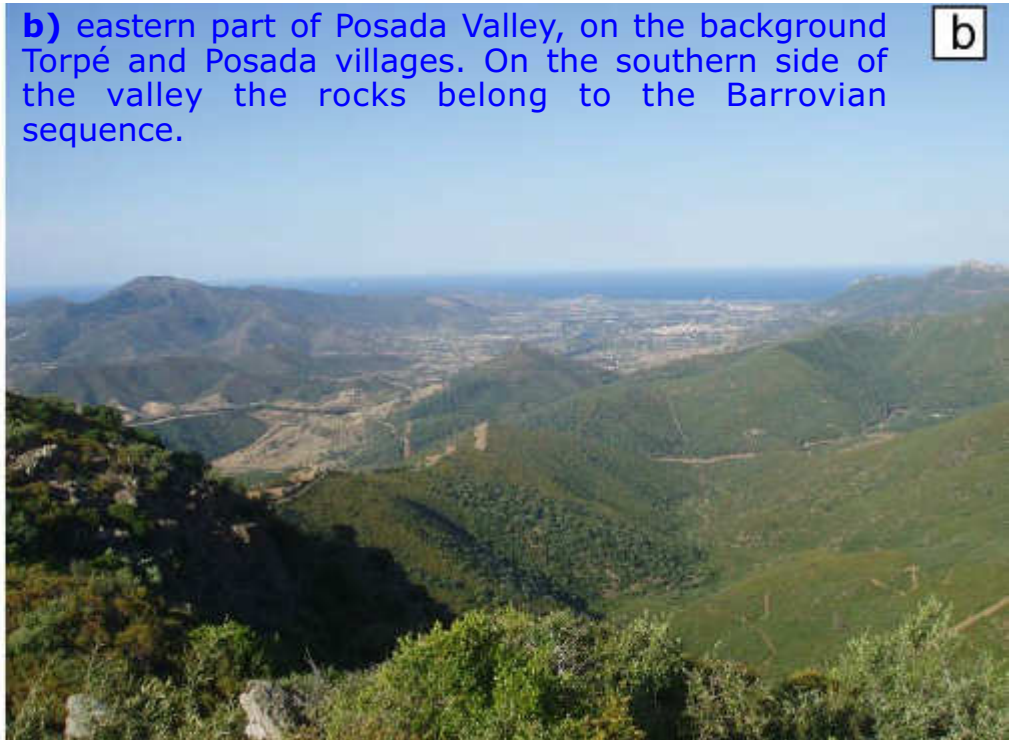

b) eastern part of Posada Valley, on the background Torpé and Posada villages. On the southern side of the valley the rocks belong to the Barrovian sequence.

DOI: 10.3301/GFT.2015.03

F2 folds are recumbent and northeast verging becoming tighter and isoclinal towards the high-strain zone in the Posada Valley. The F2 synform with a core of paragneiss and micaschist surrounded by orthogneiss is bordered to the north by the F2 Lodè antiform and by tighter synforms and antiforms that become rootless in the high-strain zone. At the microscale, staurolite and biotite porhyroblasts are deformed and wrapped around by the S2 foliation. They are well-preserved inside the D2 microlithons. The 1:10.000 scale mapping of the F2 folds enables the staurolite+biotite isograd in the Mamone synform to be linked with the previously known isograd in the Posada valley. Restoring the F2 folds we obtain a geometry in which the HGMC is above the L-MGMC with an inverted geometry of Barrovian isograds, showing a metamorphic grade increasing from bottom to top. According to Carosi & Palmeri (2002), this geometry is the result of the overthrusting of the HGMC onto the L-MGMC which caused the inversion of the isograds by ductile shearing and top-to-the south tectonic transport and the start of the decompression of the HGMC.
The D2 transpression affected the Barrovian index minerals from biotite, garnet up to kyanite, telescoping and the bending the Barrovian isograds. This explains the previously unrecognized large outcrops of staurolite-bearing micaschist nearly 10 km south of the staurolite isograd of the classical metamorphic framework of Northern Sardinia (Carosi et al., 2008). Moreover, the overall Barrovian prograde sequence in the field from kyanite to sillimanite is apparent, since kyanite was pre-S2 and sillimanite from syn- to post S2. Whereas kyanite porphyroblasts grew during increasing pressure and temperature conditions, sillimanite crystallized during the decompression from medium-pressure conditions. Existing petrological data and P-T-t paths support this picture. In particular, the D2 transpressional deformation associated with the exhumation of rocks at high depths strongly affects the occurrence and distribution of metamorphic rocks in the inner part of the belt during post-collisional tectonics.

STOP 2.2: Punta Batteria – Punta dell'Asino. Migmatite and associated rocks of sillimanite+K-feldspar zone; paragneiss with fibrolite nodules at Punta Ainu (N 40° 41' 34.7", E 9° 44' 12.5").

A typical sequence of the migmatite complex exposed at Punta Ainu consists of (Franceschelli et al., 1991):

- stromatic migmatite with minor calc-silicate nodules;
- biotite-sillimanite mesocratic gneiss locally very rich with fibrolite nodules;
- granodioritic to granitic orthogneiss.

The fibrolite nodules occur within the paragneiss in the northern and southern side of Punta Ainu.
In the field, the gneiss consists of an irregular alternation of Al-silicate rich foliated layers and Al-silicate-poor massive

DOI: 10.3301/GFT.2015.03

to poorly foliated layers (Fig. 2.10a). In the former the abundant Al-silicates (fibrolite sillimanite) are concentrated into white fibrolite-rich nodules. The nodules vary from 0.2 to 4 cm in length and from 0.1 to 1 cm in width.
The main foliation is the regional S2 foliation striking ~ N030E and dipping towards the SE. Macroscopic evidence of pre-S2 foliation is scarce whereas later folds with variable geometries are common. Two fold systems are seen: F2 folds and F3 folds, frequently highlighted by quartz veins (Fig. 2.10b, c).

Fig. 2.10 - **a)** Alternation of nodule-rich and nodule-poor layers in paragneiss; **b)** D2 fold in migmatite adjacent to fibrolite–rich nodules; **c)** S2 refolded by D3 deformation in the paragneiss with fibrolite-rich nodules; **d)** fibrolite-rich nodules and quartz rods defining a down dip lineation on S2 schistosity.

Biotite-sillimanite mesocratic gneiss at Punta Ainu shows oriented quartz + fibrolite rods on the foliation plane (Fig. 2.10d). The nodules are wrapped by the S2 schistosity and are sometimes surrounded by a thin biotite selvage. At the micro-scale, the nodules consist of variable amounts of fibrolite (30-70 %), quartz (20-50%), biotite (10-20%), and subordinate plagioclase, garnet, sillimanite, kyanite, apatite, tourmaline, and Fe-oxide (Fig. 2.11a). All these mineral phases, except fibrolite, also appear in the host mesocratic gneiss. Some nodules have a mineralogical zonation in which a nodule's fibrolite core has a rim of fibrolite + biotite + quartz. In some nodules, fibrolite is replaced by fine-grained potassic white mica.
The foliated layers of mesocratic gneiss consist of high amounts of biotite (50 to 70 mode %) as well as plagioclase, quartz, garnet, and accessory apatite, zircon, and tourmaline. Sometimes kyanite relics are preserved inside plagioclase crystals, whereas sillimanite (fibrolite) is associated with biotite (Fig. 2.11b).

DOI: 10.3301/GFT.2015.03

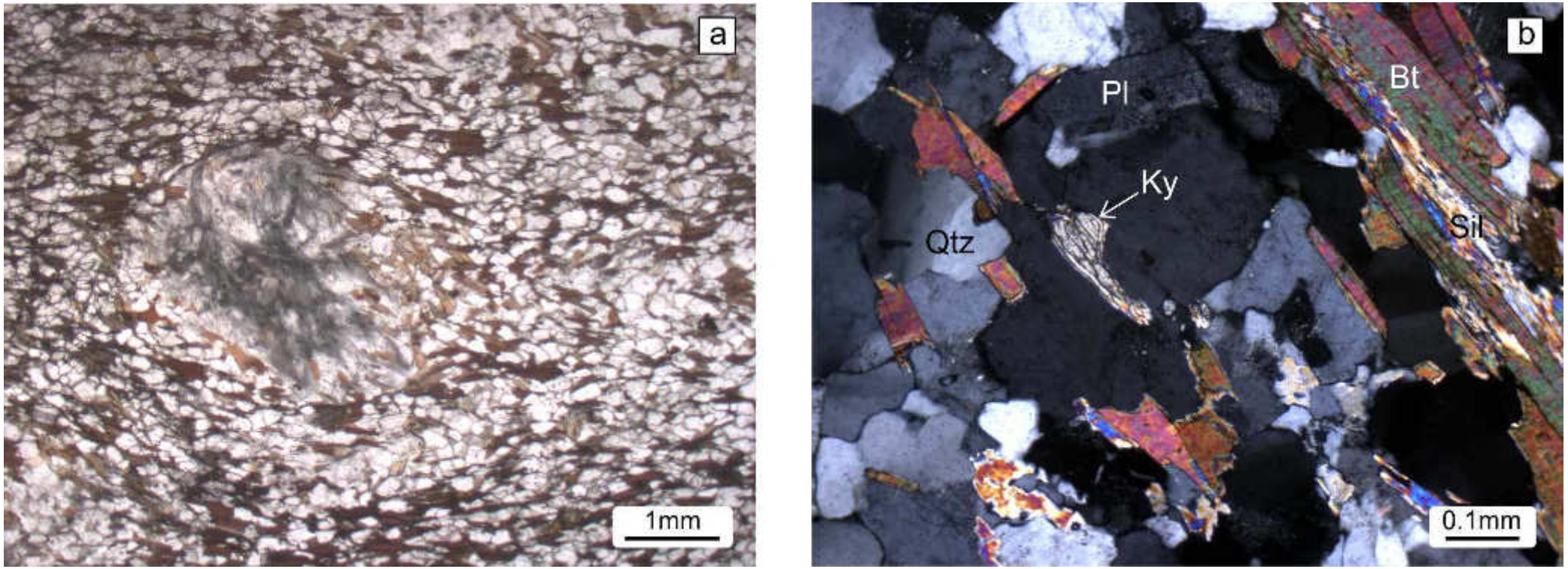

Fig. 2.11 - **a)** Photomicrograph of a fibrolite-rich nodule (PPL); **b)** kyanite relic and fibrolitic sillimanite within the quartz-feldspathic matrix of a mesocratic gneiss from Punta Ainu (CPL).

The massive to poorly foliated layers consist of the same minerals but in different modal proportions, with the biotite modal content being only 5 - 10%, and quartz and plagioclase being the most abundant minerals. Plagioclase in the gneiss and in the fibrolite nodules have the same composition, with An=21-25 mol.%. Biotite has X_{Mg} ratio 0.4-0.5, Al^{VI} between 0.65 and 0.95 and titanium lower than 0.36 a.p.f.u. No compositional differences have been found between biotite of the nodules and S2 biotite from the gneiss. Garnet is unzoned with the following composition: Alm_{65}, Sps_{19}, Pyr_{13}, Grs_3. Si content in muscovite ranges from 6.05 to 6.18 a.p.f.u. The X_{Mg} content of muscovite is 0.5, and Na content in the 0.08-0.12 a.p.f.u. range.
The fibrolite nodules were probably formed in two main steps: **(i)** fibrolite forming into lens-shaped aggregates; and **(ii)** nodules forming by stretching of the aggregates associated with tectonic deformation. The association of the fibrolite nodules and quartz veins suggests that the nodule formation was related to

DOI: 10.3301/GFT.2015.03

fluid circulation resulting from deformation of two rheologically heterogeneous rock bodies. The lens shaped segregations may be derived from metasomatic interaction between the host gneiss and acidic fluid(s) introduced into the rocks.
The presence of fibrolite indicates that the nodules formed in the sillimanite stability field at a temperature higher than 620-635 °C, probably near to P-T conditions estimated in the adjacent migmatite (T 700°C, P 0.6 GPa).
Several late- to post-tectonic granitic dykes crosscut the metamorphic fabric, the latest ones having a basic composition.

From Punta Ainu, drive north towards Porto Ottiolu. The Porto Ottiolu outcrop is one of the southernmost outcrops of the migmatite complex in Northeastern Sardinia. Walk a few hundreds meters along the Tyrrhenian coast from Porto Ottiolu north to Punta de Li Tulchi. On the way, notice the different types of sedimentary- and igneous-derived migmatite belonging to the sillimanite + K-feldspar zone, calc-silicate nodule, and retrogressed eclogite bodies embedded within the migmatite.

STOP 2.3: Porto Ottiolu - Punta de li Tulchi. Contact between the migmatized orthogneiss and its metasedimentary host rock (N 40°44’ 26.70”, E 9° 42’ 42.18”).

At the Porto Ottiolu beach (Fig. 2.12) we see migmatized orthogneiss in contact with its sedimentary host rock, which now consists of paragneiss and layered migmatite (Fig. 2.13a).
The contact (Fig. 2.13a) is parallel to the regional schistosity (S2). The migmatized orthogneiss is slightly schistose with a regional foliation oriented N 100° 45° SW. The paragneiss is dark-colored, and consists of alternating medium and fine-grained layers, with occasional calc-silicate nodules. On the basis of SiO_2/Al_2O_3 vs. K_2O/Na_2O ratios (Wimmenauer, 1984), the paragneiss protoliths were classified as greywackes to arkoses. The paragneiss sometimes preserves intrafoliar folds which transposes an earlier S1 foliation (Fig. 2.13b). S1, the oldest structure observed in the field, pre-dates the most pervasive folding phase, D2, which is characterized by tight folds with sub-horizontal axes (Fig. 2.14a,b). In the paragneiss and layered migmatite, a N-S 48°S muscovite down-dip lineation and isoclinal folds with axial plane schistosity are recognisable. The regional schistosity is transposed by shear bands oriented at E-W 25° S with kinematic indicators (S-C planes) corresponding to a top-to-the-N shear component. The D3 deformation caused symmetric folds with sub-horizontal axes with no axial plane schistosity (Fig. 2.14b).

DOI: 10.3301/GFT.2015.03

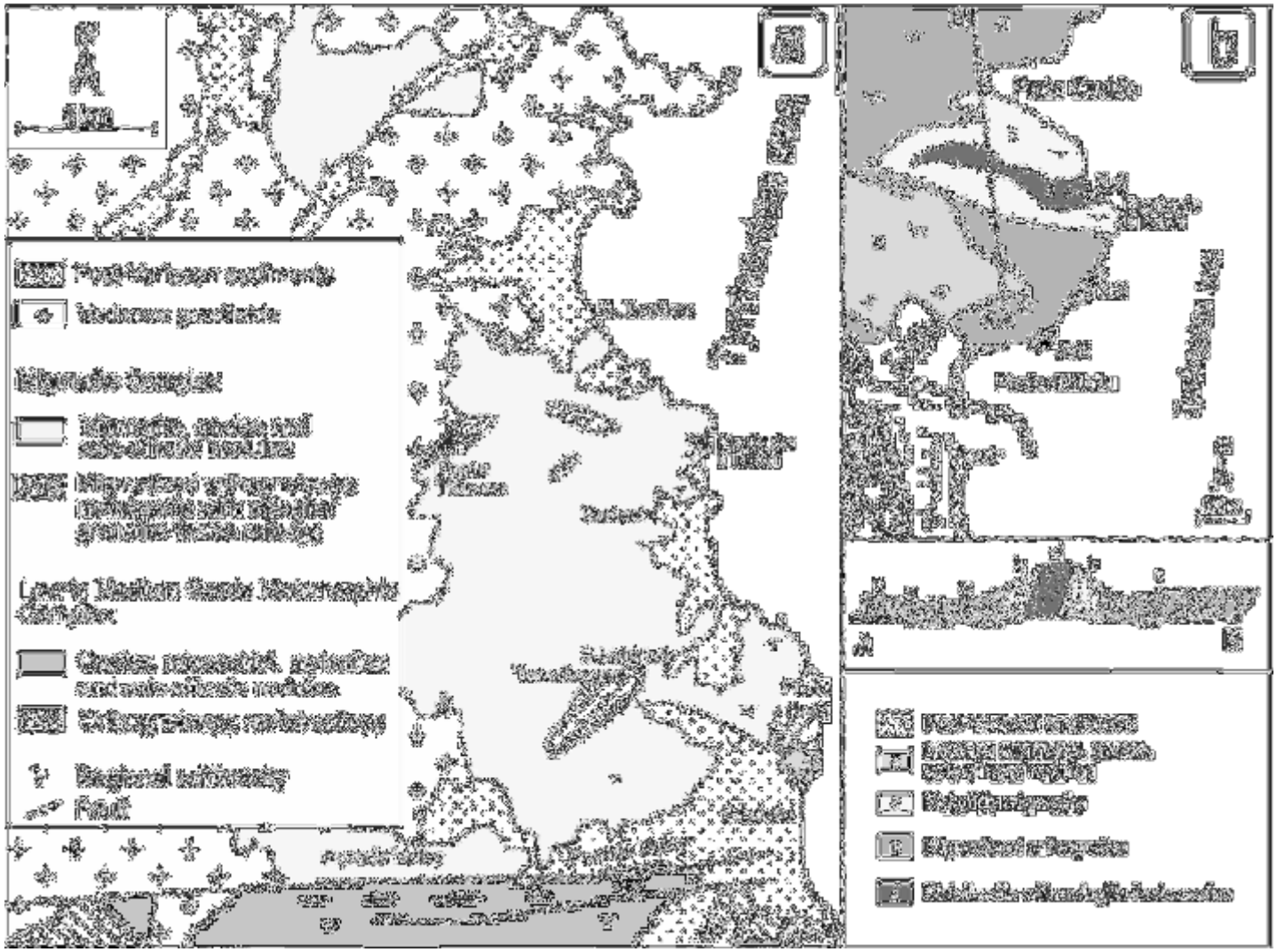

Fig. 2.12 - **a)** Geological sketch map of the Porto Ottiolu-Punta de li Tulchi area. Stops 2.2, 2.3, 2.4 and a cross-section are also shown **(b)**.

One hundred meters to the north, the layered migmatite consists of biotite, quartz, plagioclase (An_{5-31}), sillimanite, with rare small kyanite relics, garnet and retrograde muscovite. The kyanite relics are enclosed in plagioclase or quartz, and are sometimes surrounded by retrograde muscovite (Fig. 2.15).
Leucosomes are trondhjemitic in composition, coarse-grained, and show a faint foliation. They consist of quartz, plagioclase, rare K-feldspar, muscovite, biotite, fibrolite, and rare kyanite. Plagioclase is unzoned oligoclase, though in some cases a thin albite rim was observed.
Three muscovite textures have been distinguished: a) single small- to medium-grained flakes enclosed in feldspar; b) coarse grains with biotite, fibrolite, and opaques, often overgrowing plagioclase and K-feldspar and showing textural evidence of retrograde growth; and c) muscovite interleaved with biotite along the S2 schistosity, representing pre to syn-D2 muscovite. Mesosomes are medium-grained, schistose rocks, consisting of muscovite, K-feldspar, biotite, quartz, plagioclase, fibrolite, ±garnet. Garnet is present as small-sized crystals. Fibrolite and biotite are associated with each other, and oriented parallel

DOI: 10.3301/GFT.2015.03

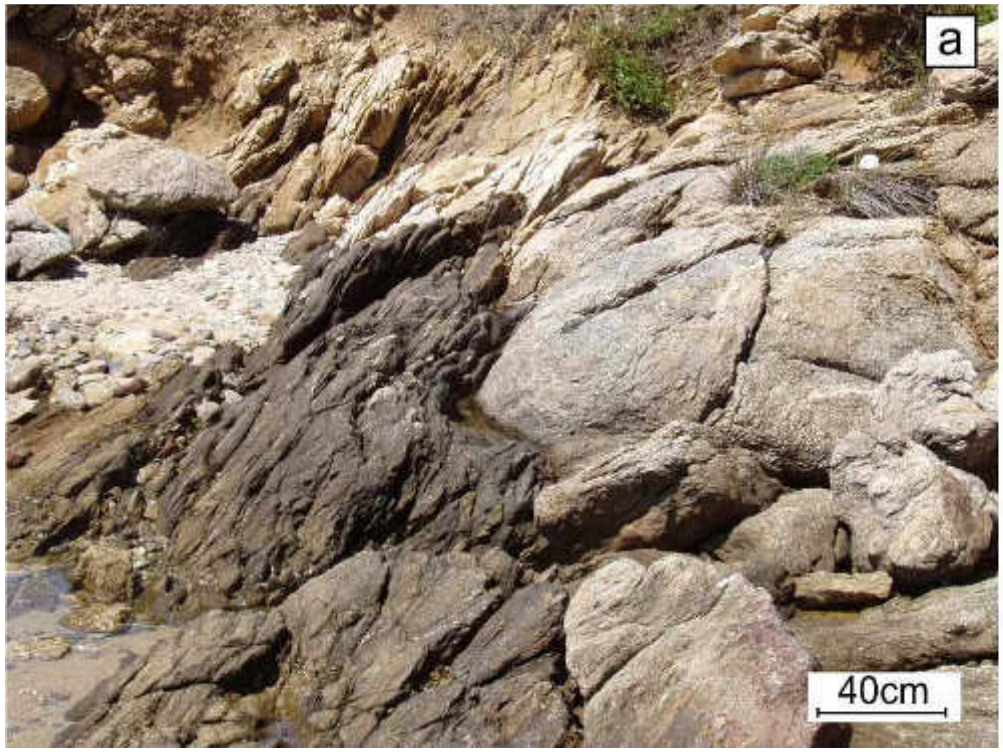

Fig. 2.13 - **a)** Contact between the migmatized orthogneiss (right) and the sedimentary-derived migmatite (left); **b)** intrafoliar D2 fold in the paragneiss of Porto Ottiolu with S2 axial plane schistosity which transposes an early S1 foliation.

to the fabric. A few mm-thick melanosome is usually present at the boundary between the leucosomes and mesosomes.

According to Cruciani et al. (2001, 2014a), partial melting in the pelitic rocks of the "Sant'Anna Formation Auctt." to which the pelite of Porto Ottiolu belongs (Elter et al., 1986), started in the kyanite field. The sequence of kyanite, fibrolite, and crosscutting coarse-grained muscovite reflects the evolution of migmatite during the exhumation. The trondhjemitic leucosome and the less common granitic leucosome of the layered migmatite are formed by H2O-fluxed melting and dehydration melting of muscovite, respectively. The garnet–biotite-plagioclase-fibrolite assemblages give P-T values of T 650C and P= 0.4-0.6 GPa. According to Franceschelli et al. (1989) and Ricci et al. (2004), the garnet-biotite geothermometer does not record the peak metamorphic conditions, but only reflects re-equilibration along the retrograde path.

DOI: 10.3301/GFT.2015.03

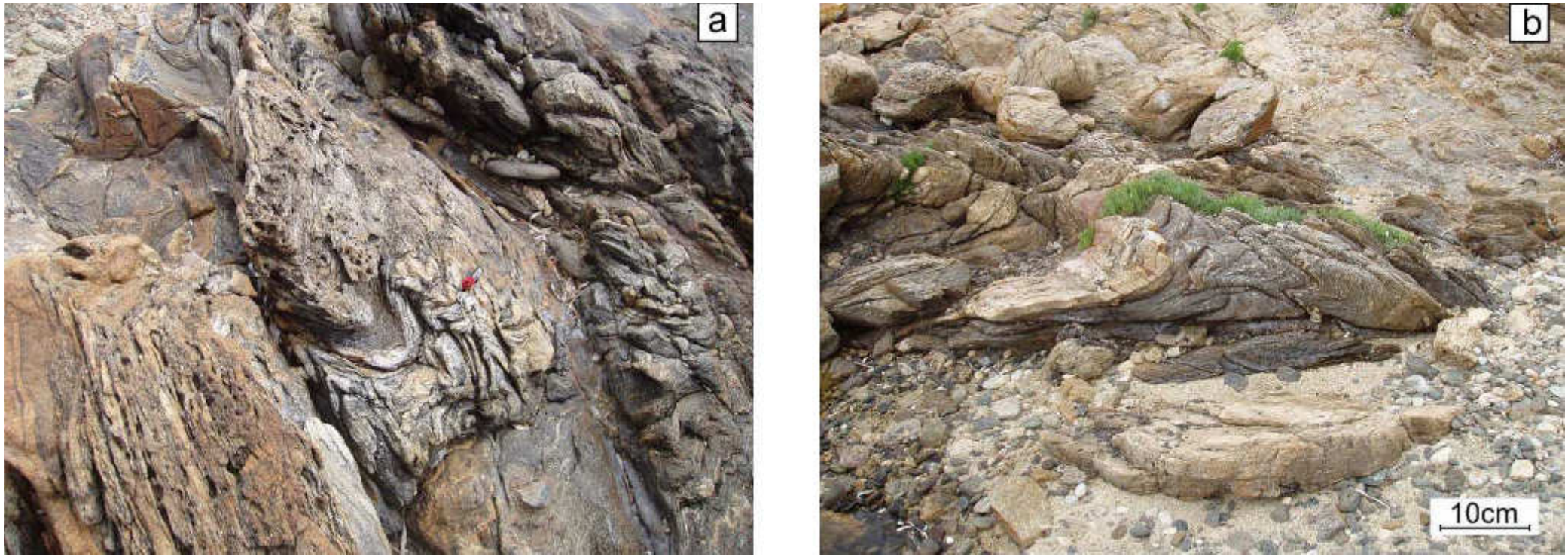

Fig. 2.14 - **a)** D2 leucosome folds with subhorizontal axis in the layered migmatite; **b)** D3 fold in the layered migmatite with subhorizontal axis lacking any axial plane foliation.

STOP 2.4: Migmatitic orthogneiss, paragneiss with fibrolite nodules, granitic and pegmatite dykes (N 40° 44’ 31,5”; E 9° 42’ 53,2”).

The migmatized orthogneiss consists of zoned K-feldspar (microcline), biotite, quartz, plagioclase (An_{20-33}), ± garnet, and coarse-grained retrograde muscovite. The leucosomes are generally granitic in composition, but the modal ratio of biotite and K-feldspar varies between leucosomes and even within a given leucosome. Based on their structural relationships with the S2 schistosity, two types of leucosomes can be identified in the migmatized orthogneiss (Fig. 2.16): folded leucosomes and leucosomes emplaced along shear zones. The first type are deformed by D2 folds with sub-vertical axes and are frequently characterized by the occurrence of biotite trails within the leucosome (Fig. 2.16a, b). The contact between these leucosomes and the migmatized

DOI: 10.3301/GFT.2015.03

orthogneiss is marked by a biotite-rich selvage (Fig. 2.16a, b). The second type of leucosome is emplaced along shear zones (Fig. 2.16c). Tension gashes (Fig. 2.16d) with synkinematic intrusion of leucosome are also present (Corsi & Elter, 2006). In the tension gashes, the leucosome intrusion corresponds to a Riedel fracture system with the master fault oriented at N 170°

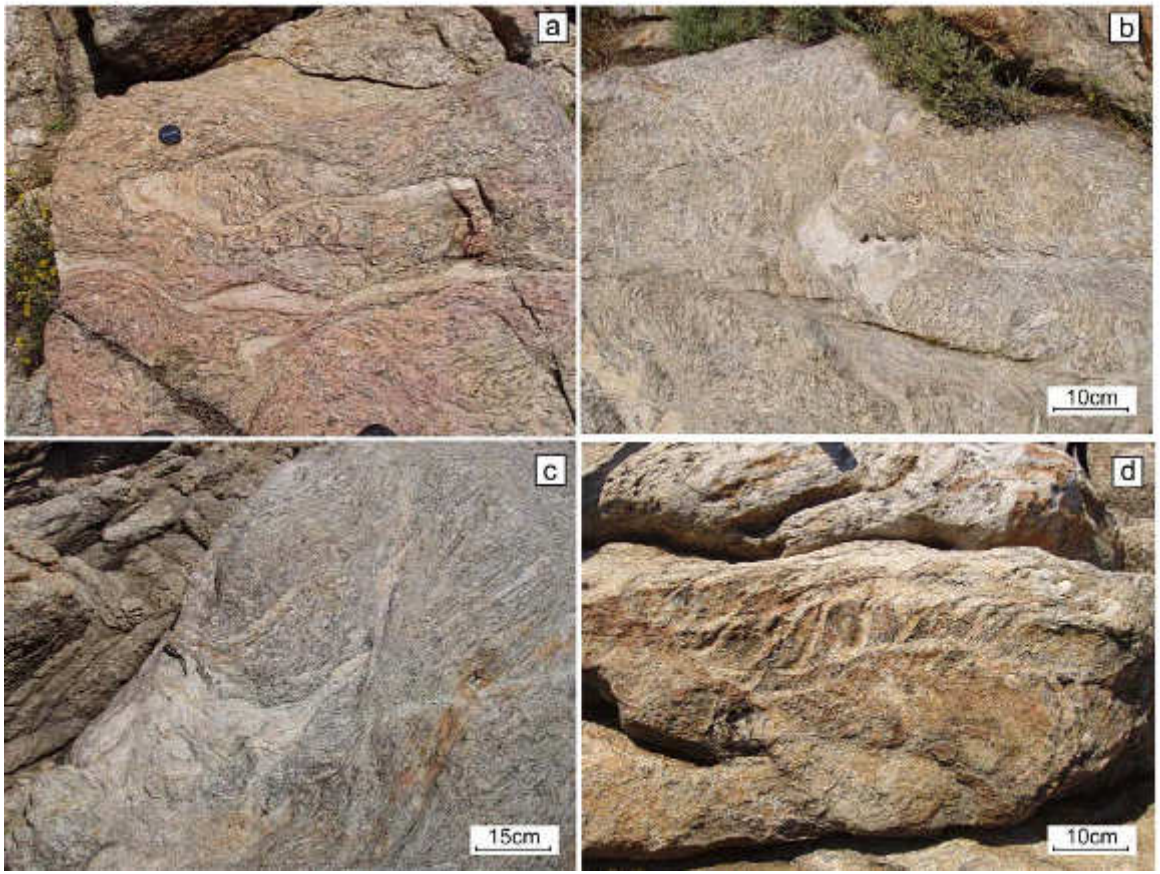

Fig. 2.16 - **a)**, **b)** Folded leucosomes in the migmatized orthogneiss of Porto Ottiolu; the leucosome/mesosome interface is marked by biotite-rich melanosomes; **c)** leucosome emplaced along a shear zone; **d)** tension gashes with synkinematic intrusion of leucosome in the migmatized orthogneiss.

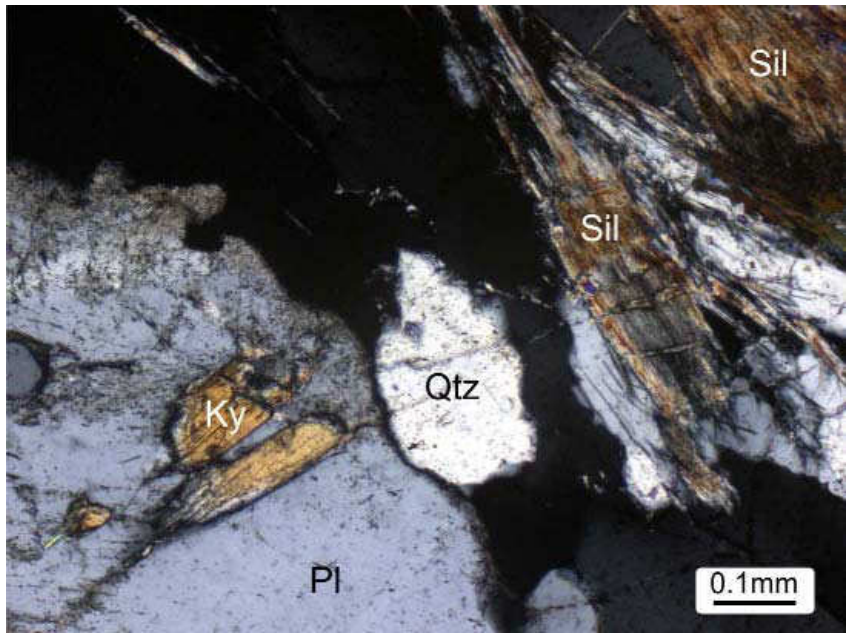

Fig. 2.15 - Kyanite and sillimanite in a quartz-feldspathic matrix in the sedimentary-derived layered migmatite of Porto Ottiolu (CPL).

and R2 oriented at N 115°. The cm-sized shear bands that are related to emplacement of leucosomes have been interpreted by Elter et al. (1999, 2010) and Padovano et al. (2012) as a regional system of shear zones, connected to a network of extensional shear zones in the migmatite complex of NE Sardinia.

The leucosomes show the following composition: SiO_2: 69-74, Al_2O_3: 13-15, Fe_2O_3tot: 0.9-3.5, MgO: 0.3-1.8, CaO: 1.4-3.1, Na_2O: 1.9-3.7, K_2O: 1.7-7.7 wt.% (Cruciani et al., 2001). The ASI index ranges

DOI: 10.3301/GFT.2015.03

between 1.01 and 1.10. The mesosomes are enriched in MgO, Fe_2O_3tot, TiO_2 and depleted in SiO_2 and K_2O as compared to the leucosomes. The positive correlation of MgO with Na_2O+CaO and the negative correlation with K_2O suggest that K_2O content is mainly controlled by K-feldspar.
The leucosomes are enriched in Rb, Sr, Ba, and Pb, and depleted in Li, Sc, V, Cr, Co, Y, Zr, Nb, Cs, Th, and U as compared with the mesosome. ∑REE varies from 40 to 100 ppm in the leucosomes and from 120 to 180 ppm in the mesosomes. The mesosomes have strongly fractionated chondrite-normalized REE patterns characterized by LREE enrichment and, in most cases, by a negative Eu anomaly.
Most leucosomes show a positive Eu anomaly and moderately fractionated chondrite-normalized REE patterns. Leucosomes containing garnet are characterized by a higher HREE content than those without garnet.
The petrography and chemical composition of the Porto Ottiolu orthogneiss are quite similar to those of the Tanaunella orthogneiss, which has been dated at 456±14 Ma (Helbing & Tiepolo, 2005) and interpreted as an Ordovician calc-alkaline granitoid.
According to Palmeri (1992), the leucosome in the migmatized orthogneiss may be formed by dehydration melting of the biotite+muscovite+ quartz assemblage. The leucosome along the shear zone may be the result of a congruent melting reaction involving the quartz-feldspatic component of the host orthogneiss, possibly favored by fluid channelled along shear zones.

Micaschist, paragneiss with fibrolite nodules

Towards Punta de li Tulchi a zone of micaschist and paragneiss with fibrolite-rich nodules is encountered.
The paragneiss lens contains an elliptically shaped (1 m x 15 cm) zoned calc-silicate nodule (Grt + Qtz + Am + Ep + Cpx) with the long axis parallel to the regional schistosity.
Near the contact with the paragneiss the nodule is characterized by a dark-coloured, fine-grained thin rim.
About 100 m north of the calc-silicate nodule, lenses of micaschist and paragneiss with cm-sized fibrolite-rich nodules recur (Figs. 2.17a, b). The nodules are flattened and stretched along the S2 foliation plane. The fibrolite nodules are strongly oriented and are composed of variable amounts of sillimanite (as fibrolite), quartz, plagioclase, minor biotite, and coarse-grained muscovite (Fig. 2.17b).
In the micaschist the phyllosilicate content increases, with the rocks comprising quartz, plagioclase, biotite chlorite, and abundant muscovite and fibrolite. Coarse-grained muscovite contains fibrolite needles. Muscovite also appears as smaller fibrolite-free randomly oriented crystals. The micaschist has a mylonitic appearance and typically contain S-C planes.

DOI: 10.3301/GFT.2015.03

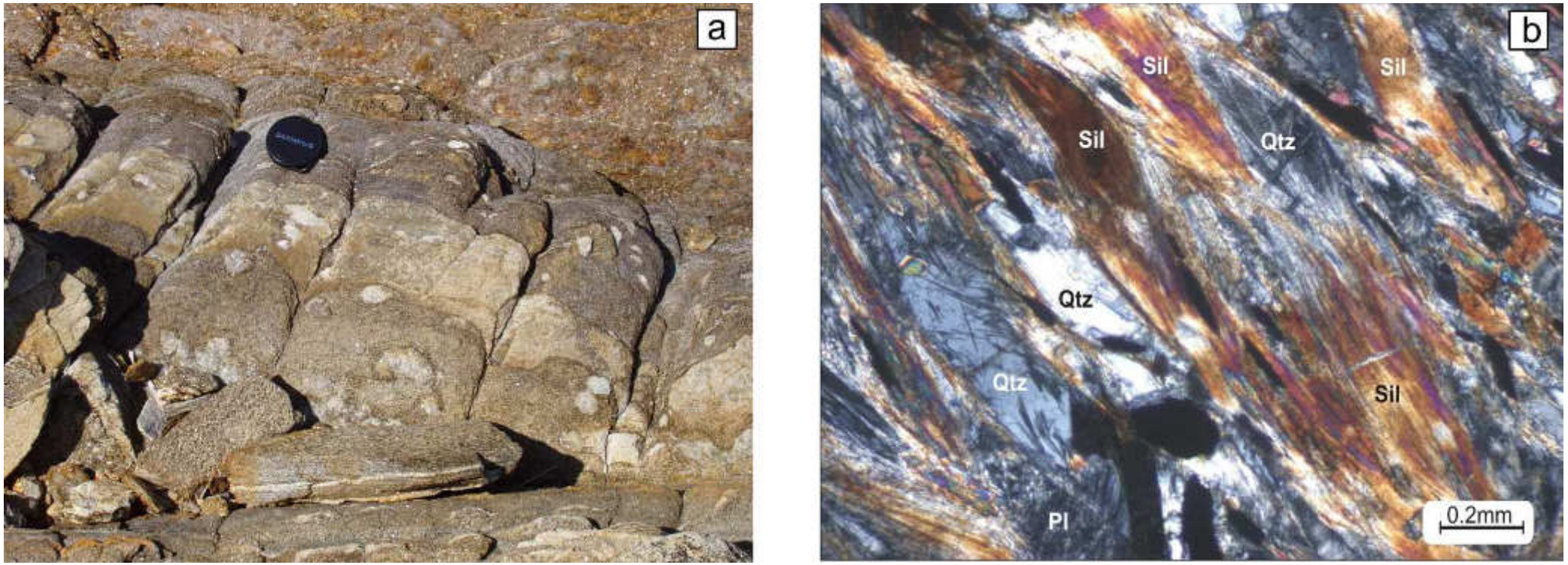

Fig. 2.17 - **a)** Fibrolite + quartz nodules (white) flattened and oriented along the S2 schistosity of micaschist and paragneiss; **b)** microstructure of a fibrolite + quartz nodule with fibrolite mats following S2 schistosity (PPL).

Leucogranite and pegmatite dykes

The leucogranite and pegmatite dykes (Fig. 2.18a, b) that crosscut the migmatites and paragneiss range in thickness from 10 cm to 1 m. The leucogranite is fine-grained and consists of quartz (30-35 vol.%), plagioclase (35-45%), K-feldspar (15-20%), biotite (1-5%), muscovite (3-15%), and garnet (1-2%). The leucogranite has the following properties: apatite and zircon as accessory phases; plagioclase as zoned oligoclase-andesine; K-feldspar with microcline twinning and perthitic veins and an average value of the triclinicity index of 0.83; biotite with a XFe ratio of 0.63 and titanium content of 0.215 - 0.295 a.p.f.u.; muscovite (2M1 polytype) with Si content in the range 6.16 - 6.31 a.p.f.u.; and garnet that is almandine-rich (62-64%), with spessartine (28-30%), and subordinate grossularite (>3%) and pyrope (6-8%) contents.

DOI: 10.3301/GFT.2015.03

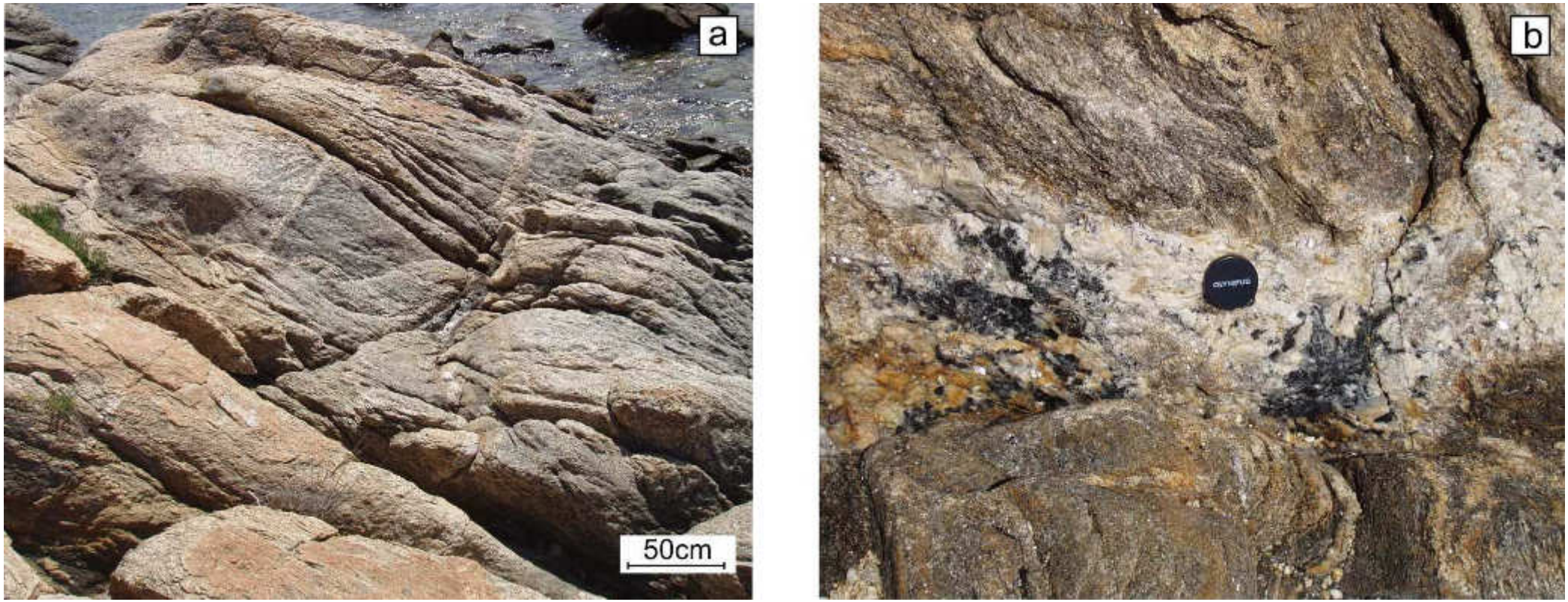

Fig. 2.18 - **a)** Leucogranite dykes croscutting the migmatized orthogneiss of Porto Ottiolu; **b)** pegmatite dyke in the layered migmatite of Porto Ottiolu. The black mineral is tourmaline.

Pegmatites consist of quartz (10-15 vol%), plagioclase (20-40%), K-feldspar (50-65%), muscovite (2-5%), and tourmaline (1-2%) (Fig. 2.18b) with the following properties: plagioclase is an unzoned oligoclase/andesine and K- feldspar belongs to the low microcline structural state with a triclinicity index of 0.92-0.99; muscovite (2M1 polytype) has Si content in the 6.16- 6.17 a.p.f.u. range and Ti content from 0.003 to 0.014 a.p.f.u.; tourmaline, up to 2-3 cm in size, is a solid solution between dravite (32-44%), schorl (39-44%), and elbaite (15-22%).
The Porto Ottiolu leucogranite is a peraluminous (ASI: 1.25-1.44) S-type granite with normative corundum < 1.1 vol.% (Caredda et al. 1999) with a composition similar to that of other Variscan leucogranites from Sardinia. They

DOI: 10.3301/GFT.2015.03

have the following composition: SiO_2=70.5-72.8, Fe_2O_3=1.16-2.09 ; MgO=0.64-1.09; Na_2O=2.7-3.0, CaO=0.8-1.6; K_2O=4.4-4.7 wt.%, being enriched in MgO, TiO_2, Fe_2O_3tot, P_2O_5, Zr, V, Cr, Co, Nb and depleted in K_2O, Rb, Sr, Ba, and Cs as compared to the pegmatite.
REE content varies between 60 and 110 ppm; chondrite-normalized REE patterns are moderately fractionated with the La_N/Lu_N ratio between 5 - 17. Granite samples show no Eu anomaly or a moderately negative Eu anomaly.

STOP 2.5: Nebulite and metabasite with eclogite-facies relics of Punta de li Tulchi
(N 40° 44' 37.06", E 9° 42' 53.55")

Nebulite
Along the footpath from Porto Ottiolu to Punta de li Tulchi, the migmatized orthogneiss gradually changes texture and fades into a nebulitic migmatite towards north (Fig. 2.19). The typical field appearance of the

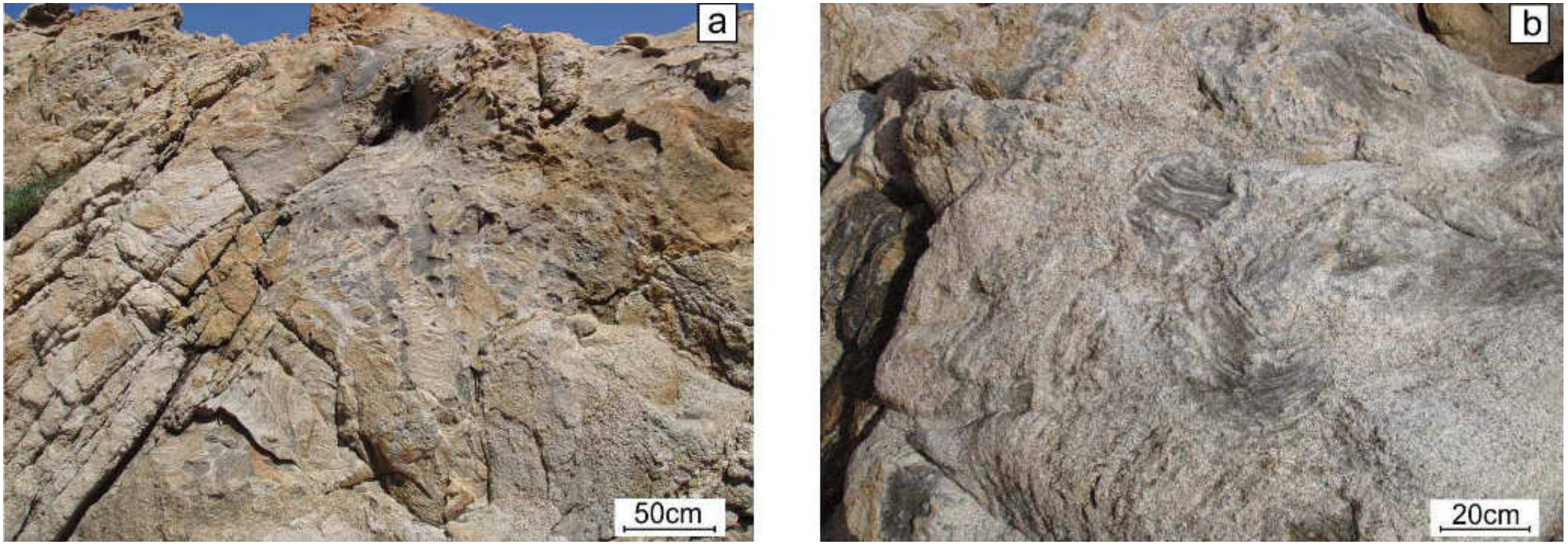

Fig. 2.19 - **a)** Nebulitic migmatites at the contact with the metabasite with eclogite facies relics at Punta de li Tulchi; **b)** detail of the nebulite structure.

DOI: 10.3301/GFT.2015.03

nebulitic migmatite can be observed near the contact with the metabasites with eclogite facies relics at Punta de li Tulchi. Compared to the migmatized orthogneiss, the nebulitic migmatites are characterized by a faint foliation, lower biotite content, and a homogeneous texture in which leucosomes are absent, or at least not easily seen at outcrop scale (Fig. 2.19a). Some foliated and/or folded portions of migmatite appear to have been trapped within the nebulite (Fig. 2.19b).

Metabasites with eclogite-facies relics

At Punta de li Tulchi, eclogite enclosed within migmatite forms a 100 m by 20-30 m thick lens (Fig. 2.20a) with a N80°-60° orientation. The northern contact between eclogite and nebulitic migmatite is marked by a 20-30 cm thick dark amphibole-rich layer and quartz-rich veins. Moving south, orthogneiss in contact with eclogite shows evidence of brecciation.

The eclogite consists of alternating garnet-pyroxene-rich (GP) and amphibole-plagioclase-rich (AP) layers (Fig. 2.20a, b) parallel to the main schistosity (Franceschelli et al., 1998, 2005a, 2007).

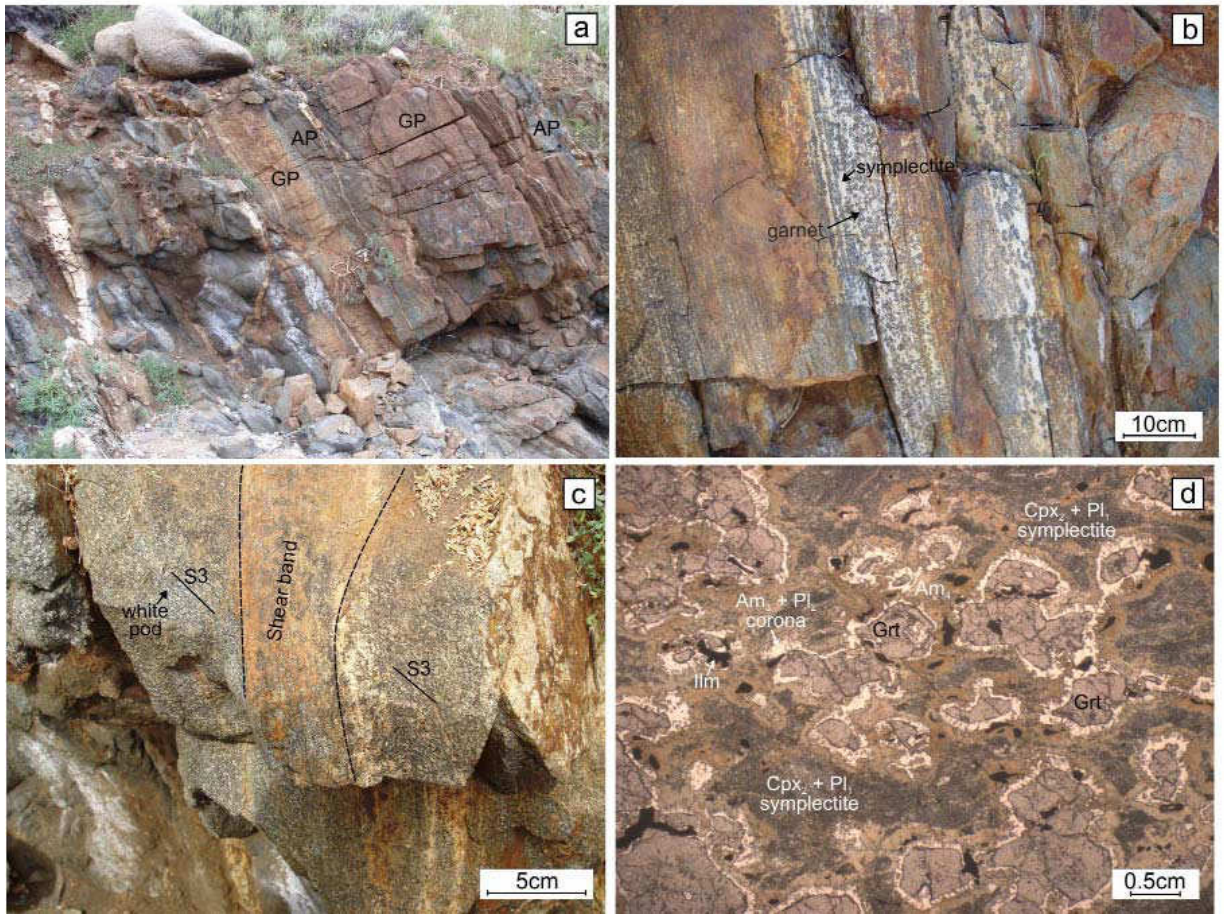

Fig. 2.20 - (a) Alternation of decimeter-scale brownish Grt-Px layers and greenish Am-Pl layers; (b) detail of the Grt-Px layer with reddish garnet crystals with a dark corona surrounded by the clinopyroxene + plagioclase symplectite (white); (c) elongated white pods in the Am-Pl layers forming the S3 schistosity, which is cut by millimeter-scale shear bands; (d) photomicrograph showing microstructures in a Grt-Px layer of the Punta de li Tulchi granulitized eclogites with coronitic garnet set in a Cpx2+Pl1 symplectite matrix. PPL.

DOI: 10.3301/GFT.2015.03

The major element composition of selected GP and AP layers from the Punta de li Tulchi eclogite is shown in Table 1. According to the SiO_2–Zr/TiO_2 diagram (Winchester & Floyd, 1977) the rocks plot in the sub-alkaline basalt field. Except for Rb, the GP and AP layers show quite similar trace element contents. Both GP and AP layers exhibit a slightly convex light-REE pattern, generally a slight negative Eu anomaly, and a flat heavy-REE pattern (Franceschelli et al., 1998; Cruciani et al., 2010). In the Ti-Zr-Y discrimination diagram of Pearce & Cann (1973), they plot in the field of Mid-Ocean Ridge basalts.

Table 1. Major element composition for some selected samples of garnet-pyroxene (GP) and amphibole-plagioclase (AP) layers of the eclogite from Punta de li Tulchi (from Franceschelli et al., 1998).

Layer	*GP*	*GP*	*AP*	*AP*
(wt%)				
SiO	45.50	49.07	52.66	48.17
TiO	2.33	1.14	1.45	1.82
Al	11.71	16.06	11.71	14.92
Fe	16.56	12.08	14.81	12.87
MnO	0.24	0.18	0.21	0.21
MgO	7.12	4.44	5.86	6.14
CaO	11.51	12.43	9.65	11.53
Na	4.04	2.06	2.46	3.23
K	0.06	0.40	0.52	0.27
P	0.30	0.29	0.22	0.34
LOI	0.63	1.84	0.45	0.51

The layers, sharply to poorly defined, show a preferred 50° N dip with an E-W strike. Locally, at the micro-scale, individual lobes of the symplectic lamellae are roughly aligned along a preferred orientation (Fig. 2.20c) forming a high angle with the S2 foliation, which is defined by garnet elongation. Moreover, the amphibolitization of the original granulitic rock is clearly recognisable in some parts of the outcrop where an amphibolitic front with faded contours cuts the S2 or replaces granulitic layers.

The GP layers (Figs. 2.20a, b) are mainly composed of medium/coarse-grained and poikiloblastic garnet up to 5 mm in size with inclusions of omphacitic pyroxene, euhedral amphibole (from actinolite to tschermakite), quartz, rutile, and epidote. The matrix consists of fine-grained symplectites of plagioclase (An_{19-36}) plus small lath-shaped clinopyroxene (diopside-augite) replacing omphacite, orthopyroxene, various types of amphibole and minor Fe-oxides. Amphibole in the matrix commonly shows a pale-green core surrounded by a brown rim with composition from tschermakite to Mg-hornblende. The colourless amphibole replacing orthopyroxene is a cummingtonite with X_{Mg} = 0.7. The garnet composition is: Alm_{50-62} Prp_{19-27} Grs_{16-26} Sps_{1-3}. In some zoned garnet crystals, X_{Mg} increases smoothly from the core (0.25) to an intermediate zone (0.36) and then decreases in the rim (0.24). The grossularite content generally decreases gradually from core to intermediate zone and rim (0.748; 0.668; 0.584 a.p.f.u., respectively). Garnet margins in contact with clinopyroxene-plagioclase symplectites are surrounded by a radial kelyphytic corona consisting of pale-green prismatic blebs of brown to

DOI: 10.3301/GFT.2015.03

green amphibole (from tschermakite to Mg-hornblende) and plagioclase (An_{51-96}). The late pale green amphibole is an actinolite with X_{Mg} = 0.6-0.7.

The AP layers consist of elongated white pods (Fig. 2.20c) of plagioclase-amphibole oriented along a N 80°-SE 30° S_3 foliation. Relics of clinopyroxene + plagioclase symplectites, orthopyroxene, and colourless amphibole occur in the matrix. The modal proportion of amphibole reaches 50-60vol%. The S1 schistosity is completely obliterated and the main rock foliation is defined by the orientation of the matrix amphibole crystals. Most of the white pods are strongly aligned with a later S_3 foliation, which, in turn, is crosscut by a later shear band.

The metamorphic history and evolution of the eclogite may be summarized by the stages represented in Fig. 2.21 (Cruciani et al., 2012). The metamorphic evolution is characterized by an increase in temperature during the early stage of exhumation (Franceschelli et al., 1998; Giacomini et al., 2005; Cruciani et al., 2011, 2012).

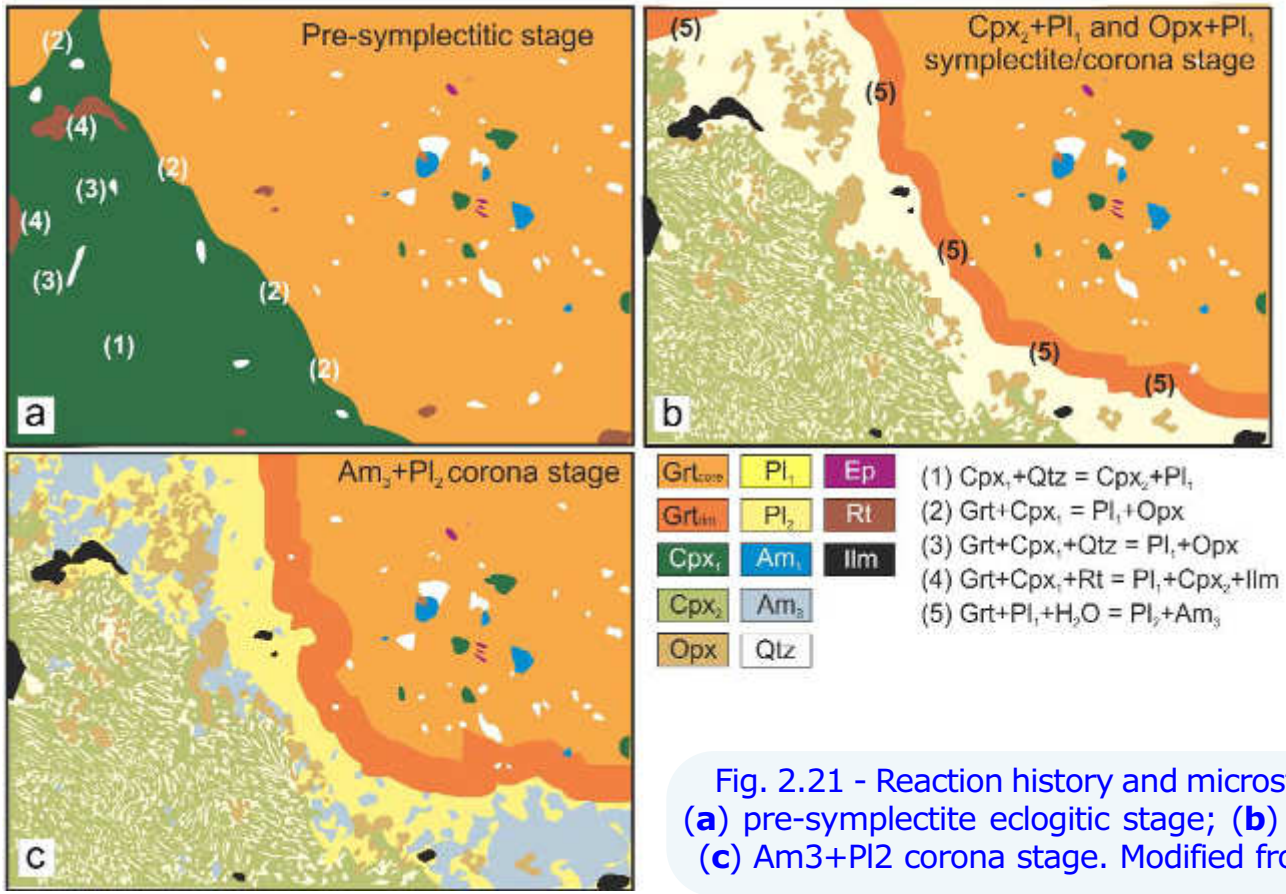

Pre-symplectite stage: the earlier stage of the metamorphic history corresponding to eclogite facies P-T conditions is documented by the occurrence of inclusions of omphacite, rutile, quartz, epidote, amphibole in poikiloblastic garnet (Fig. 2.21a), the high jadeite content of omphacite (X_{Na} ratio up to 0.38), and by the compositional zoning of garnet. Euhedral amphibole and epidote only found as armoured inclusions in garnet could represent pre-eclogite facies minerals.

Fig. 2.21 - Reaction history and microstructure of Punta de li Tulchi retrogressed eclogite. (**a**) pre-symplectite eclogitic stage; (**b**) Cpx2+Pl1 and Opx+Pl1 symplectite/corona stage; (**c**) Am3+Pl2 corona stage. Modified from Cruciani et al. (2012).

DOI: 10.3301/GFT.2015.03

Cpx2-Pl1 and Opx +Pl1 symplectite/corona stage: This stage is documented by the formation of Cpx2+Pl1 and Opx+Pl1 symplectites through reactions (1) and (2) in Fig. 2.21. The first symplectite type is breakdown product of omphacite, whereas the second was generated by the reaction between omphacite and garnet.

Pl2 + Am3 corona stage: this stage is characterized by the pervasive development of amphibole (Am_3) + plagioclase (Pl_2) growing on $Opx_1+Pl_1\pm$ Ilm corona around garnet. Pl_2+Am_3 coronae grow around garnet porphyroblasts (Fig. 2.21c), whereas coronitic amphibole replaces symplectitic Cpx_2 and coronitic Opx and Ilm grains. The growth of amphibole implies that H_2O was available in the system.

Late stage: this stage is documented by the growth of actinolite, chlorite, epidote, and titanite in the matrix. The syn-D_4 biotite growth along shear bands is also tentatively attributed to the late stage.
The eclogites underwent a clockwise P-T path from the eclogite, through granulite and up to amphibolite stage. The pre-symplectite stage occurred with prograde metamorphism from 660-680°C, 1.6-1.8 GPa to 660-700°C at 1.7-2.1 GPa (Fig. 2.22a, b).
Pseudosections calculated for clinopyroxene + plagioclase and orthopyroxene + plagioclase symplectitic coronae indicate temperatures in excess of 800°C and pressures of 1.0-1.3 GPa for the formation of these microstructures (Fig. 2.22b). Decompression then led to the formation of plagioclase + amphibole coronae around garnet at P-T conditions of 730-830°C, 0.8-1.1 GPa.
Water isomodes suggest that eclogites were H_2O-undersaturated at peak-P conditions (Fig. 2.22b) and during most of their subsequent heating and decompression, allowing preservation of prograde garnet zoning in spite of the strong granulite-facies overprint.
Zircons from Punta de li Tulchi eclogites have been dated by the U-Pb SHRIMP method (Palmeri et al., 2004),yielding three weighted means of 453 ± 14, 400 ± 10 and 327 ± 7 Ma. These are interpreted to represent the protolith age, the high-pressure eclogitic event (or Pb loss during the Variscan event), and amphibolite facies retrogression, respectively.

Return to road 131 D.C.N. and drive towards Nuoro. Take the crossroad to S.Lorenzo and then to Tamarispa.

DOI: 10.3301/GFT.2015.03

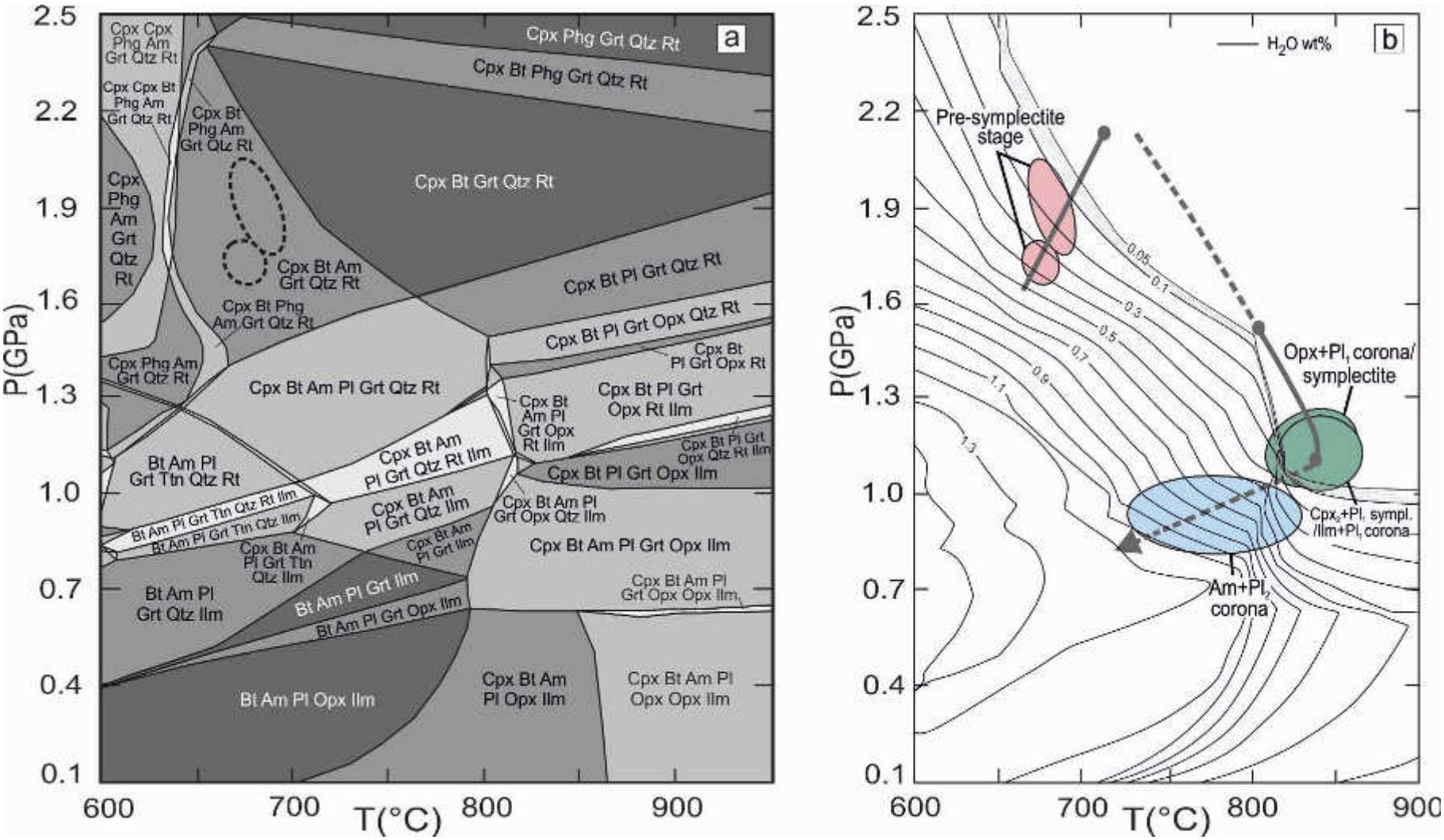

Fig. 2.22 - **a)** P–T pseudosection (NCKFMASTH system) calculated at $aH_2O = 1$ for the bulk composition of a selected sample of Grt-Px layer. **b)** P-T path of the Punta de li Tulchi granulitized eclogites. Orange dotted ellipses represent P-T conditions for pre-symplectite stages shown in (a). An early prograde stage is constrained by the composition of omphacite (preserved as inclusions in garnet) and garnet inner core. A later prograde stage is constrained by the composition of outer cores of garnets as well as by omphacite composition. Green and blue ellipses show P-T conditions of Opx-Pl corona/Cpx +Pl symplectite and Am-Pl corona formation obtained by the P-T pseudosection approach as in Cruciani et al. (2008c). H_2O isomodes (wt%) show that the sample was H_2O-saturated during prograde evolution (continuous P-T path), whereas it was H_2O-undersaturated at peak-P conditions and during most of the following heating and decompression (dashed P-T path). Modified from Cruciani et al. (2012).

DOI: 10.3301/GFT.2015.03

STOP 2.6: Tamarispa (N 40° 40’ 58.14”, E 9° 39’ 48.83”).

Calc-silicate rocks

These rocks, known in the literature as calcsilicate marbles or as grossularite - wollastonite marbles, crop out as two adjacent lenses of about 3 m by 11-15 m. They are embedded within a sequence of multideformed migmatites from the Variscan metamorphic basement near Tamarispa and are characterized by a compositional layering and weak foliated matrix and poikiloblastic garnet grains up to 15 cm in diameter (Fig. 2.23). Wollastonite, calcite, small garnet crystals, diopside, pectolite, quartz, and minor plagioclase, epidote, apatite, and sphene have been identified in the matrix.

Poikiloblastic garnet contains mainly small clinopyroxene and wollastonite inclusions, forming a millipede-like structure. Garnet is a poorly zoned grossularite (Grs_{88-96}; Alm_{4-9}) with low spessartine content. Clinopyroxene is salitic, with X_{Mg} = 0.60-0.71 and an Al_2O_3 content up to 1.20 %.

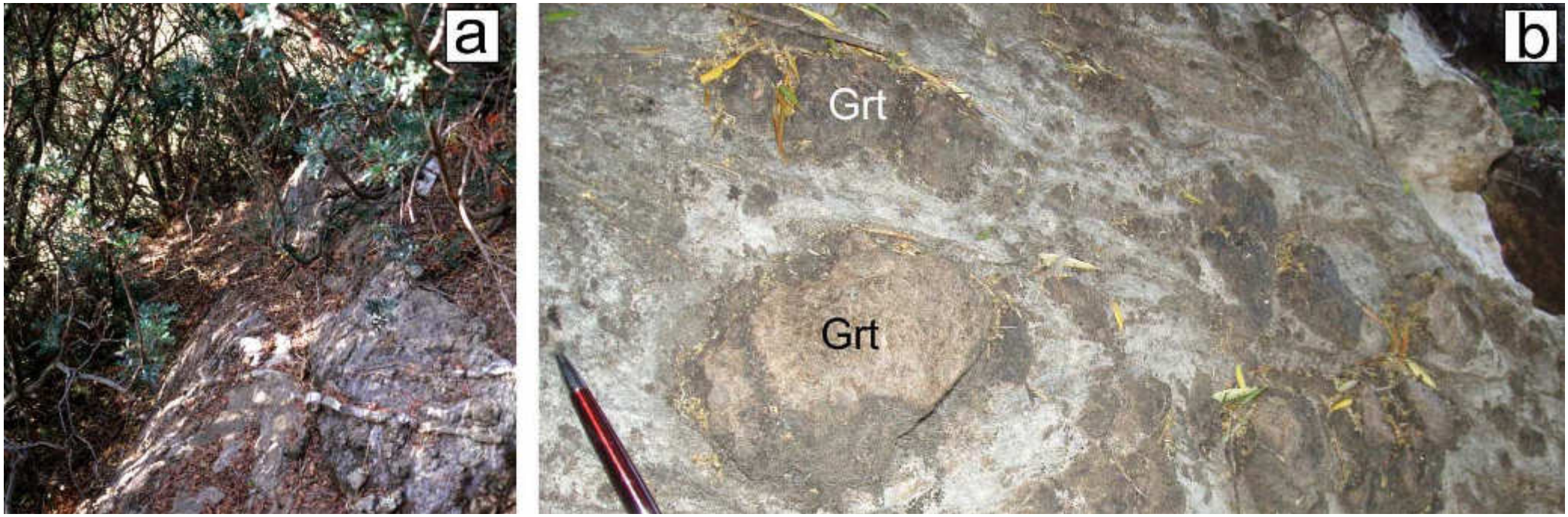

Fig. 2.23 - **a)** Overview of the Tamarispa outcrop; note the white vein crosscutting the wollastonite-grossularite calc-silicate rocks; **b)** decimeter-sized garnet porphyroblasts.

DOI: 10.3301/GFT.2015.03

Wollastonite is essentially $CaSiO_3$ with minor FeO (< 0.30 %) and Al_2O_3 (<0.10%) content. It is often partially replaced by calcite, quartz, and occasionally forms spectacular fine-scale intergrowths with calcite.
Pectolite occurs as fine-grained crystals growing in the microfractures of wollastonite and poikiloblastic garnet or as a thin, discontinuous rim, developed around wollastonite grains.
These rocks are crosscut by two types of veins (I and II): i) type I veins, up to 8-10 cm thick and 4-5 m long, originating from the surrounding biotite-rich migmatite; and ii) type II veins, a few millimeters in thickness, often originating from type I veins.
Quartz, calcite, epidote, K-feldspar, Fe-rich- clinopyroxene, apatite, titanite, albite, and muscovite were found in the type I veins. Calcite, pectolite, and quartz are the principal minerals found in type II veins.
Pectolite has quite a homogeneous chemical composition, which, on average, is: SiO_2 =54-55%, CaO =34-35%, Na_2O=7-8%. The wollastonite-grossularite calc-silicate rocks share a common metamorphic and deformational history with the surrounding migmatite. Temperatures from 650 to 700 °C and pressures between 0.4 and 0.7 GPa have been determined using conventional thermobarometry on the migmatites of NE Sardinia (Franceschelli et al., 1989). Temperatures from 650 to 850 °C and X_{CO2} between 0.006 and 0.13 have been estimated by Elter & Palmeri (1992).

DOI: 10.3301/GFT.2015.03

San Teodoro: *Altitude: 15m a.s.l.; Surface Area: 104,87 km²; Population: 4630.*

San Teodoro, one of the most important tourist villages of north-eastern coast of Sardinia, is located in the so called "Gallura d'Oviddè" and lies on the slopes of M.giu Nieddu. The town's name comes from the church dedicated to San Teodoro di Amasea, a Roman soldier and martyr of the fourth century A.D. San Teodoro is the ideal destination for a seaside holidays on its beautiful beaches (such as La Cinta, among the others). A variety of natural environments start from the wetlands and the lagoon near the shore, home of many bird species, up to the hills with the main peak of Mt. Nieddu. From San Teodoro, there is a wonderful panoramic view of Tavolara.

San Teodoro and, to the north, La Cinta beach.
In the background, Tavolara Island is made up of carbonatic sediments
from: http://www.topsardinia.it

DOI: 10.3301/GFT.2015.03

Third day

Posada, Olbia, Punta Sirenella, Montiggiu Nieddu, Terrata, Olbia, Monte Plebi

From the Hotel in Posada, take SS131 (d.c.n) northwards along the coast. We cross the metamorphic basement and the Carboniferous – Permian granitoids. On the right is Tavolara Island composed of Mesozoic rocks lying unconformably on the metamorphic basement. Go through the centre of Olbia and take SP 82 along north-east coast up to Pittolungu.

The Variscan basement along the NE Olbia coast up to Golfo Aranci area (Fig. 3.1) is a very interesting geological zone of Sardinia's Variscan basement. It has several high-grade rocks such as migmatized orthogneiss, amphibole-bearing migmatite, and calc-silicate nodules enclosed in sedimentary-derived migmatite. At Montiggiu Nieddu (Fig. 3.2) mafic and ultramafic amphibolite and metabasite with relic eclogite facies minerals at Terrata and Iles are enclosed within the migmatite.

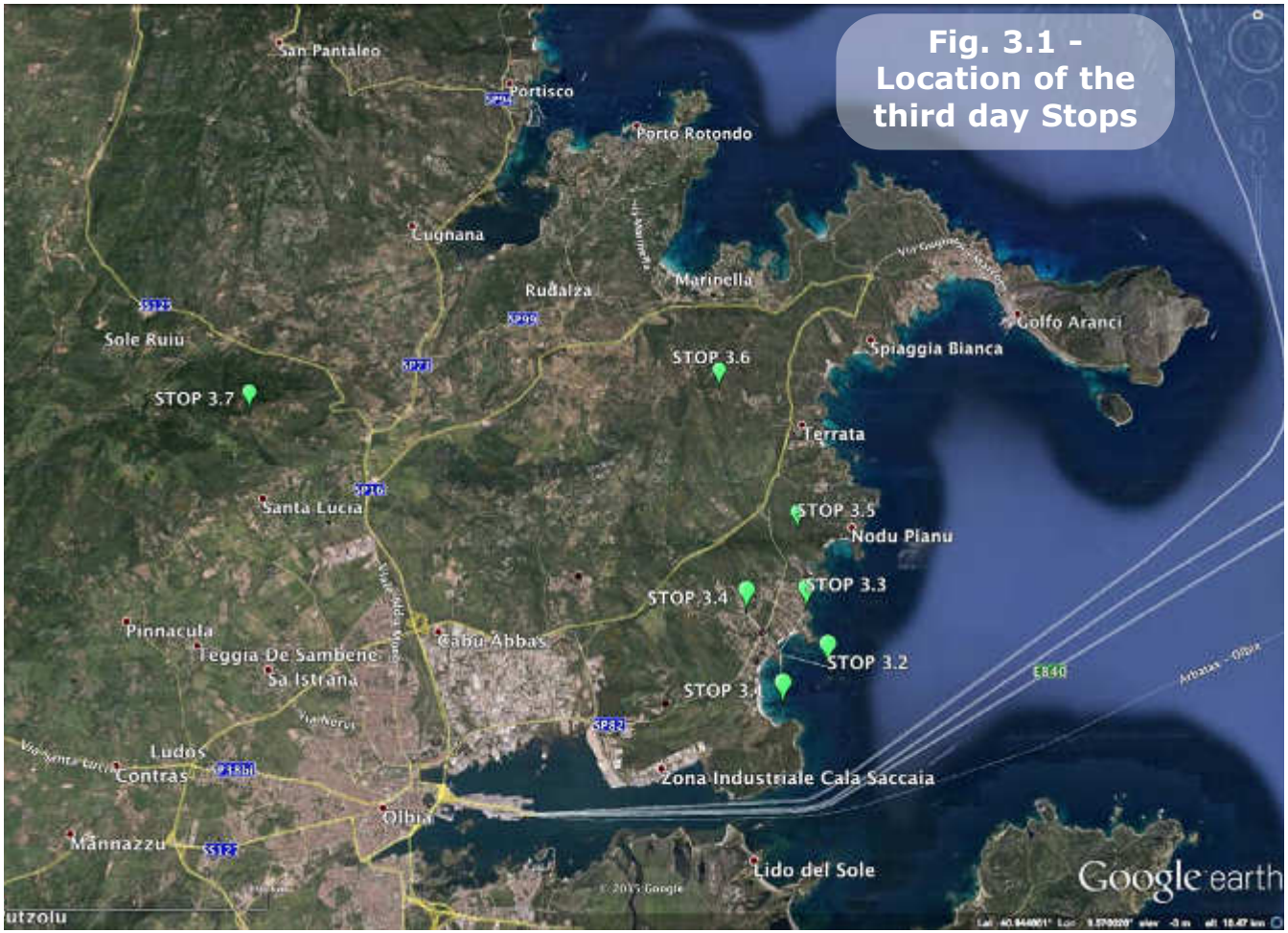

Fig. 3.1 - Location of the third day Stops

DOI: 10.3301/GFT.2015.03

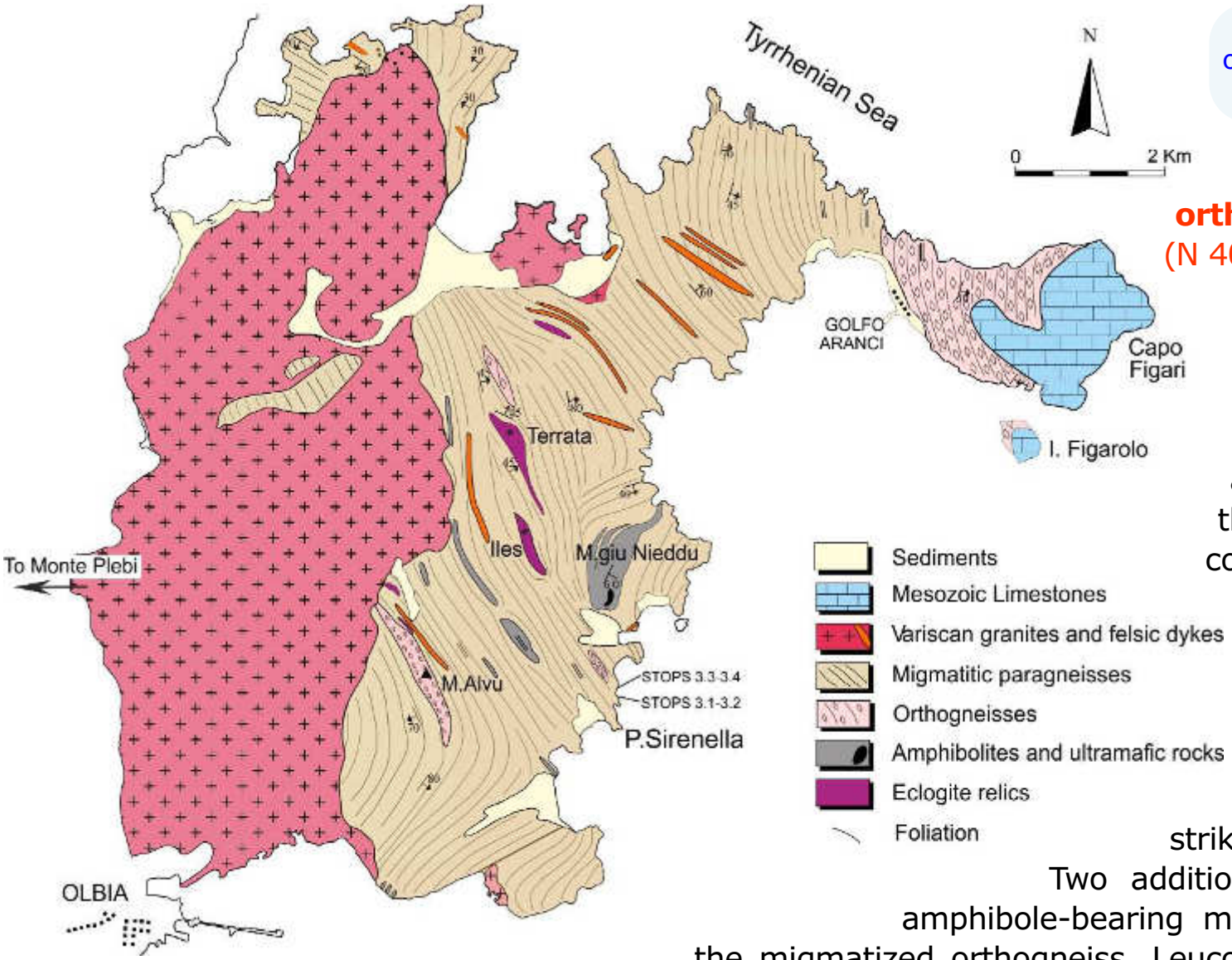

Fig. 3.2 - Geological sketch map of Olbia-Golfo Aranci area (modified from Giacomini et al., 2005).

STOP 3.1: Migmatized orthogneiss from Punta Sirenella (N 40° 56′ 38,6″; E 9° 34′ 19.6″).

The migmatized orthogneiss from Punta Sirenella lies between Al-silicate-bearing migmatite to the south and amphibole-bearing migmatite to the north (Fig. 3.3a, 3.4). The contact between the migmatized orthogneiss and the other two migmatite types is parallel to the regional foliation (S_2). The migmatized orthogneiss is massive to moderately foliated, with the foliation striking N155° and dipping 60° NE. Two additional 2-3m by 100m lenses of amphibole-bearing migmatites (Fig. 3.3a) lie within the migmatized orthogneiss. Leucosomes occur as elongated and deformed whitish layers alternating with mesosomes (Fig. 3.3b), or as deformed and folded pods and patches hosted in the orthogneiss (Fig. 3.3c). The leucosomes, granitic to granodioritic in composition, are made up of quartz, plagioclase, K-feldspar, rare biotite, ± garnet. Zircon has been identified as accessory mineral. Quartz, plagioclase and K-feldspar occur as anhedral crystals with strongly variable size and shape. K-feldspar is microcline at times with perthite exsolutions. Garnet is rare in leucosomes and consists of small, submillimetric crystals,

DOI: 10.3301/GFT.2015.03

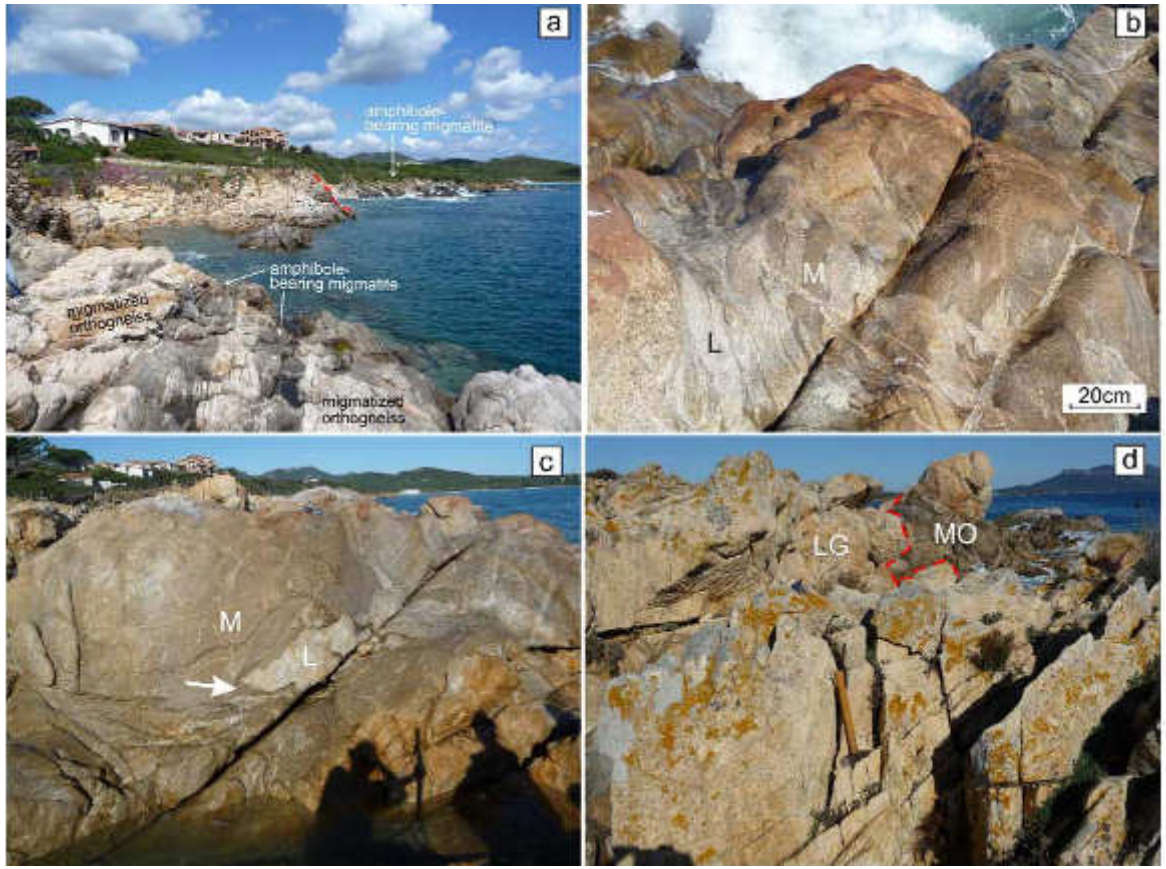

Fig. 3.3 - Field aspect of migmatized orthogneiss cropping out at Punta Sirenella. **a)** Panoramic view of migmatized orthogneiss with two lenses of amphibole-bearing migmatite; **b)** migmatized orthogneiss with locally nebulitic appearance; (L): leucosome; (M): mesosome; **c)** pod or patch of leucosome (L) hosted in migmatized orthogneiss (M); the boundary between leucosome and orthogneiss is marked by biotite concentrations (arrow); **d)** the migmatized orthogneiss of Punta Sirenella (MO) is crosscut by foliated muscovite-bearing leucogranite (LG).

undetectable by the naked eye. The mesosome, made up of the same minerals with additional muscovite, shows the same microstructural features but is characterized by an increase of garnet and oriented biotite. Muscovite in mesosomes occurs sporadically and comprises single crystals within the matrix or inside plagioclase crystals. The migmatized orthogneiss of Punta Sirenella is crosscut by garnet-bearing leucogranite dykes (Fig. 3.3d). The leucogranite consists of quartz, plagioclase, K-feldspar, ± biotite, garnet, and muscovite. Syntectonic granites at Capo Ferro (N Sardinia) have been dated using U–Pb in zircon at 318 ± 3 Ma and 317 ± 2 Ma by Padovano et al. (2014). The migmatized orthogneiss composition is SiO_2:73-76, Al_2O3: 11-15, Fe_2O_3tot: 0.4-2.4, MgO>0.4, CaO: 1, Na_2O: 3.2-5.3, K_2O: 2.8-5.0 wt.%. Barium ranges between 69 and 160 ppm; rubidium and strontium average 190 and 45 ppm respectively.

STOP 3.2: Amphibole-bearing migmatite at Punta Sirenella (N 40° 56′ 39,7″; E 9° 34′ 18.2″).

The amphibole-bearing migmatite forms a 100–150m × 50–70m lens-shaped body located between Al-silicate-bearing migmatite (Figs. 3.4; 3.5b) to the north and migmatized orthogneiss to the south. The contact

DOI: 10.3301/GFT.2015.03

Fig. 3.4 - Geological sketch map of the Punta Sirenella–Punta Bados area, NE Sardinia showing the location of the four Stops.

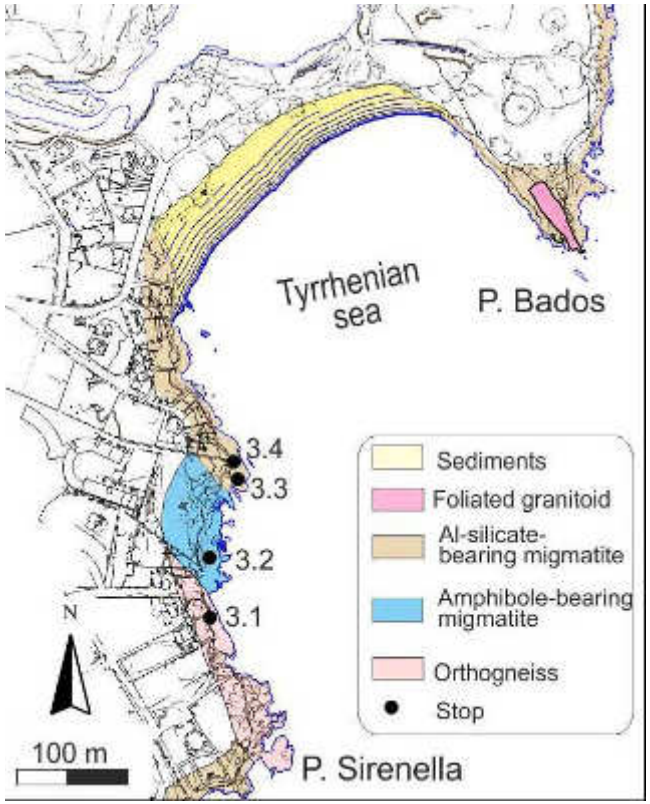

Fig. 3.5 - **a)** Panoramic view of amphibole-bearing migmatites with the contact with the Al-silicate bearing-migmatite visible in the background; **b)** closer view of the contact between the amphibole-bearing and the Al-silicate-bearing migmatites parallel to the regional S2 schistosity. At left, a late pegmatite dyke crosscuts the amphibole-bearing migmatite.

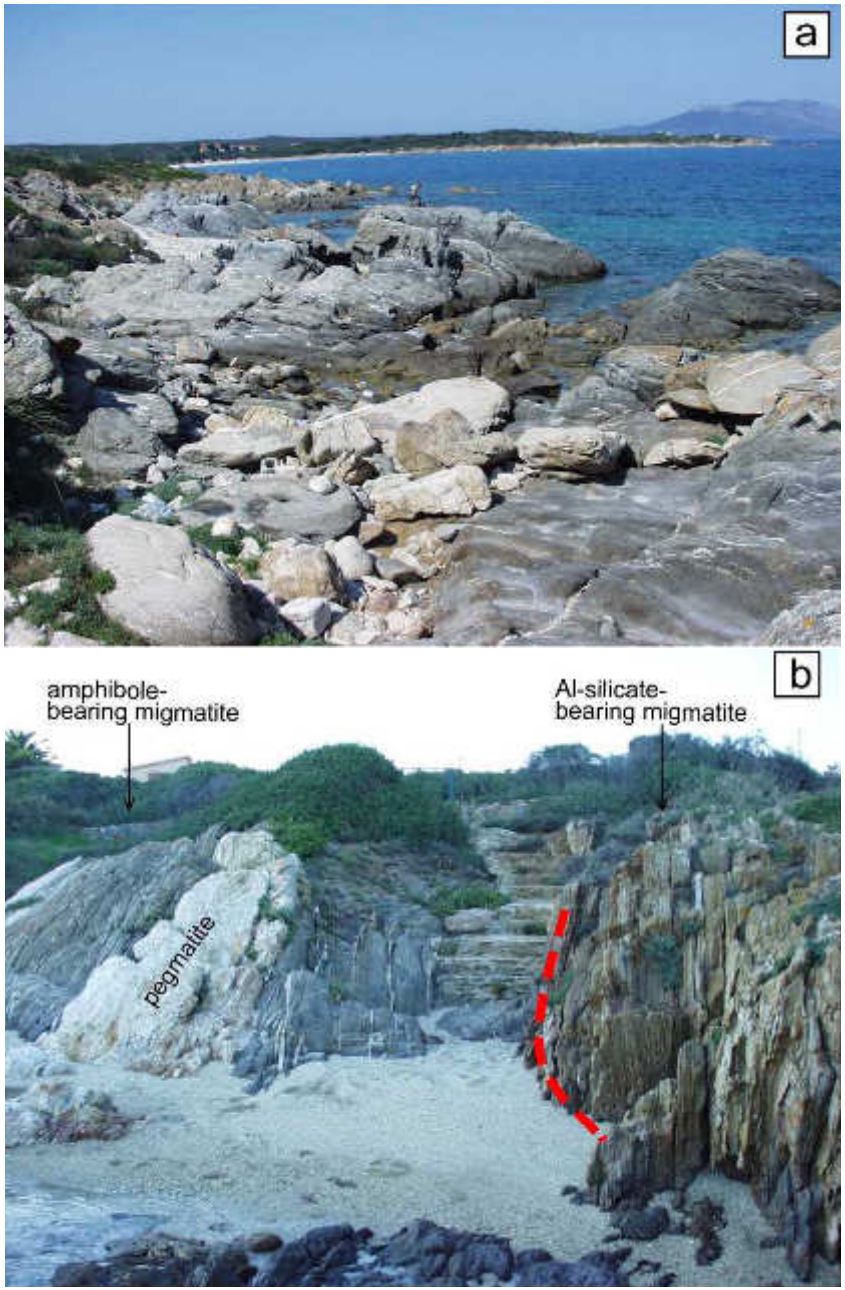

between the amphibole-bearing migmatite and the other two migmatite types is parallel to the regional main foliation (S_2). Two additional 2-3m x 100m lenses of amphibole-bearing migmatite (Fig. 3.3a) are included in the migmatized orthogneiss. Zircon morphology reveals that the amphibole-bearing migmatite originated from an igneous protolith, whose emplacement age was constrained at 452±3 Ma with Pb–Pb zircon evaporation analyses and at 461±12 Ma with Pb-Pb isochrons (Cruciani et al., 2008b).

DOI: 10.3301/GFT.2015.03

The amphibole-bearing migmatite shows an N 145° 80° NE foliation, which transposes leucosomes and rods of quartz + feldspars on the XY plane oriented N 135° 25° SE. The only evidence of a pre-D2 deformation is the occurrence of a gneissose layering (D1) pre-dating the most pervasive D2 folding phase. An oriented biotite lineation trending N139° and plunging 15° to the SE has been observed on S2 schistosity. Sheath folds also occur. The amphibole-bearing migmatite shows discontinuous banding on the scale of 5–10 cm to a few meters, which is defined by alternating, well-foliated biotite-rich mesosomes and poorly-foliated quartz-feldspathic leucosomes parallel to the main foliation or folded by D2 deformation. The leucosomes are coarse-grained and poorly-foliated, and occur as elongated, folded leucosomes ranging in thickness from 2 to 4 cm, as discordant leucosomes, and as pods or patches up to 30–50 cm long (Fig. 3.6a, b, c, d). Coarse-grained pegmatite type leucosomes have also been observed. The most striking feature of the leucosomes is the occurrence of idioblastic amphibole grains up to 2 cm in size. Variable amphibole content has been observed within individual leucosomes or between different leucosomes. Some leucosomes are flanked by mafic selvages up to a few mm thick, consisting of oriented biotite trails. In the amphibole-bearing migmatites, two different types of leucosomes can be observed: tonalitic leucosomes and granodioritic to granitic leucosomes. The tonalitic leucosomes are made up of quartz, plagioclase, amphibole, garnet (<1-2%), and minor

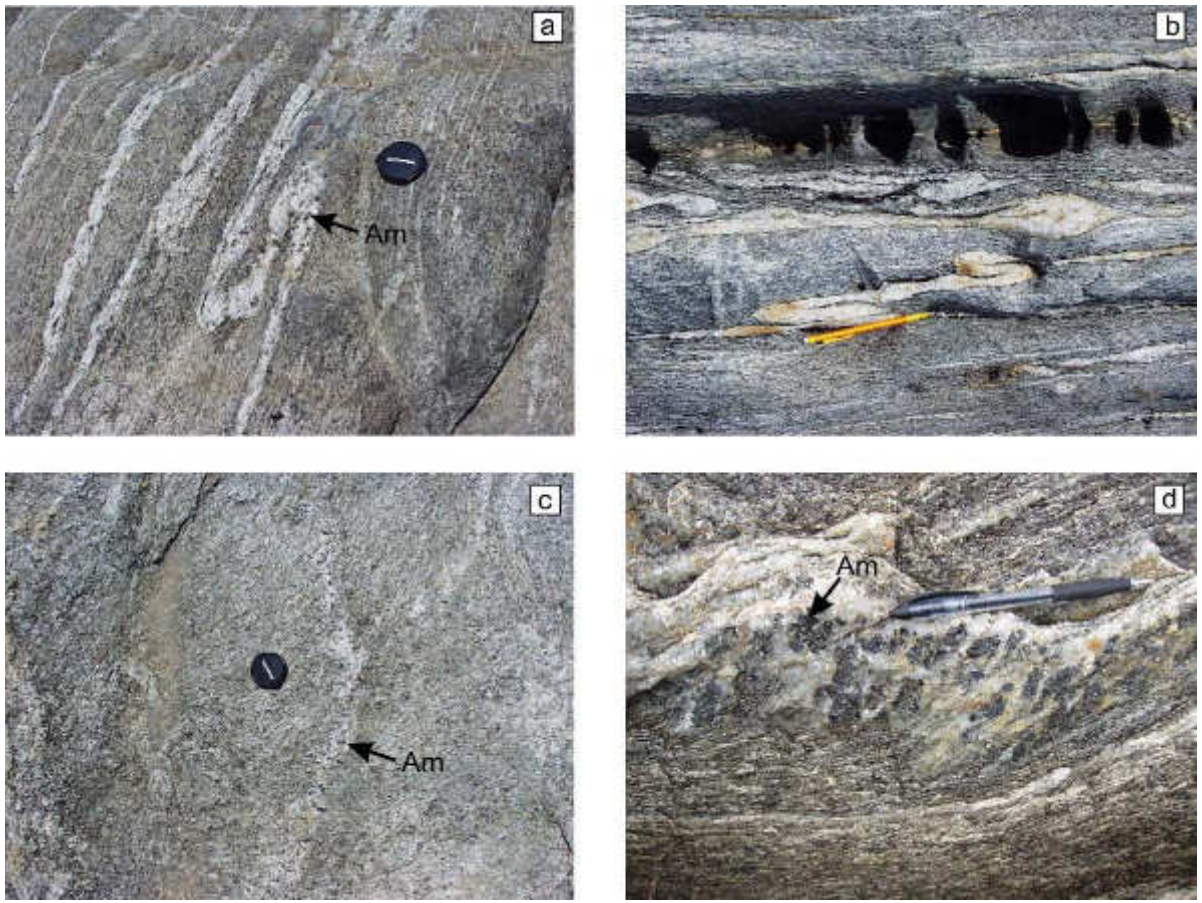

Fig. 3.6 - **a)** Amphibole-bearing leucosome folded by the D2 folding phase; **b)** folded and boudinaged leucosome; **c)** elongated leucosome, discordant with respect to the main D2 regional foliation; **d)** leucosome patch oriented parallel to the main D2 regional foliation.

DOI: 10.3301/GFT.2015.03

biotite (<5%). Accessory phases are apatite, zircon, and titanite. Trace amounts of K-feldspar are rarely preserved as wormy intergrowths in plagioclase. Albite content in plagioclase ranges from Ab_{42-56}.
Amphibole is a K-rich-pargasite ($X_{Mg} \cong 0.51$) showing several small and rounded inclusions of plagioclase, quartz, garnet, and biotite (Figs. 3.7a, b). Retrograde biotite growth on amphibole as well as worm-like microstructures at the amphibole-biotite interface have been observed. Garnet (Alm_{51-53} $Prp_{\sim 7}$ Grs_{32-34} $Sps_{\sim 7}$) occurs as small grains (0.6 mm in diameter), usually enclosed in amphibole (Fig. 3.7b). Less common granodioritic to granitic leucosomes are restricted to the two lenses in the migmatized orthogneiss (Fig. 3.3a). They are fine-grained and characterized by the occurrence of abundant K-feldspar (up to 30%).

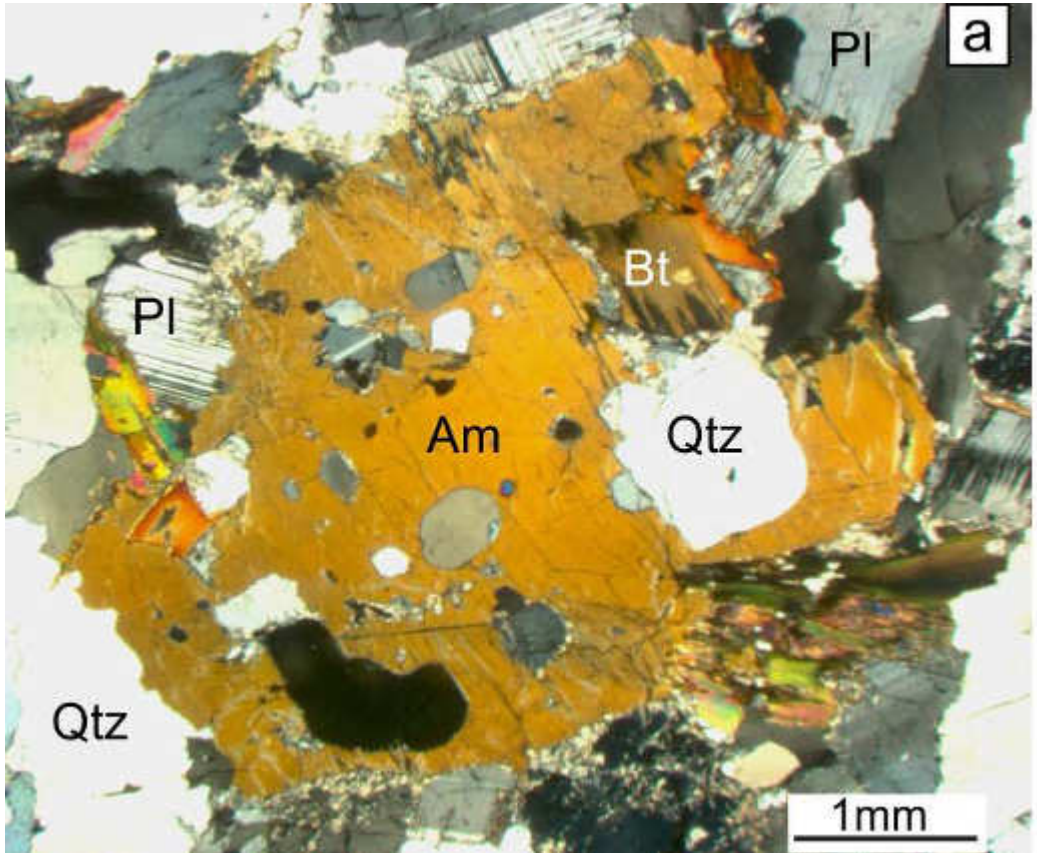

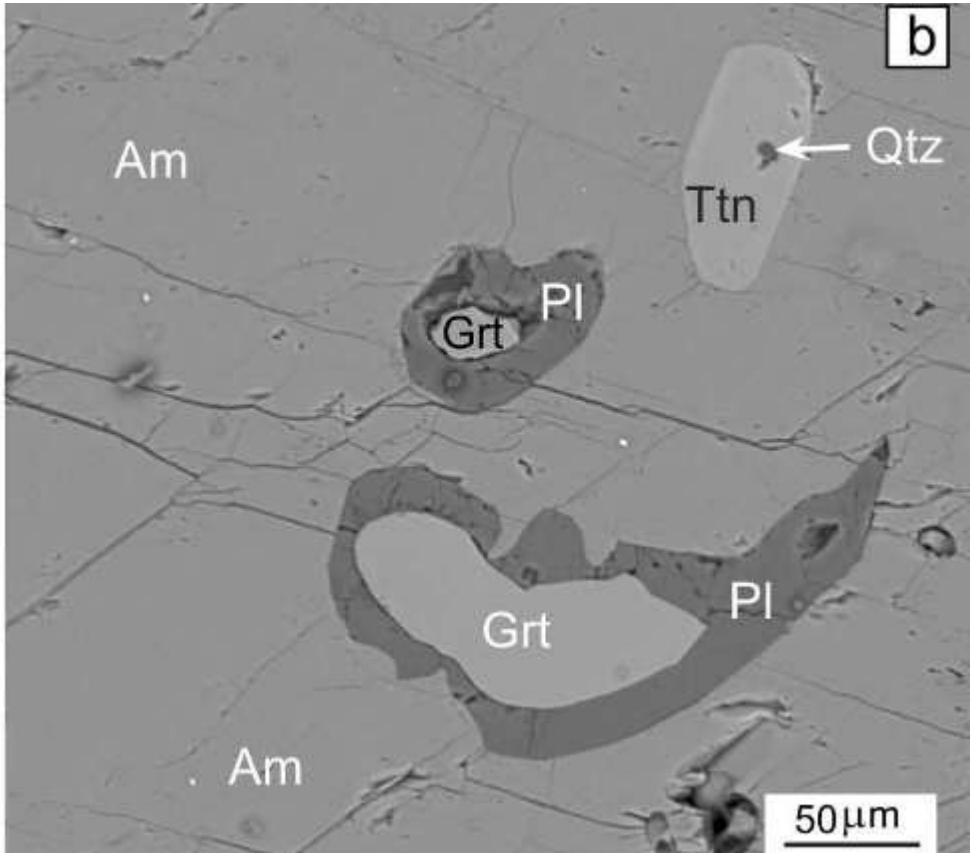

Fig. 3.7 - **a)** Photomicrograph of a tonalitic leucosome from the amphibole-bearing migmatite. Amphibole contains inclusions of quartz and feldspar; biotite occurs at the margin of the amphibole crystal, CPL; **b)** SEM image of garnet crystals surrounded by a plagioclase rim enclosed in amphibole (from Cruciani et al., 2008b).

DOI: 10.3301/GFT.2015.03

The mesosomes of the amphibole-bearing migmatite are made up of the same minerals in different modal proportions (Qtz: 35-45vol.%, Pl: 35-45%, Bt: 10-20%, Am: <5%, Grt <2%).
The composition of amphibole, averaged from 23 analyses, is as follows: Si: 6.25 a.p.f.u., Ti: 0.10; Al: 1.26; Fe^{2+}: 1.74; Fe^{3+}: 0.4; Mg: 1.93; Ca: 1.85; Na: 0.35; K: 0.29; 0.5 Na + K a.p.f.u. (Massonne et al., 2013). The most Si-rich amphibole was found at the outermost rim, with a Si content of 6.91 a.p.f.u. The Si-rich amphibole is richer in iron and poorer in cations occupying the 12-fold coordinated site such as K (Fig. 3.8). Amphibole shows trace element patterns partly similar to those observed for the bulk leucosomes and mesosomes. The most significant differences are the lower concentrations of Cs, Pb, Cu, and U in amphiboles as compared to the bulk rocks. REE in amphibole are enriched relative to chondritic values with absolute concentrations ranging from 19 to 114 ppm. Rim-core-rim traverses revealed that amphibole rims have higher REE, and a wide range of negative Eu anomalies compared to the cores, which show lower REE and slight to marked positive Eu anomalies (Cruciani et al., 2014b).
P-T pseudosections, calculated for an average mesosome composition are used to estimate P-T conditions of the anatectic event, whereas P-T pseudosections calculated for the average bulk composition of leucosomes are used to determine which mineral phases crystallized from the anatectic melt (Massonne et al., 2013).

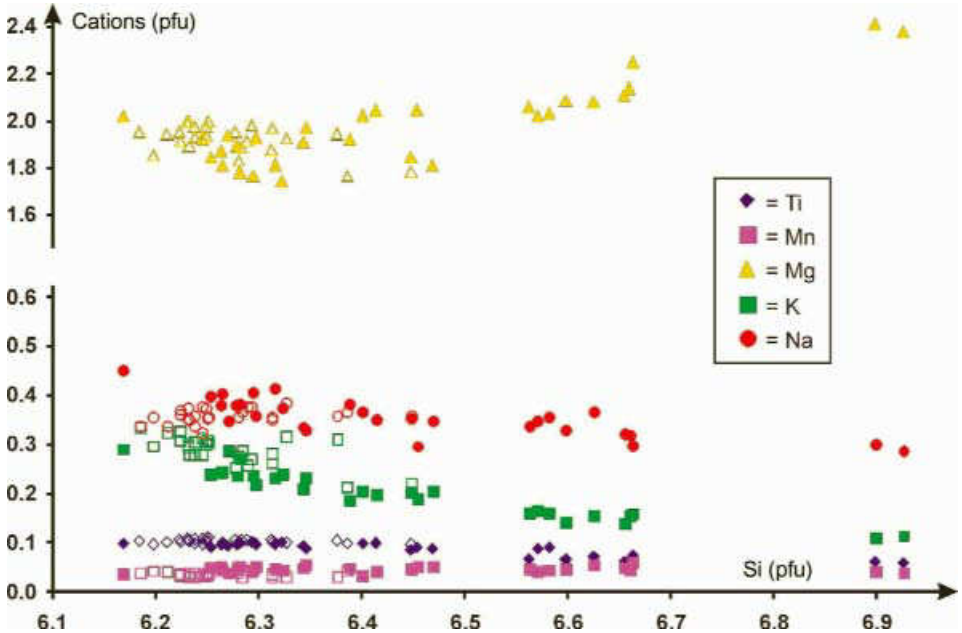

P–T conditions close to 1.3 GPa and 700°C are interpreted as the conditions of partial melting.
Similarly, contoured values for amphibole composition and amphibole modal content calculated for the P-T pseudosection for the leucosome composition resulted in conditions of about 1.05 GPa and 700°C for the crystallization of amphibole in the leucosome melt, and 0.9 GPa and 680°C for complete crystallization of the melt (Massonne et al., 2013).

Fig. 3.8 - EMP analyses of amphibole plotted as various cations versus Si content (a.p.f.u.). Open symbols refer to analyses in the extended core area, whereas closed symbols are related to analyses of outermost amphibole rims (Massonne et al., 2013).

DOI: 10.3301/GFT.2015.03

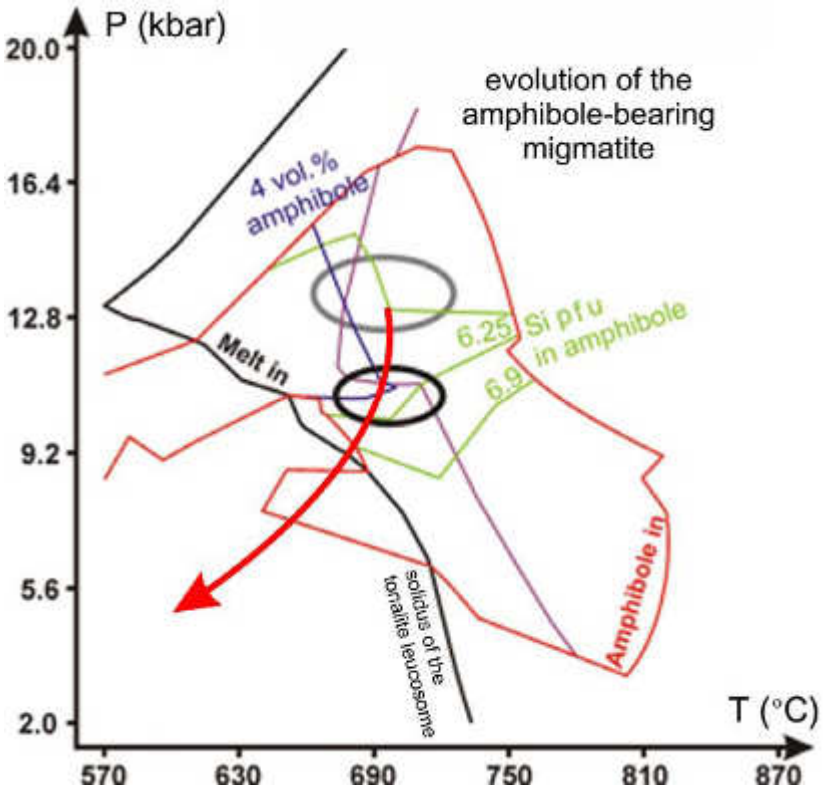

These P-T conditions are compatible with those obtained by Cruciani et al. (2008; 1.0–1.2 GPa, 700–750◦C) with conventional geothermobarometry. The clockwise P-T path shown in Fig. 3.9 implies that the melt must have resided in the rock during exhumation from about 45 to 30 km depth and thus over a long period of time.

Fig. 3.9 - P-T evolution of the amphibole-bearing migmatite modified from Massonne et al. (2013). The red line represents the amphibole stability field, the violet line is 60 vol. % melt, the blue line is 4 vol. % amphibole, the black line is the melt-in curve, and the green line is Si (a.p.f.u.) content in amphibole. Grey ellipse: P-T conditions of the migmatization event; black ellipse: P-T conditions of crystallization of the leucosome melt. The red arrow corresponds to P-T path of the amphibole-bearing migmatite.

STOP 3.3: Al-silicate-bearing migmatite at Punta Sirenella-Punta Bados (N 40° 56’ 40,3”; E 9° 34’ 18.05”).

The Al-silicate bearing migmatite of Punta Sirenella (Fig. 3.4) is layered with centimeter-sized leucosomes (Fig. 3.10a, b) that have a trondhjemitic and occasionally granitic composition (Cruciani et al., 2008a). In a few spots, as in the Stop 3.3, they are strongly mylonitized. The leucosomes, with length varying from a few centimeters to 1–2 m, occur as elongated layers which are often deformed, stretched and strongly folded. Leucosomes also occur as discontinuous to boudin-shaped centimeter-sized patches parallel to the main regional schistosity. Another type of leucosome, often coarse-grained and quartz-rich, has a pegmatitic appearance. The trondhjemitic leucosomes are locally bordered by millimeter-thick biotite-rich melanosomes. Fibrolite folia, patches, or veinlets, and coarse-grained muscovite (up to a few cm) are very common in the migmatite.

DOI: 10.3301/GFT.2015.03

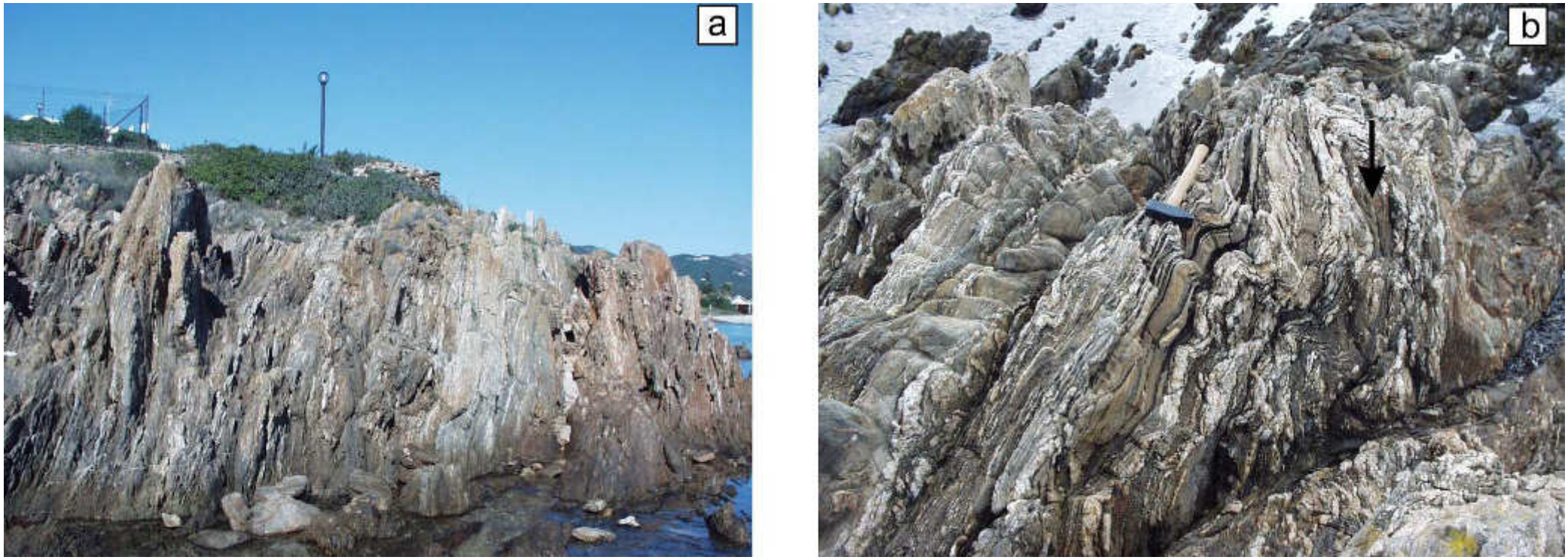

Fig. 3.10 - **a)** Panoramic view of the Al-silicate bearing migmatite outcrop from Punta Sirenella-Punta Bados; **b)** coarse-grained, deformed and gently folded trondhjemitic leucosome bordered by a thin melanosome.

At least three deformation phases (D1, D2, D3) have been identified in the migmatite. D1, not clearly recognizable in the field, is manifested by the transposition of centimeter-sized leucosomes. The D2 phase is revealed by N140° trending isoclinal folds with a SE plunge of 2–18°.
Three different poly-mineralogical lineations along the S2 schistosity have been recognized: the oldest consists of rods and/or pencils of plagioclase+quartz; the second is a fibrolite+quartz mineralogical lineation (Fig. 3.11a) trending N 158° and plunging 20–30° to the SE, at a 0–20° angle with the previous mineralogical lineation; and the third consists of muscovite (Fig. 3.11b), which may overprint the fibrolite+quartz lineation. Shear folds, shear band boudins, sigma porphyroclasts, and kinematic indicators related to the rods and pencils of plagioclase+quartz indicate a top-to-the NW sense of shear, while those associated with the fibrolite+quartz and muscovite (D2 phase) lineations suggest a top to the SE component of shear. The

DOI: 10.3301/GFT.2015.03

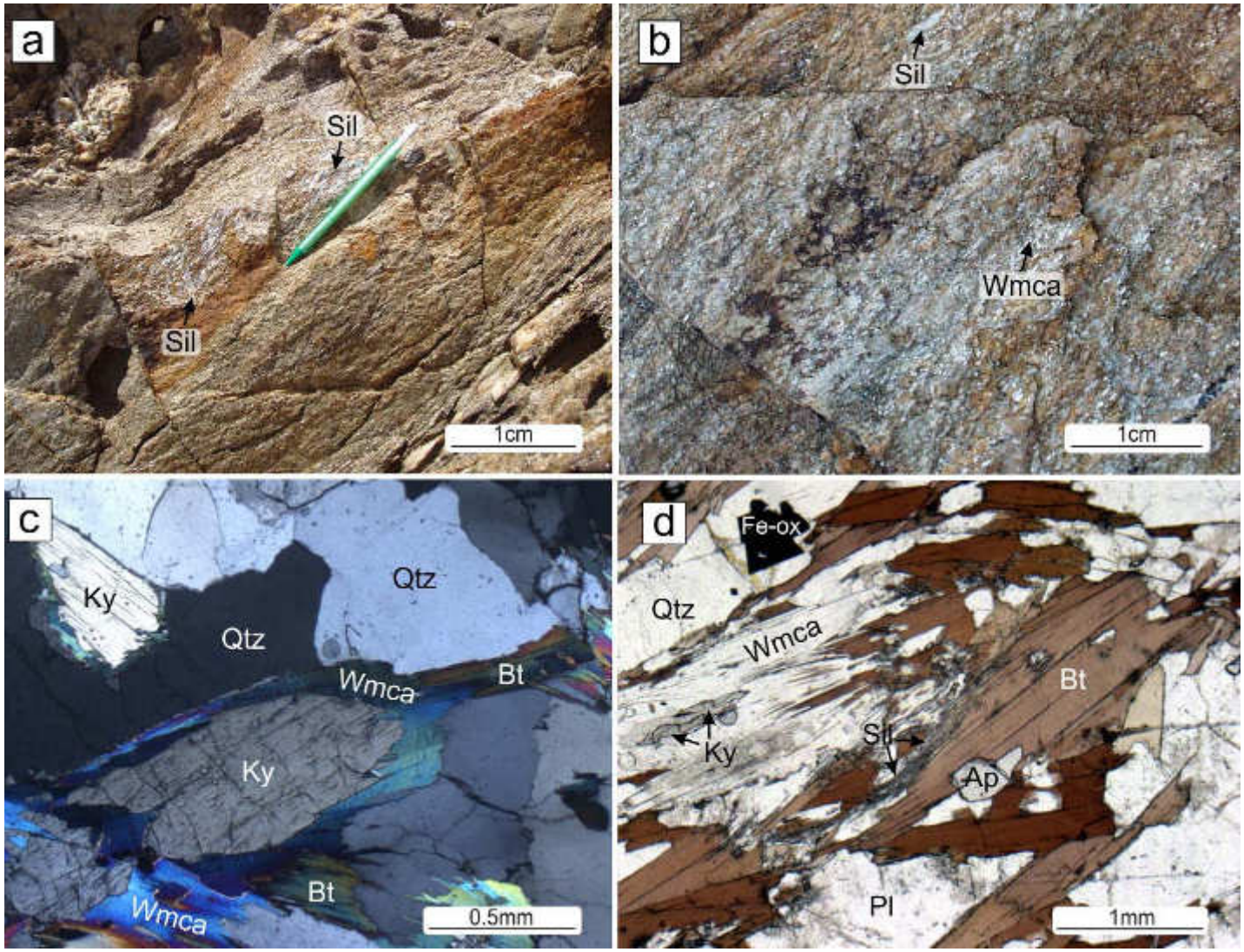

Fig. 3.11 - **a)** Sillimanite lineation along the S2 schistosity; **b)** late crosscutting muscovite along the S2 schistosity; **c)** kyanite surrounded by retrograde muscovite in a matrix mainly made up of quartz, plagioclase, and biotite, CPL; **d)** biotite and fibrolitic sillimanite surrounded by a quartz-feldspathic matrix made up of plagioclase and quartz. PPL.

trondhjemitic leucosomes (Figs. 3.11c, d) consist of plagioclase (oligoclase An_{20-23} surrounded by a thin, discontinuous albite rim), quartz, biotite (X_{Mg}~0.4-0.5), ± garnet (Alm_{65-72} Prp_{12-17} Grs_{3-5} Sps_{8-20}), ± kyanite, ± sillimanite, trace amount of K-feldspar, and abundant retrograde muscovite (Si: 6.04-6.15 a.p.f.u.). The accessory minerals are zircon, apatite, rutile, and monazite.

The rare granitic leucosomes differ from trondhjemitic ones only by the increase in modal content of K-feldspar, which ranges up to 25%. The mesosome is made up of the same minerals but in different modal proportions, though in some cases, mesosomes only consist of quartz, plagioclase, biotite and muscovite. The melanosomes are characterized by a high biotite content.

The main textural features of the kyanite migmatite are the following: i) kyanite is partially replaced and

DOI: 10.3301/GFT.2015.03

rimmed by fine- to medium-grained muscovite (Fig. 3.11c); ii) fibrolite occurs as isolated needles growing on and mantling biotite flakes (Fig. 3.11d); iii) in trondhjemitic leucosomes, K-feldspar occurs as small rare crystals; and iv) coarse-grained muscovite crosscutting the fabric includes fibrolite needles.

According to the CIPW norm, the leucosomes are corundum–hypersthene normative. In the normative An–Ab–Or classification diagram by Barker (1979), most leucosomes have trondhjemite-like compositions, whereas only a few of them plot in the granite field (Fig. 3.12b).

The leucosomes have higher SiO_2, CaO, Na_2O, and Sr and lower Al_2O_3, Fe_2O_3, MgO, TiO_2, K_2O, P_2O_5, Rb, Ba, Cr, V, Zr, Nb, Zn, and REE content with respect to the mesosome. In some leucosomes, the relatively high content of calcium and ferromagnesian elements suggests entrainment of restitic plagioclase, biotite and accessory phases. Most leucosomes show low REE content, moderately fractionated REE patterns, and a marked positive Eu anomaly. On the basis of

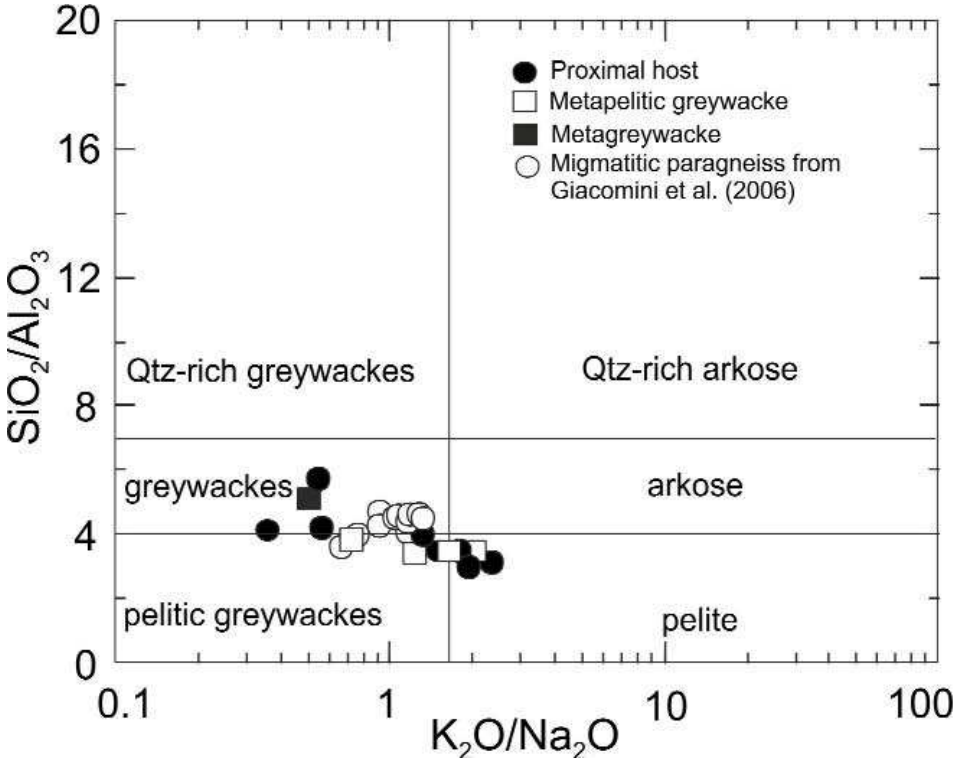

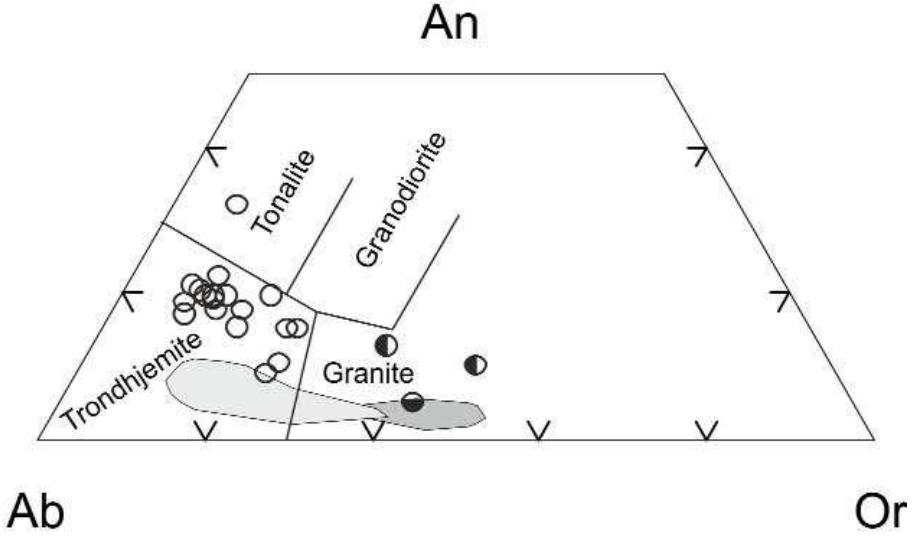

Fig. 3.12 - (**a**) Geochemical composition of selected unmelted rocks (metapelitic greywacke, metagreywacke) and proximal hosts (mesosome) from the Al-silicate-bearing migmatite; composition of migmatitic paragneisses north of Punta Sirenella area (Giacomini et al., 2006) is reported for comparison; (**b**) normative Ab–An–Or content of leucosomes in the classification diagram proposed by Barker (1979). Compositional ranges of experimental melts generated by muscovite dehydration melting (grey) and H_2O-fluxed melting (light-grey) from muscovite–biotite schist (Patiño Douce & Harris, 1998) are also shown.

DOI: 10.3301/GFT.2015.03

SiO_2/Al_2O_3 vs. K_2O/Na_2O ratios, the original sedimentary sequence is classified as an alternating sequence of greywackes, pelites, and pelitic greywackes (Fig. 3.12a).
The protolith of Al-silicate-bearing migmatite underwent partial melting at high-pressure with approximately 1.5-2.0 wt.% of H_2O (Cruciani et al., 2014a). Subsequently, pressure release and slight cooling resulted in the crystallization of the leucosome melt to form, among other phases, kyanite and biotite. After the formation of kyanite-bearing leucosomes, the migmatite of Punta Sirenella underwent some metamorphic re-equilibration including the formation of fibrolite and coarse-grained muscovite. The last stage of mineralogical re-equilibration is documented by the widespread formation of coarse-grained muscovite in leucosome and mesosome. The P-T estimates obtained using a P-T pseudosection yielded T ~ 700-740 °C, P ~ 1.1-1.3 GPa for the partial melting event and ~ 660-730 °C, ~ 0.75-0.90 GPa for melt crystallization (Cruciani et al., 2014a). The trondhjemitic leucosomes were generated by H_2O-fluxed melting whereas the rare granitic leucosomes reveal peritectic K-feldspar produced by muscovite-dehydration melting.

STOP 3.4: Calc-silicate nodule of Punta Sirenella (N 40° 56′ 38,6″; E 9° 34′ 19.6″).

Calc-silicate nodules hosted in migmatite are very common in the HGMC of NE Sardinia and in the Posada Valley. Calc-silicate nodules have been classified as either oblate or prolate ellipsoids by Elter et al. (2010). The calc-silicate nodules cropping out at Punta Sirenella (Figs. 3.13a, b) have rounded to elliptical shapes with the longer axis parallel to the S2 schistosity of the enclosing migmatites. Based on colour and grain size, up to six different layers are recognizable, though usual just the following three are seen: i) medium-grained, light-brown core; ii) intermediate and concentric epidote-rich layers; and iii) fine-grained, dark-colored rim.

Fig. 3.13 - (**a**), (**b**) field appearance of calc-silicate nodules hosted in the Al-silicate-bearing migmatite outcrops north of Punta Sirenella.

DOI: 10.3301/GFT.2015.03

The core (Fig. 3.14a) is made up of fine to medium-grained quartz, diopside (X_{Mg}:~0.60; up to 40% modal content), garnet ($Alm_{\sim 45}$ $Prp_{\sim 8}$ $Grs_{\sim 39}$ $Sps_{\sim 8 mol.\%}$; up to 48% modal amount), anorthite, and subordinate Mg-hornblende.
The intermediate layers (2 to 5 cm thick) are fine to medium-grained. They consist of a variable amount of epidote (35-60vol.%), opaque minerals (20-30%), plagioclase (5-30%), garnet (5-10%), and clinopyroxene. These layers are cut by several epidote-rich veins. Fe^{3+} content of epidote ranges from 0.40 to 0.56 a.p.f.u.
The dark-colored, fine-grained rim (Fig. 3.14b) ranges in thickness from 5 to 10 mm. It consists mainly of pale-green coarse-grained amphibole (30%), quartz (20%), garnet (20%), plagioclase (30%), and rare clinopyroxene. Amphibole is Mg-hornblende (Si: 6.5 - 6.7 a.p.f.u., X_{Mg}: 0.6 - 0.7, Na: ~ 0.2 a.p.f.u.). Fine-grained titanite has occasionally been observed.
The nodules do not show a systematic and regular trend of variation of major elements. However, among these elements, only Fe_2O_3tot shows a rather flat, constant pattern from core to rim. All the other elements show

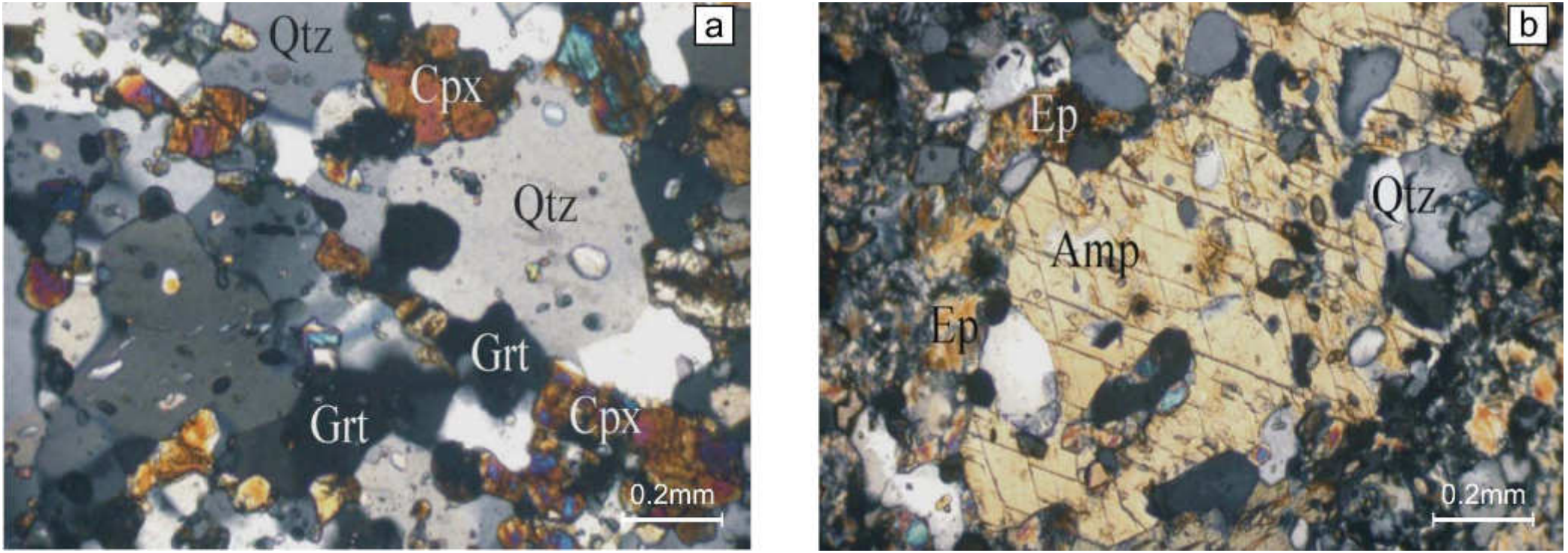

Fig. 3.14 - **a)** Microstructure of the core of the calc-silicate nodule mainly consisting of quartz, garnet and diopside; CPL; **b)** microscopic appearance of the amphibole-rich outer rim of the calc-silicate nodule; CPL.

DOI: 10.3301/GFT.2015.03

an irregular rim-core-rim pattern which probably reflects the strong variability in mineralogical composition observed among different layers. The high Al_2O_3 (19.65wt%) and alkali (Na_2O=1.15 wt%; K_2O=3.18wt%) and low CaO (12.70 wt%) content of the intermediate layer is indicative of the contribution of Al- and alkali-rich phases (such as epidote and amphibole, respectively) and the depletion of Ca-rich phases (e.g. garnet). The garnet abundance of the other layers is reflected by their high CaO content (19.4 - 25.8 wt.%).
Geothermobarometric calculations have been performed on the cores of nodules that do not show significant hydration and re-equilibration during retrogression. The temperatures estimated using the Grt-Cpx thermometer (calibration after Ellis & Green, 1979 and Powell, 1985) range from 680 to 750 °C, while the Grt-Cpx-Pl-Qtz barometer (calibration after Newton & Perkins, 1982) yields pressures between 0.6 and 0.8 GPa. Slightly higher temperatures and pressures (of about 50 °C and 0.1-0.2 GPa) have been obtained in the Grt-Cpx-Pl-Qtz assemblage.

Return to Strada Provinciale 82, drive on a few of km, and turn left onto the road to M.giu Nieddu.

STOP 3.5: Ultramafic, massive and plagioclase-banded amphibolites of Montiggiu Nieddu (N 40° 57′ 44.75″; E 9° 34′ 35.77″).

Three main lithotypes outcrop at Montiggiu Nieddu: ultramafic amphibolite, massive amphibolite, and plagioclase-banded amphibolite (Figs. 3.15, 3.16a, b, c, d; Franceschelli et al., 2002, 2005a). The ultramafic amphibolite (Figs. 3.15, 3.16a) forms an elongated body of ~ 100 m in length and ~ 40-60 m in thickness cropping out on top of the hill. They are massive to poorly schistose rocks with garnet and amphibole visible to the naked eye. The massive, plagioclase-banded amphibolite (Fig. 3.16b) that represents the dominant lithology at Montiggiu Nieddu, consists of alternating dark-green and white bands, possibly reflecting an original magmatic layering. They form a N-S oriented body, ~ 1000 m in length and ~ 60 m in thickness. The dark bands, from some decimeters to a few meters in thickness, consist

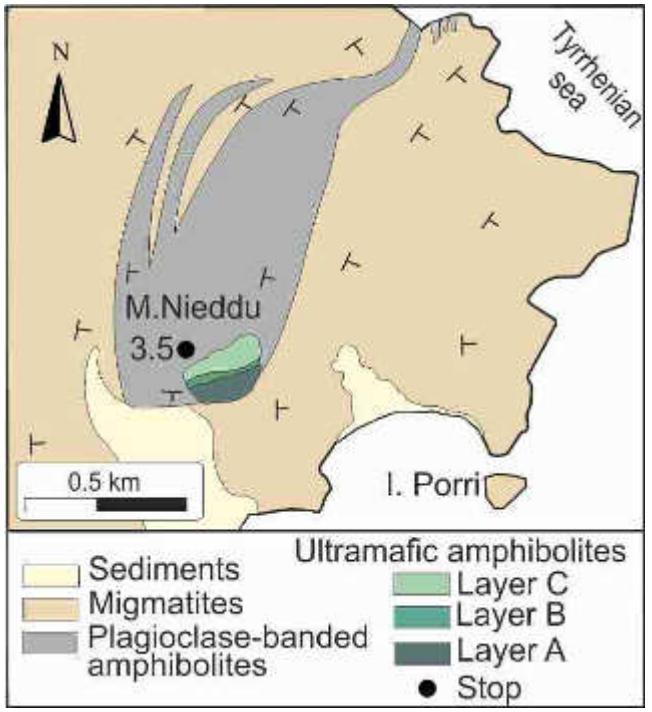

Fig. 3.15 - Geological sketch map of the Montiggiu Nieddu area from Franceschelli et al. (2002).

DOI: 10.3301/GFT.2015.03

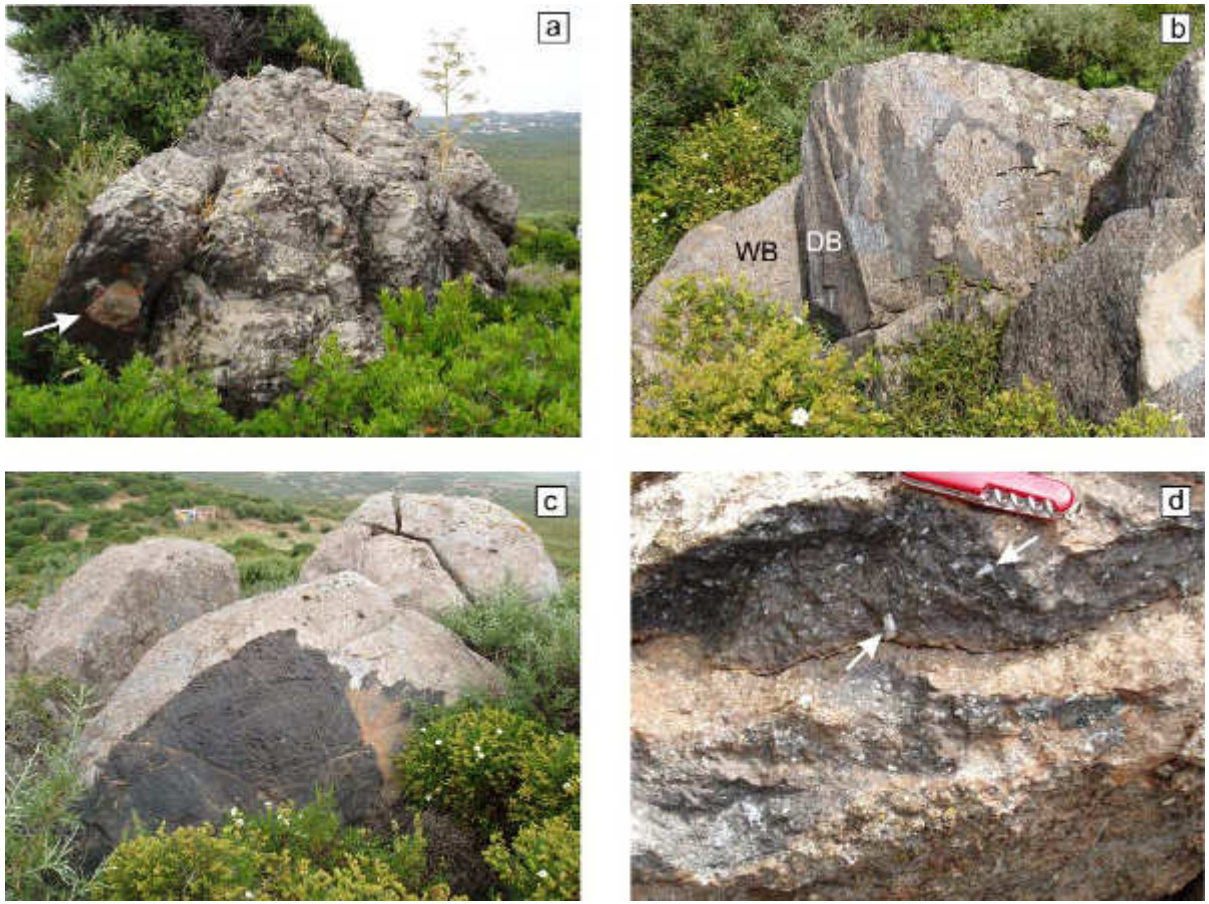

Fig. 3.16 - **a)** Ultramafic amphibolite at the top of Montiggiu Nieddu; the arrow points to a garnet-rich nodule; **b)** white plagioclase-rich (WB) and dark amphibole-rich bands (DB) in the banded amphibolite; **c)** sharp contact between the ultramafic amphibolite and the massive amphibolite; **d)** millimeter-sized plagioclase crystals (arrows) in Layer B of the ultramafic amphibolite.

mainly of amphibole, plagioclase, and rare garnet and pyroxene. The white bands are characterized by an increase in plagioclase content. The regional S2 schistosity is the axial plane foliation of decameter folds.
The contact between the ultramafic amphibolite and the plagioclase-banded amphibolite is sharp and strikes N 40° and dips SE 45° (Fig. 3.16c). It is cut by the secondary foliation, striking N 40° and dipping SE 30°. On the XY plane, a down-dip lineation striking N 160° and dipping 30° to the SE composed of amphibole is seen, while on the XZ plane, some kinematic indicators related to a top-to-the-SE component of shear are recognisable (porphyroclast of amphibole surrounded by plagioclase coronas and quartz + feldspar ribbons folded by isoclinal folds).
The ultramafic amphibolites consist of relics of igneous phases (plagioclase: An_{89-98}; olivine: Fo_{68-71}; orthopyroxene: En_{74-76}; clinopyroxene: Di_{80-88}) and metamorphic minerals (mainly orthopyroxene; diopsidic clinopyroxene; plagioclase: $An_{0.1-74}$; garnet: Alm_{49-62} Prp_{18-27} Grs_{16-25} Sps_{1-3}; Mg-rich chlorite; clino and orthoamphibole) in varying proportions.
Based on the distribution of the relic igneous minerals, three main compositional layers (Layer A, Layer B, Layer C) have been identified in the ultramafic amphibolites.

DOI: 10.3301/GFT.2015.03

Layer A, 20 m in thickness, is made up of coarse-grained olivine, chlorite, amphibole, spinel, and minor pyroxene, garnet, and rare plagioclase.
Layer B is 5 m in thickness and is composed of millimeter-sized plagioclase (Fig. 3.16d), olivine, pyroxene, spinel, garnet, and amphibole. Layer B shows corona textures around igneous olivine and plagioclase (Fig. 3.17). Olivine grains (1–5 mm in size) are surrounded by a shell of orthopyroxene, whereas two different types of amphibole (brown and green amphibole: Am_1, Am_2) surround igneous pyroxene.
Layer C, which is 20-30 m in thickness, is characterized by the presence of porphyroblastic garnet, pyroxene, large amphibole grains (up to 5 cm), and minor plagioclase. Layer C encloses garnet-rich nodules up to 20 cm in diameter (Fig. 3.16a). The nodules are made up of garnet, amphibole, spinel, and large amounts of epidote. Garnet-rich veins, striking N 40° and dipping NW 25°, surrounded by dark amphibole rims, and amphibole and/or epidote-rich veins are also present.
The dark-green and white bands are made up of plagioclase (Ab_{13-88}), amphibole (Mg-hornblende), garnet (Alm_{45-50} Prp_{26-37} Grs_{10-18} $Sps_{1-2.5}$), clinopyroxene (diopside, X_{Mg}: ≅ 0.80), orthopyroxene, and biotite (X_{Mg}: ≅ 0.50). In the white bands, amphibole crystals up to 5 cm in size are

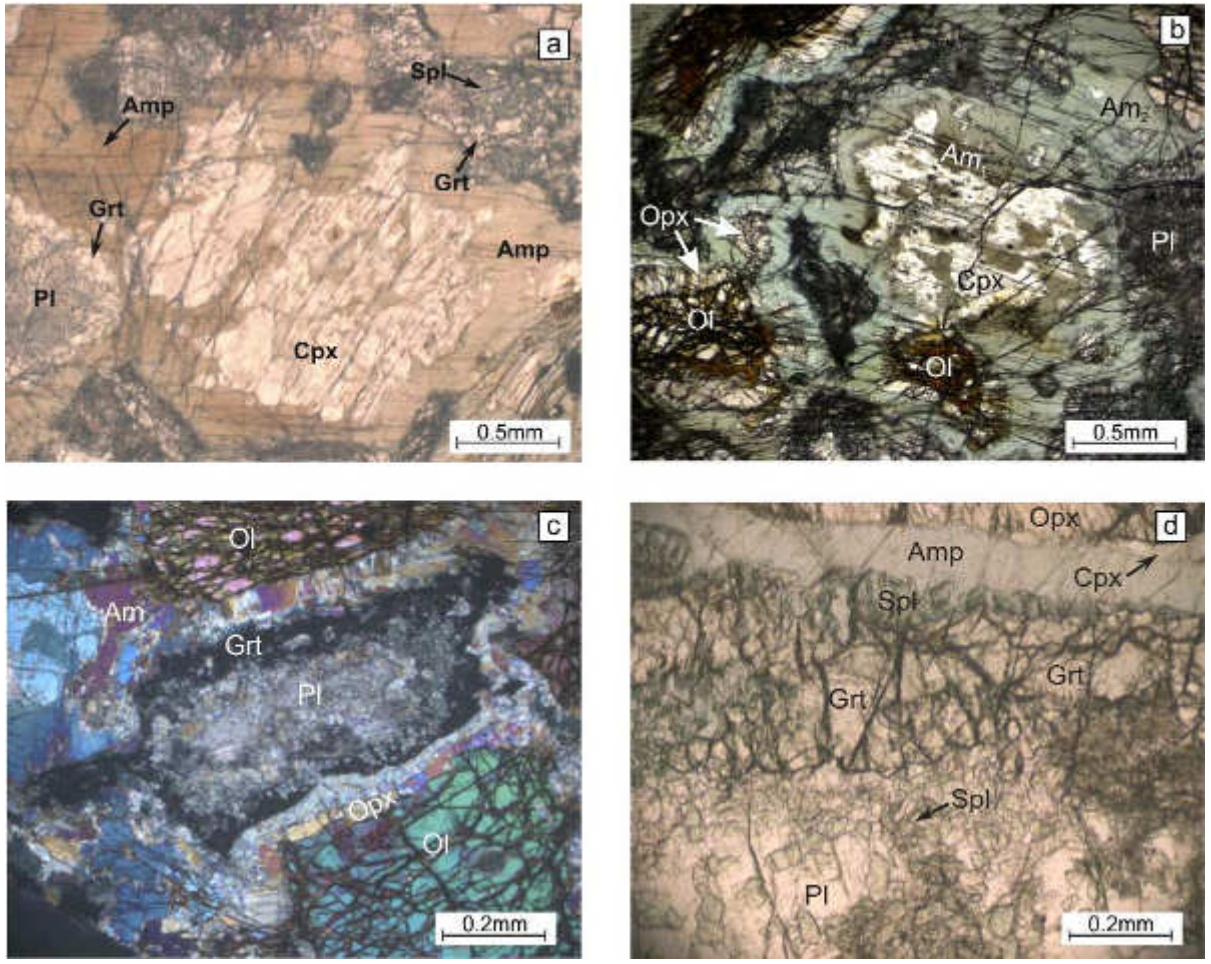

Fig. 3.17 - **a)** Magmatic clinopyroxene overgrown by brown amphibole; PPL; **b)** amphibole replacement of clinopyroxene in the rocks of Layer B of the ultramafic amphibolites; orthopyroxene around olivine can also be observed; PPL; **c)** garnet coronas around plagioclase at the interface between plagioclase and olivine in the rocks of Layer B; CPL; **d)** detail of corona between plagioclase and orthopyroxene; PPL, from Franceschelli et al. (2002).

DOI: 10.3301/GFT.2015.03

visible with the naked eye. Amphibole and garnet show -porphyroclast structures on the XZ plane related to a top-to-the-SE component of shear correlated with the tectonic framework of the surrounding migmatites.
Major elements of selected samples of Layers A, B, C are shown in Table 2. On the basis of the CIPW norm, the rocks of M.giu Nieddu show a composition ranging from olivine meta-gabbros, quartz-gabbros, and leuco-gabbros to trondhjemite. According to Ghezzo et al. (1979), the mafic-ultramafic amphibolites are genetically related by processes of cumulitic differentiation of an original continental rift type tholeiitic basaltic magma.
This conclusion is supported by the fractionation trend in the CaO versus MgO diagram (Fig. 3.19a) redrawn from Cruciani et al. (2002). The Ti/Y-Nb/Y diagram suggests a tholeiitic affinity (Fig. 3.19b).

The metamorphic evolution of the Montiggiu Nieddu metabasite (P-T path in Fig. 3.18) may be divided into three stages (Franceschelli et al., 2002): granulite, amphibolite and greeschist.

Table 2 - Major element composition for selected samples of Layers A, B, C of the ultramafic amphibolite as well as dark (DB) and white bands (WB) of the banded amphibolite and garnet-rich nodules (N) from M.giu Nieddu (from Cruciani et al., 2002).

Layer	A	B	C	N	DB	WB
(wt%)						
SiO_2	41.13	41.12	44.18	41.09	48.95	60.36
TiO_2	0.13	0.10	0.60	0.27	1.24	0.81
Al_2O_3	8.85	13.90	15.29	15.82	13.86	14.78
Fe_2O_{3tot}	18.08	15.49	12.38	14.23	13.92	7.44
MnO	0.24	0.21	0.13	0.25	0.20	0.12
MgO	22.84	17.86	9.94	12.35	7.50	4.28
CaO	6.27	9.60	14.30	13.28	11.13	7.82
Na_2O	0.78	0.72	1.05	1.00	2.41	3.47
K_2O	0.07	0.05	0.22	0.12	0.07	0.09
P_2O_5	0.06	0.02	0.03	0.04	0.15	0.14
LOI	1.55	0.93	1.88	1.55	0.57	0.69

Stage I is characterized by the development of orthopyroxene coronas, clinopyroxene, green spinel, and garnet around igneous olivine and anorthite. In some samples, garnet containing corundum inclusions has completely replaced the igneous plagioclase. A remarkable feature of the coarse-grained orthopyroxenes is the inclusion of opaque mineral trails that can be interpreted as exsolution textures of an igneous Fe-rich pyroxene.
Stage II is dominant and represents pervasive growth of large amphibole grains containing coronas around olivine and plagioclase grains. Brown and green clinoamphibole, colourless amphibole, and orthoamphibole replace pyroxene and garnet. Often the amphibole growing on igneous pyroxene shows a brown core and a green rim. The other minerals developed during the amphibolite stage are anthophyllite, Mg-rich chlorite, plagioclase, and spinel. Worthy of note is the occurrence of chlorite associated with clinoamphibole, orthoamphibole, olivine, and orthopyroxene in the rocks from Layer A.

DOI: 10.3301/GFT.2015.03

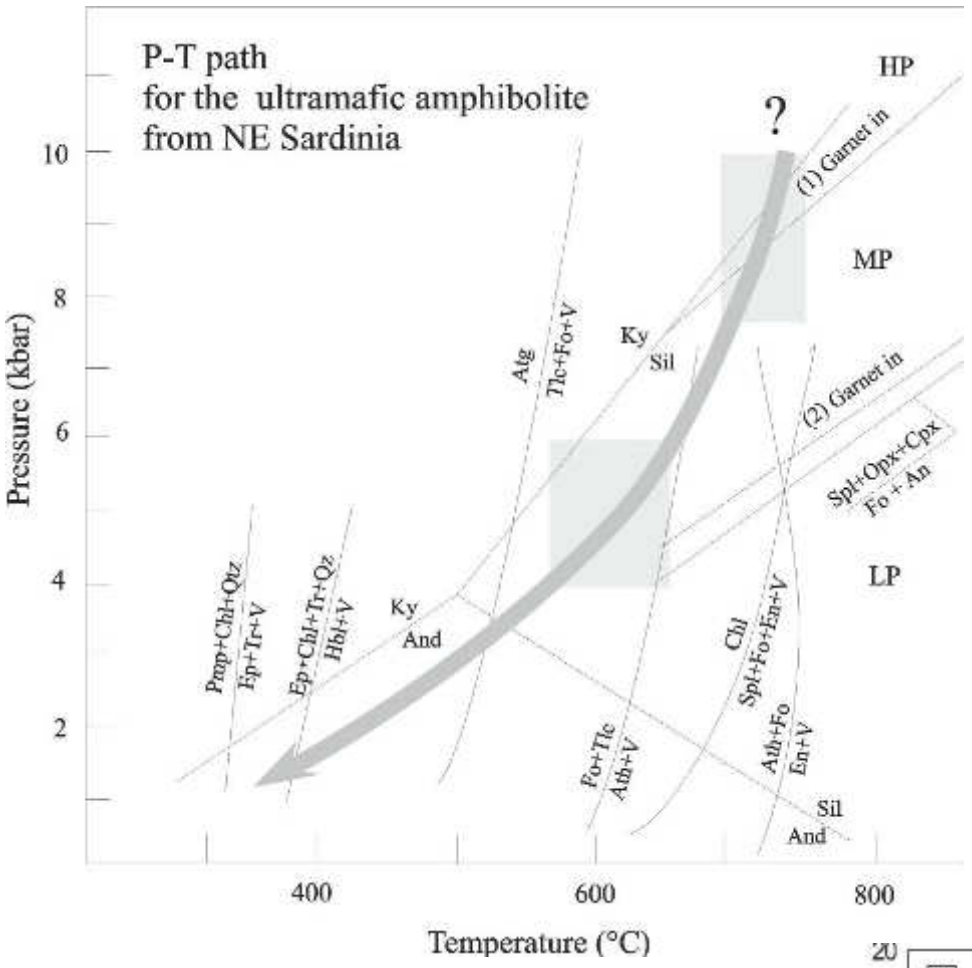

Fig. 3.18 - P–T path for ultramafic amphibolite of Montiggiu Nieddu from Franceschelli et al., 2002 (modified). Aluminium silicate triple points from Holdaway (1971). Pmp + Chl + Qtz = Ep + Tr +V and Ep + Chl + Tr + Qtz = Hbl +V after Liou et al. (1987). The reactions: Atg = Tlc + Fo +V, Fo + Tlc = Ath +V, Chl = Spl + Fo + En +V, Ath + Fo = En +V, Fo + An = Spl + Opx + Cpx were calculated with TWQ 2.02 (Berman, 1991). Reaction curve (1) represents incoming garnet in a typical quartz–tholeiite composition and separates high-pressure (HP) from medium-pressure (MP) granulites (Green & Ringwood, 1967); reaction (2) represents incoming garnet in an undersaturated basalt composition (Ito & Kennedy, 1971) separating medium- and low-pressure (LP) granulites.

Stage III: minerals of this stage mostly replace mafic minerals, and consist of tremolite, chlorite, fayalite, epidote, albite, calcite, dolomite, and serpentine.
The history of the Montiggiu Nieddu mafic and ultramafic amphibolite started with igneous crystallization and continued through granulite (T = 700-750 °C, P ~ 0.8-1.0 GPa), amphibolite (T = 580-640 °C, P = 0.4-0.6 GPa), and greenschist facies (T ~ 330-400 °C, P < 0.2-0.3 GPa).

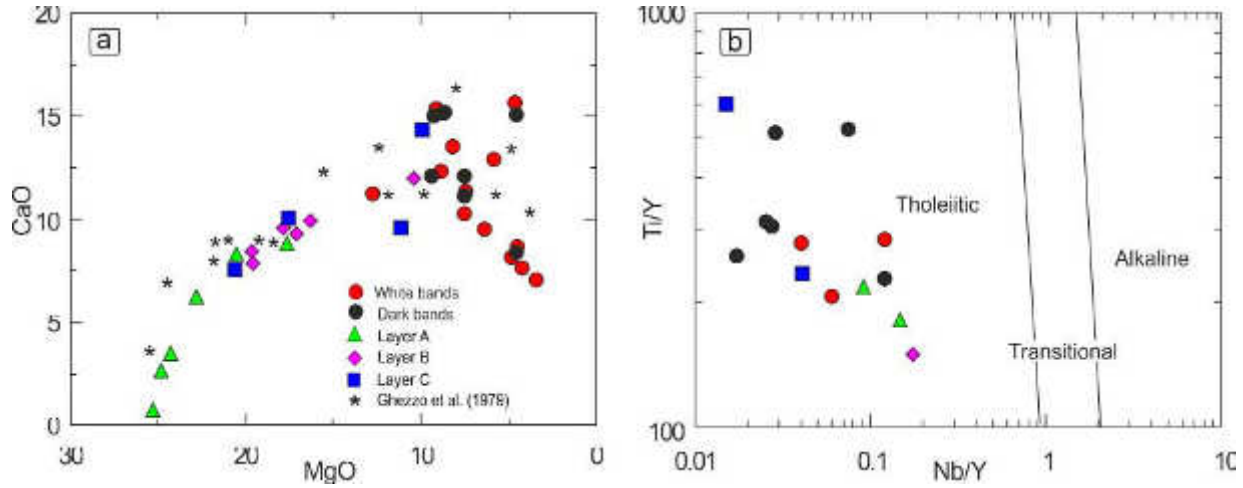

Fig. 3.19 - **(a)** Plot of CaO (wt%) versus MgO; and **(b)** Ti/Y versus Nb/Y discrimination diagram from Pearce (1982) for ultramafic and banded amphibolite from Montiggiu Nieddu; redrawn from Cruciani et al. (2002).

DOI: 10.3301/GFT.2015.03

Return to Strada Provinciale 82 towards Golfo Aranci. Drive a few of km and take a secondary road on the left to Monte Terrata.

STOP 3.6: Metabasite with eclogite facies relics from Monte Terrata and Iles (N 40° 59′ 02.9″; E 9° 33′ 43.36″).

The Migmatite Complex between Golfo Aranci and Pittulongu (Gneiss Complex of Giacomini et al., 2005) contains subordinate ellipsoidal-shaped, large boudins (up to 2 km long) of metabasite lenses with relic eclogitic parageneses and amphibolite. These rocks, hereafter called retrogressed eclogites or eclogites, crop out in lenses parallel to the schistosity of the host rocks (Fig. 3.2). These eclogites are massive (Fig. 3.20a), and are characterized by garnet-rich and garnet-poor layers. The best preserved outcrops occur at Iles and Terrata (Fig. 3.2) where two lens shaped bodies oriented NW-SE preserve omphacite + kyanite and kyanite-bearing paragenesis, respectively.

The eclogitic paragenesis is best preserved within the garnet – rich layers. In order of abundance, these layers contain garnet, clinopyroxene, ± orthopyroxene, amphibole, ± omphacite, ± kyanite, zoisite, plagioclase, rutile, quartz and apatite. Millimetric garnet porphyroblasts (Figs. 3.20b, c) contain inclusions of quartz, amphibole, zoisite,

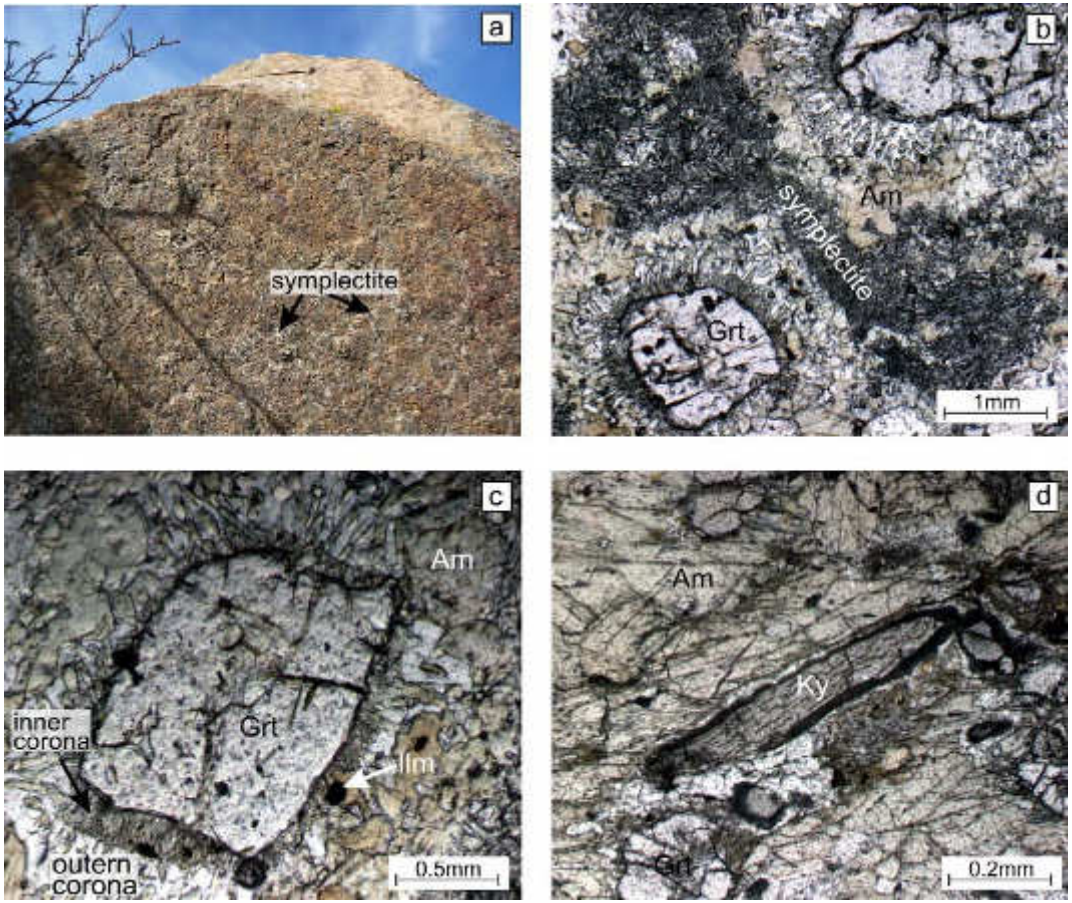

Fig. 3.20 - **a)** Field aspect of the retrogressed eclogite of Terrata: the whitish microstructure indicated by arrows are symplectites. Photomicrographs : **b)** garnet porphyroblasts hosted within the symplectite and surrounded by amphibole + plagioclase coronas; PPL; **c)** inner and outer coronas around garnet; PPL; **d)** elongated kyanite crystal in a strongly re-equilibrated eclogite sample; PPL.

DOI: 10.3301/GFT.2015.03

omphacite, rutile, apatite, kyanite, albite, and zircon preferentially concentrated in the garnet core. Garnet is compositionally zoned with a systematic decrease in calcium, and an increase in magnesium from core to rim. Omphacite, preserved inside the garnet, is partially replaced by Cpx–Pl symplectites; omphacite inclusions are also often associated with inclusions of zoisite and amphibole. Kyanite (Figs. 3.20d, 3.21a) is commonly without inclusions, but inclusions of plagioclase, amphibole and rutile can occasionally be found.

Kyanite is surrounded by a thin corona of anorthite (Ab_{5-10}) + symplectitic spinel lamellae, in turn surrounded by an outer corona of symplectitic sapphirine + Ca-rich ($Ab_{\sim 20}$) plagioclase (Fig. 3.21a). The contact between the two symplectites is sharp and the size of the symplectite lamellae varies. In the symplectites the spinel lamellae are very fine-grained whereas sapphirine lamellae are fine –medium grained. Both spinel and sapphirine lamellae have a well-defined orientation, radiating from kyanite inside the corona. In the kyanite-free-corona, the nucleus of the corona consists of an intergrowth of acicular corundum crystals and Ca-rich plagioclase ($Ab_{\sim 13}$) (Fig. 3.21b).

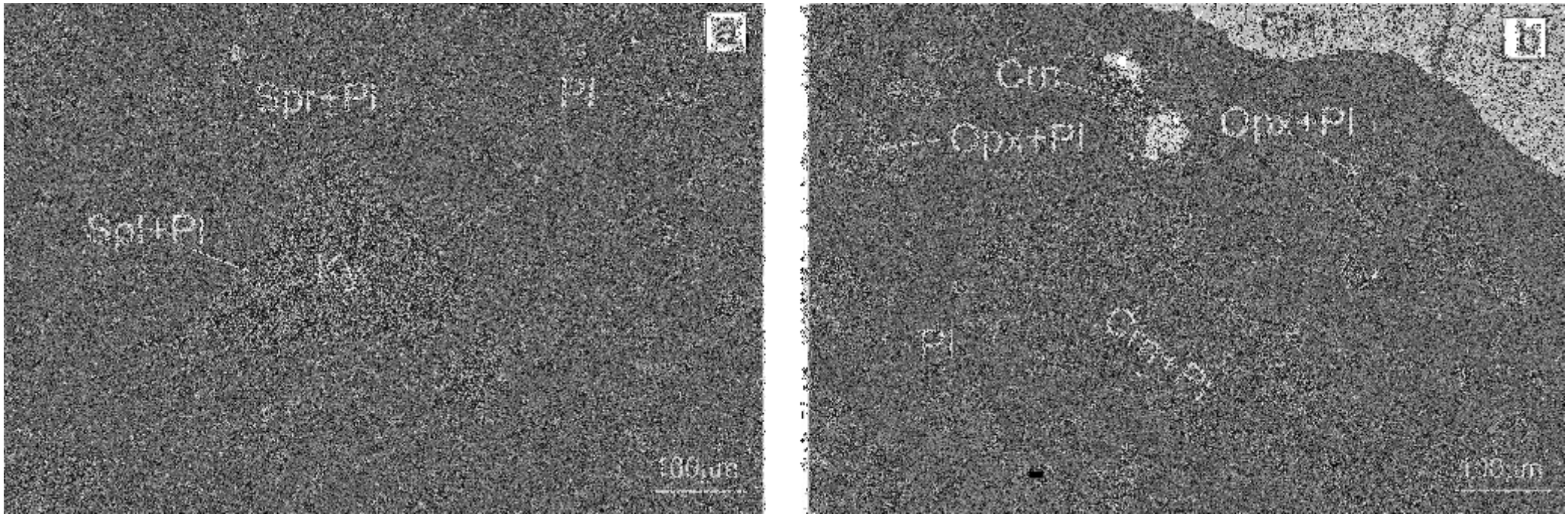

Fig. 3.21 - SEM images showing microstructural features of the retrogressed eclogite: **a)** kyanite surrounded by a thin layer of spinel + anorthite symplectite, in turn surrounded by a thicker layer of symplectitic plagioclase + sapphirine; **b)** corundum + plagioclase intergrowth.

DOI: 10.3301/GFT.2015.03

The symplectite assemblages are in turn surrounded by a continuous thin layer of Na-rich plagioclase ($Ab_{\sim 60}$; Fig. 3.21a). Double-layered coronas of amphibole and plagioclase around garnet consist of an inner corona of Ca-rich plagioclase (bytownite) and Al-rich amphibole (Al-pargasite, tschermakite or Mg-hornblende X_{Mg}: 0.7-0.8), surrounded by an outer corona of Ca-Na plagioclase (andesine) and amphibole of analogous composition. Within the garnet-poor layers the eclogitic relics are rarely preserved and the texture is dominated by Cpx–Pl symplectites, quartz and garnet porphyroblasts. Matrix amphibole overgrows the Cpx–Pl symplectite. Often the modal amount of amphibole strongly exceeds that of the other phases, so that the eclogites are almost completely re-equilibrated into garnet-bearing amphibolites.

The metabasites from Iles and Terrata have a Qtz-poor tonalite to gabbro composition. The most primitive mafic rocks have low alkali contents and a subalkaline tholeiitic affinity. The metabasites have nearly flat or slightly enriched a patterns, and commonly have positive Eu anomalies. This feature is consistent with protolith of N-MORB to T-MORB affinity. The Th/ Yb and Ta/Yb ratios suggest that the rocks did not originate from subduction related mantle sources (Giacomini et al., 2005). The emplacement of the mafic protolith occurred in the Ordovician (460 ± 5 Ma).

According to Giacomini et al. (2005), the eclogite of Golfo Aranci underwent the following stages (Fig. 3.22): prograde amphibolite stage (PR-A), eclogite stage (E), granulite stage (GR), high temperature amphibolite stage (HT-Amp), and medium temperature amphibolite stage (MT-Amp). The basic rocks were buried in a subduction–related environment with formation of the kyanite-bearing eclogitic paragenesis (650°C, 1.9 GPa), followed by strong re-equilibration under granulite (sapphirine–bearing paragenesis, 700-800°C ~ 1.9 GPa), and then amphibolite facies with pervasive growth of amphibole dated at 352 ± 3 Ma.

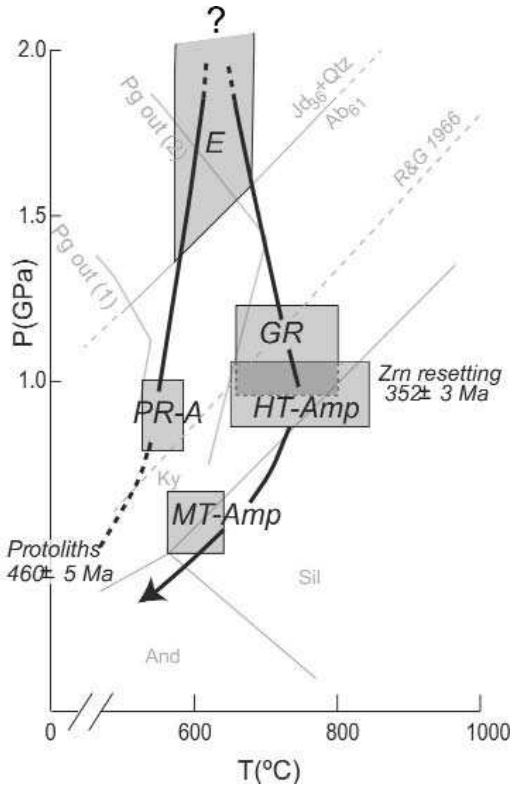

Fig. 3.22 - P–T–t path for retrogressed eclogite. Grey fields represent the calculated P-T conditions for the inferred equilibrium assemblages. PR-A=prograde amphibolite; E=eclogite; GR=granulite; HT-Amp=high-temperature amphibolite; MT-Amp=medium-temperature amphibolite. Pg out 1 and Pg out 2 are the paragonite-out curves (aH_2O: 0.1 and 0.9, respectively). R&G 1966 is the eclogite–granulite boundary after Ringwood & Green (1966). From Giacomini et al. (2005).

DOI: 10.3301/GFT.2015.03

Return Olbia on Strada Provinciale 82. After Olbia, turn off the main road towards Monte Plebi, whose 350 meters-high relief makes it quite prominent.

STOP 3.7: Layered amphibolite sequence of Monte Plebi (N 40° 58' 52,2"; E 9° 28' 07.9").

At Monte Plebi, a few kilometers north of Olbia (Figs. 3.2, 3.23), a 250m x 60-70m lenticular body of a layered amphibolite sequence is tectonically enclosed in migmatites of the HGMC. The sequence includes ultramafic (Figs. 3.24a, b), mafic (dark bands), and silicic (white bands) layers, with moderate foliation parallel to the S2 regional schistosity. Four layers (A, B, C, D; Fig. 3.23) were recognized in the sequence by Franceschelli et al. (2005b). From bottom to top, they are: *Layer A* (Fig. 3.24c), a 20-30m x 10m layer with alternating white and dark bands, generally ranging from a few millimeters to a few centimeters thick, but reaching a maximum of 90-100cm in thickness for white bands and 20 cm for dark bands. Dark bands are massive whereas white bands are moderately foliated. The thickness of the dark bands increases from bottom to top within Layer A. *Layer B* consists of two lenticular bodies maximum thickness of 5m, made up of dark, massive ultramafic rocks, locally with mm-sized garnets: the first lenticular body (B_1) is completely enclosed in layer A whereas the second body (B_2) occurs at the boundary between layer A and overlying layer C.

Layer C is 20-30m x 6m and alternates between larger dark bands and subordinate white bands. Millimeter-sized garnets are only found in the dark bands.

Layer D (Fig. 3.24d), 60m x 15m, lies at the top of the amphibolite sequence and consists of major white bands and minor dark bands.

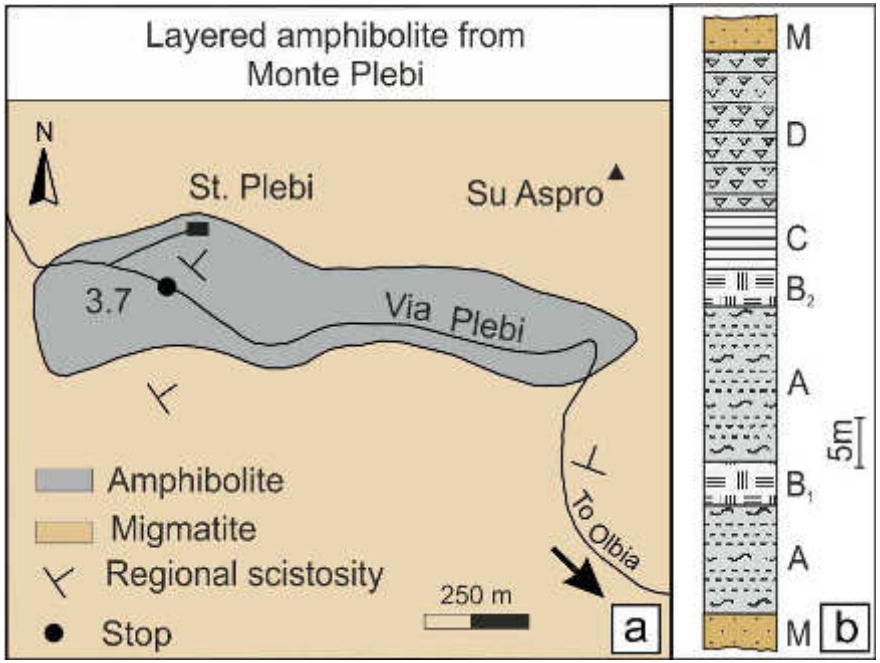

Fig. 3.23 - (a) Geological sketch map of the Monte Plebi area; (b) layered amphibolite sequence. A, B_1, B_2, C, D: layers of the amphibolite sequence; M: migmatite.

DOI: 10.3301/GFT.2015.03

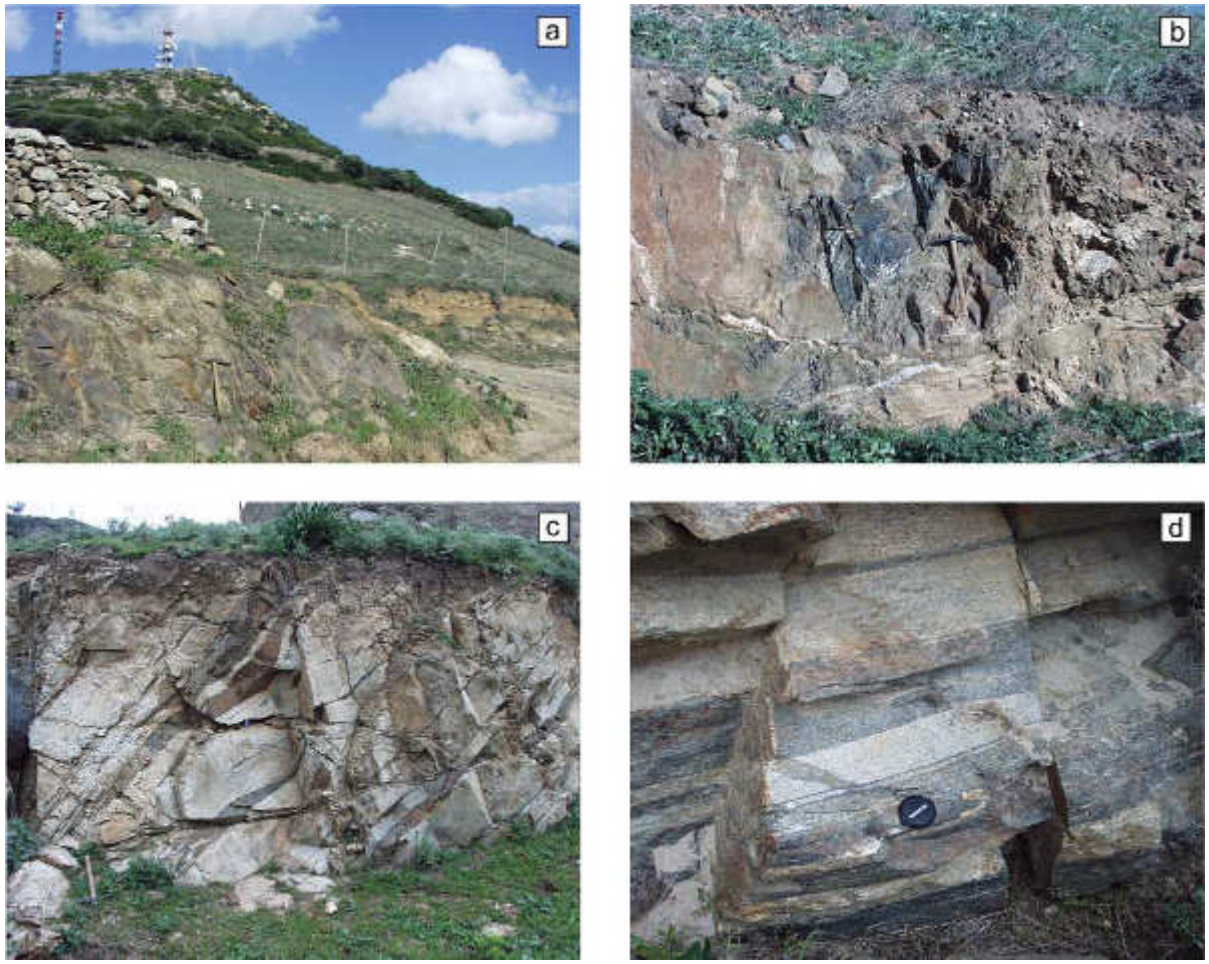

Fig. 3.24 - (a) Panoramic view of the Monte Plebi layered amphibolite sequence; (b) detailed view of ultramafic layers; (c) base of the upper part of Layer A, overlying Layer B_1 showing alternation of thick white silicic layers and thin dark mafic layers; (d) view of uppermost Layer D showing alternating decimeter-thick mafic and silicic layers.

Ultramafic layers (Layers B_1, B_2) are made up of: i) green amphibole (up to 95-98%) and opaque minerals; ii) green amphibole (75-85%), garnet (15-20%), and opaque minerals (3-5%), and iii) green amphibole (95-98%), biotite (2-3%), and opaque minerals (1%). Rare small quartz and plagioclase crystals also occur. Idioblastic garnet crystals contain small inclusions of green amphibole and epidote.

Mafic layers show different proportions of the major components: i) fine-grained green amphibole (65-75%), plagioclase (15-20%), quartz (10-15%), biotite (0-2%), opaque minerals (2-3%), and rare garnet; ii) coarse-grained green amphibole (70-80%), plagioclase (20-30%), and rare opaque minerals. The grain size of amphibole varies greatly.

Silicic layers are coarse-grained and are made up of plagioclase (60-75%), green amphibole (15-30%), and quartz (10-15%). Small amounts (1-2%) of opaque minerals and rare chlorite are also present. Green amphibole occurs as small anhedral crystals. Plagioclase occurs as coarse-grained crystals in the matrix.

The chemical composition of selected samples of ultramafic layers (UML), mafic layers (ML), and silicic layers (SL) from the Monte Plebi layered amphibolite sequence is reported in Table 3.

DOI: 10.3301/GFT.2015.03

The Monte Plebi sequence shows similarities with the bimodal suites known as "leptynite–amphibolite complexes". The main features of such complexes are the association of mafic, ultramafic, and silicic rocks, generally without rocks of intermediate composition, and the occurrence of HP relics such as retrogressed eclogites.

All Monte Plebi rocks have extremely low Nb, Ta, Zr, and Hf content, and high LILE/HFSE ratios, a feature inherited from their original mantle sources. The mafic and ultramafic layers show slight and strong LREE enrichment respectively (Fig. 3.25a). Ultramafic, mafic and silicic rocks analyzed for their Sm and Nd isotopic composition plot in the field of the inferred intrusive and effusive rocks of leptyno-amphibolite complexes (Fig. 3.25b), as defined by Innocent et al. (2003).

Table 3 - Major element composition of selected ultramafic (UML), mafic (ML), and silicic (SL) layers from Monte Plebi (from Franceschelli et al., 2005b).

Layer	UML	UML	ML	ML	ML	SL	SL	SL
(wt%)								
SiO_2	36.32	39.92	45.82	48.02	49.66	69.04	70.53	71.02
TiO_2	2.31	2.51	0.34	1.69	0.91	0.16	0.25	0.2
Al_2O_3	13.65	13.05	15.95	15.09	14.58	14.91	14.77	15.08
$Fe_2O_{3\,tot}$	23.31	19.83	11.07	12.65	12.27	3.61	2.76	2.56
MnO	0.55	0.21	0.15	0.2	0.17	0.06	0.06	0.07
MgO	7.79	9.02	10.6	7.41	7.68	1.08	0.68	0.61
CaO	11.22	11.92	10.92	9.99	10.11	5.65	5.22	4.31
Na_2O	1.21	1.34	1.78	2.77	2.62	3.75	4.57	4.46
K_2O	0.6	0.61	0.61	1.07	0.74	0.36	0.26	0.39
P_2O_5	0.77	0.52	0.03	0.31	0.05	0.17	0.1	0.1
LOI	3.81	2.61	2.75	0.8	2.09	1.43	1	1.35

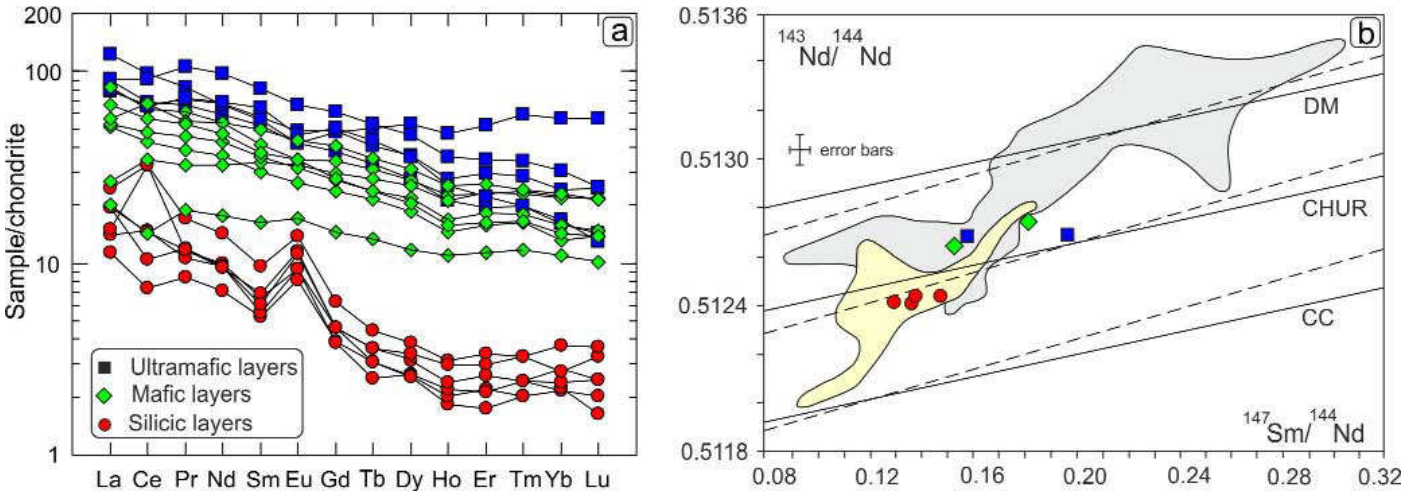

Fig. 3.25 - **a)** Chondrite-normalized REE pattern; and **b)** $^{143}Nd/^{144}Nd$ vs. $^{147}Sm/^{144}Nd$ diagram for Monte Plebi layered amphibolite (from Franceschelli et al., 2005b). Grey and yellow fields correspond to the basic-ultrabasic and felsic rocks of leptyno-amphibolite complexes, respectively (from Innocent et al., 2003).

DOI: 10.3301/GFT.2015.03

Most samples from the mafic layers are quite different from MORB as regards REE patterns and Nd, Sr isotope ratios, but show similarities with Siberian, Deccan, and proto-Atlantic rift tholeiites. Silicic layers, with Na_2O: 4–6 wt% and SiO_2: 67–71 wt%, were likely oligoclase-rich cumulates common in many mafic/silicic layered intrusions. Mafic and ultramafic samples yielded $\varepsilon_{Nd}(460)$ = + 0.79/ + 3.06 and $^{87}Sr/^{86}Sr$ = 0.702934 - 0.703426, and four silicic samples yielded $\varepsilon_{Nd}(460)$ = -0.53/-1.13; $^{87}Sr/^{86}Sr$ = 0.703239 - 0.703653. Significant differences in Nd isotope ratios between mafic and silicic rocks indicate that the groups evolved separately in deep magma chambers from different mantle sources, with negligible interaction with crustal material, and were subsequently repeatedly injected into shallower magma chambers.
Field, geochemical, and isotopic data suggest that ultramafic, mafic, and silicic layers from Monte Plebi represent repeated sequences of cumulates, basic, and acidic rocks similar to macrorhythmic units of mafic silicic layered intrusions.

Olbia: *Altitude: 24m a.s.l.; Surface Area: 383,64 km²; Population: 58003.*

Panoramic views of Olbia
from: www.settemuse.it and http://sardinias.it

Olbia (Terranóa in Sardinian language, Terranova Pausania before the 1940s) is the main city of the Olbia-Tempio Province and one of the most important in Sardinia. Its port and airport are major tourist gateways to Sardinia. In ancient times it was the capital of the Giudicato di Gallura. Over the past several decades, Olbia

DOI: 10.3301/GFT.2015.03

experienced rapid economic development, with its population doubling between 1951 and 1981. Just south of the famous Costa Smeralda, it is close to well-known tourist destinations, such as Porto Rotondo, Porto Cervo, and Portisco. The main points of interest are the "Fausto Noce" city park, the historical churches and the attractive, recently renovated walkway along the port.

Golfo Aranci: *Altitude: 19m a.s.l.; Surface Area: 37,97 km²; Population: 2206.*

Panoramic view of Golfo Aranci
from: http://www.comune.golfoaranci.ot.it

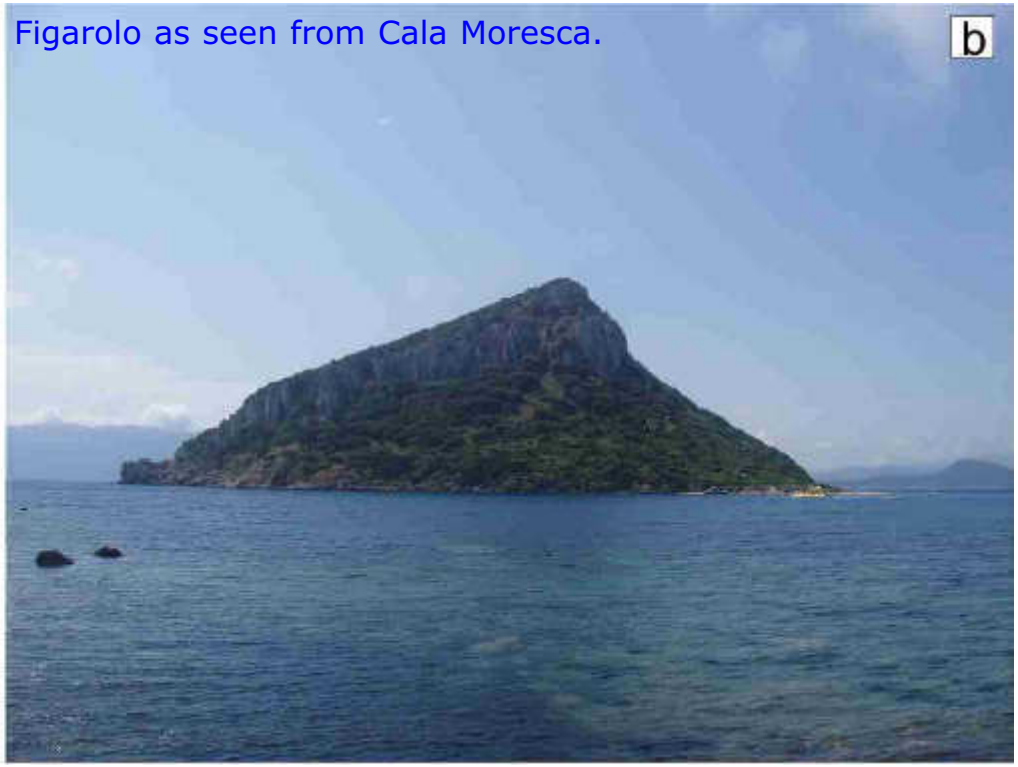

Figarolo as seen from Cala Moresca.

Golfo Aranci borders a small bay of Sardinia's northeastern coast extending up to Capo Figari. Formerly inhabited by farmers, shepherds, and fishermen, it is now an important commercial and tourist port. The name originated as a corruption of "Golfu di li ranci" (gulf of the crabs in Gallura dialect), with Golfo Aranci meaning Gulf of the Oranges in Italian. Points of interest close to the village include the Capo Figari promontory facing the island of Figarolo (both made up of Jurassic dolostones and limestones), and the beautiful Cala Moresca beach. Costa Smeralda is a short drive to the north.

DOI: 10.3301/GFT.2015.03

Fourth day

Olbia, Arzachena, Olbia end of the field trip

(L. Casini, S. Cuccuru)

Drive from Posada to Olbia and then on to Arzachena, enter the beautiful Variscan batholith landscape (Figs. 4.1, 4.2 and 4.3).

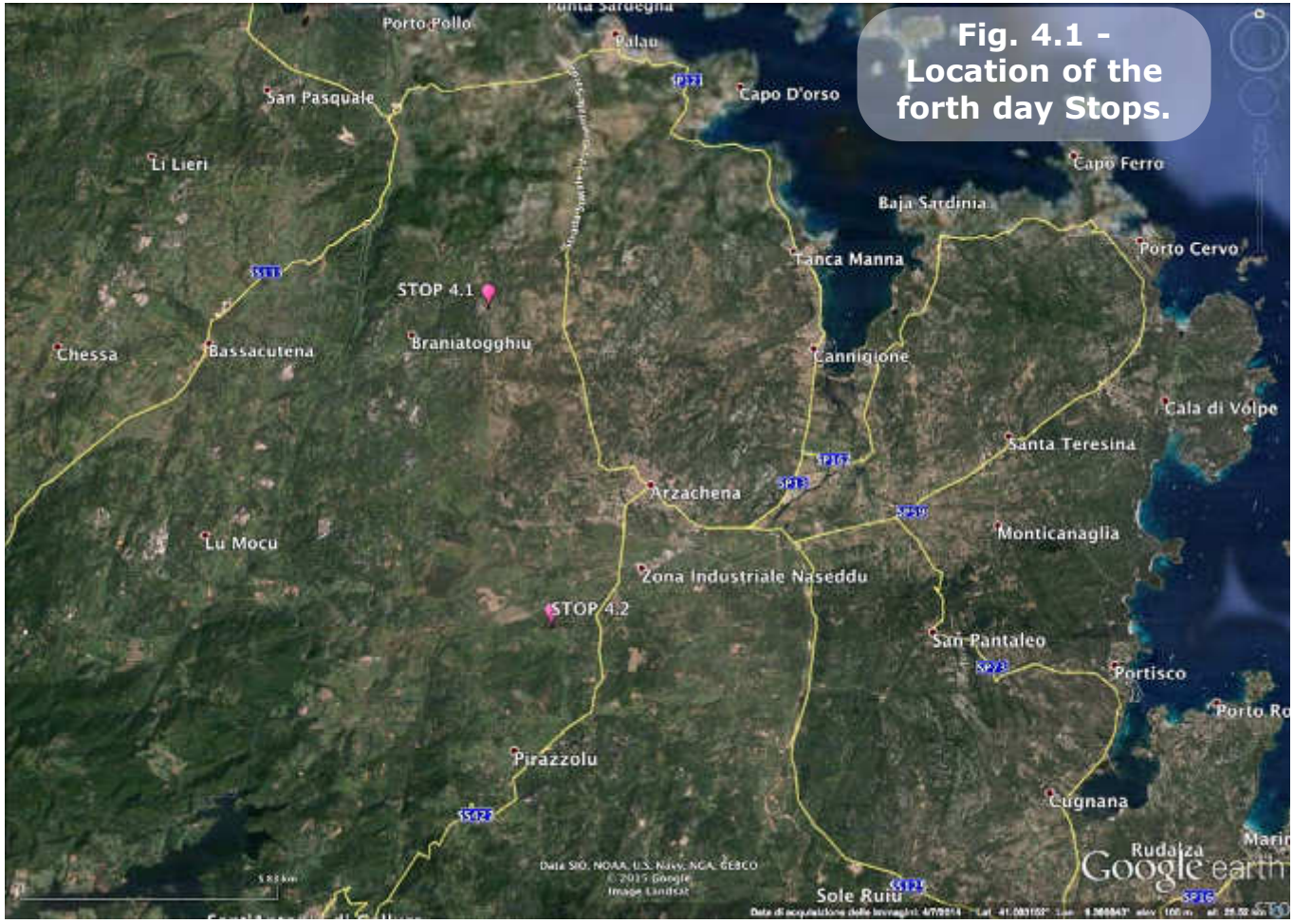

Fig. 4.1 - Location of the forth day Stops.

STOP. 4.1: Arzachena - Carboniferous magmatism. Mount Mazzolu granite quarry (N 41° 07’ 00,86; E 9° 20’ 38,25”)**.**

After Arzachena, drive north a few kilometers towards Palau, and turn left to an abandoned granite quarry.

On the quarry we see several fresh and well exposed three dimensional outcrops of the roof zone of the Arzachena pluton (Fig. 4.4) (~ 320-310 Ma; Casini et al., 2012) with a shallowly dipping magmatic foliation (Figs. 4.5 and 4.6). The area is characterized by several batches of garnet/epidote-bearing pegmatite and aplite veins roughly parallel to the pluton roof. Pegmatite veins and dykes are frequently found in the quarry (Fig. 4.7).

DOI: 10.3301/GFT.2015.03

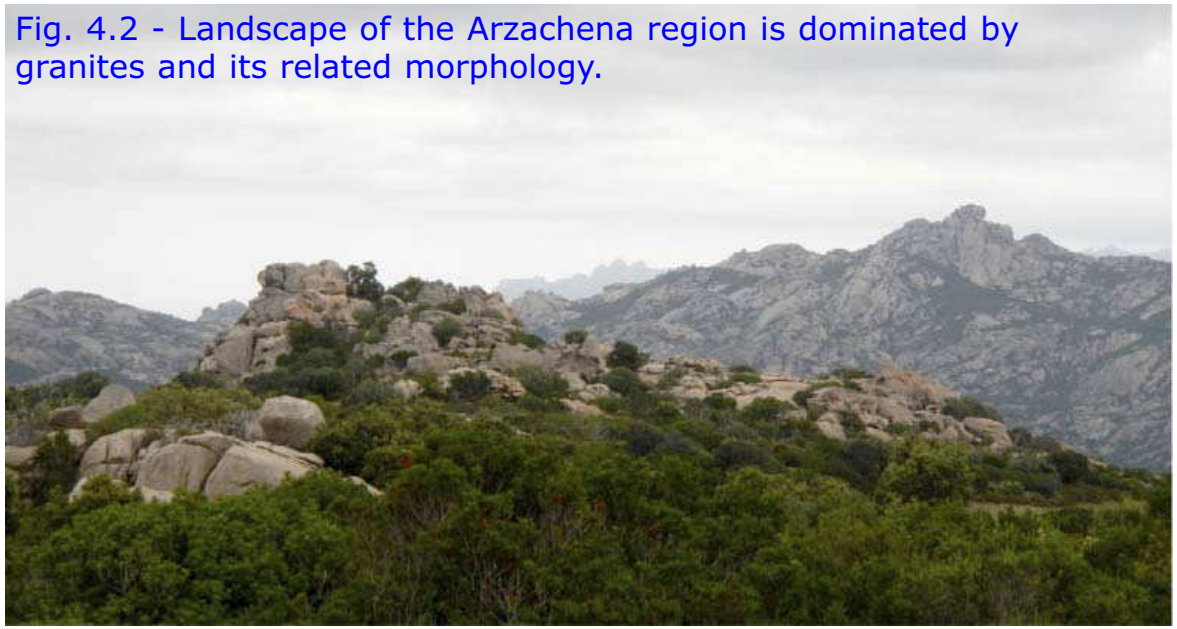

Fig. 4.2 - Landscape of the Arzachena region is dominated by granites and its related morphology.

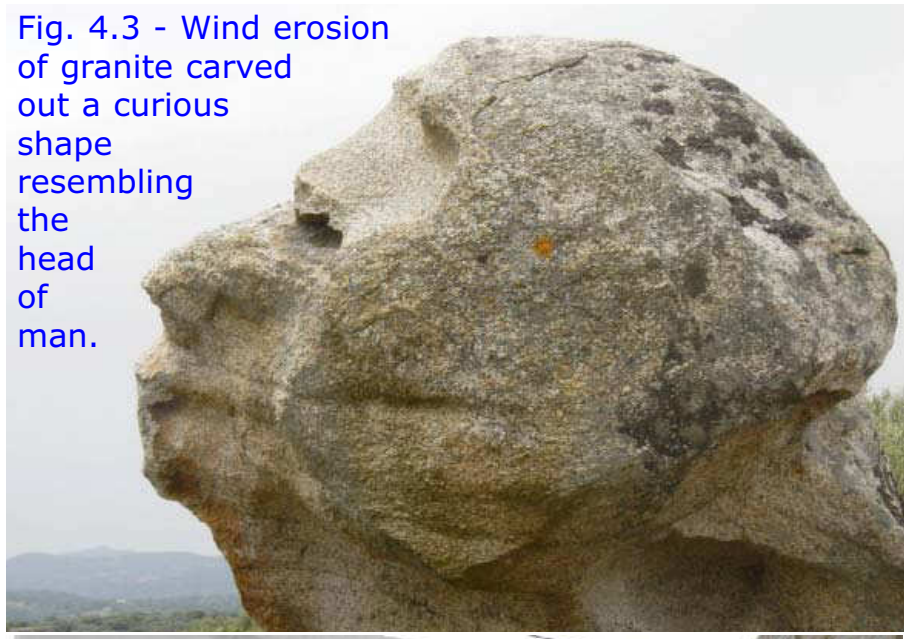

Fig. 4.3 - Wind erosion of granite carved out a curious shape resembling the head of man.

Fig. 4.4 - Arzachena monzogranite.

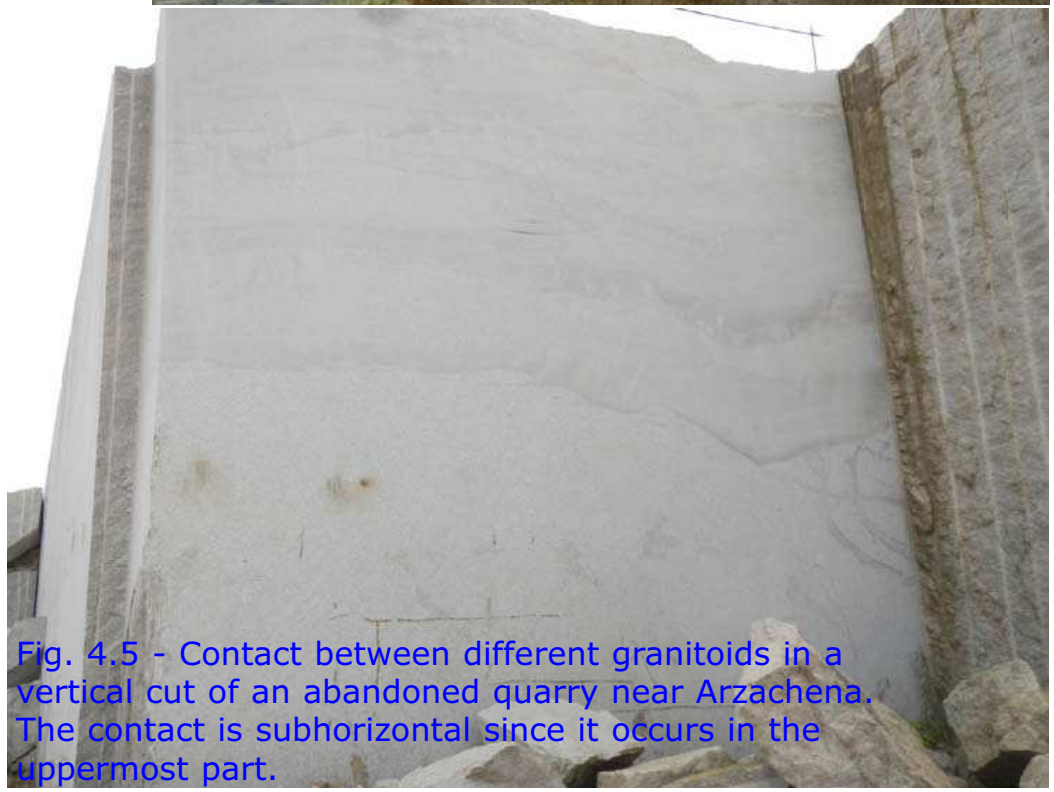

Fig. 4.5 - Contact between different granitoids in a vertical cut of an abandoned quarry near Arzachena. The contact is subhorizontal since it occurs in the uppermost part.

DOI: 10.3301/GFT.2015.03

Fig. 4.6 - Detail of the magmatic contact between a coarse-grained granodiorite (bottom) and a fine-grained granite (top) shown in the quarry cut of Fig. 4.5. of the Arzachena pluton.

Fig. 4.7 - Pegmatite vein in the Arzachena pluton.

The Arzachena pluton is one of the major calc-alkaline massifs of the Corsica-Sardinia batholith, and is one of the oldest granites in Sardinia. It is an elliptical, sill-shaped intrusion elongated in a NW-SE direction (Fig. 4.8). It consists of three nearly concentric granite shells (Casini et al., 2012). The more mafic term is a porphyritic biotite-horneblende granodiorite cropping out in the southern part of the pluton. The principal rock type is a porphyritic biotite monzogranite (~ 311 Ma; Casini et al., 2012) showing a transition to an inner, slightly more differentiated megacrystic biotite-muscovite monzogranite. Fine-grained leucogranite (biotite <5 wt%) is the more evolved magmatic product. It appears mainly at the northern edge of the pluton.
Emplacement depth of the pluton has been constrained by the hornblende-plagioclase thermometer at 0.35 and 0.41 GPa in the southern margin of the pluton and between 0.32 and 0.37 GPa in is central part (Casini et al., 2012).

DOI: 10.3301/GFT.2015.03

Growth of the Arzachena pluton started at ~320-315 Ma but the main growth stage was at ~311-312 Ma from a large volume of monzogranite melts. The final stages are represented by leucogranite emplaced at ~308 Ma within radial and peripheral dilatant fractures caused by the cooling of the pluton. Major and trace element compositions indicate that the Arzachena pluton has hybrid characteristics between that of typical S- and I-type granites. This is explained in terms of incremental melting of a heterogeneous crustal source made of metatexites and Ordovician calc-alkaline granitoids, which are common in the Variscan basement of Sardinia.

The pluton geometry and its fabric demonstrate that assembly of the main part of the batholith was related to crustal strike-slip and transpressional tectonics (Casini et al., 2012). This is further supported by the dextral Posada-Asinara shear zone and the sinistral Barrabisa shear zone to the north of Arzachena (Casini et al., 2012) (Fig. 4.8).

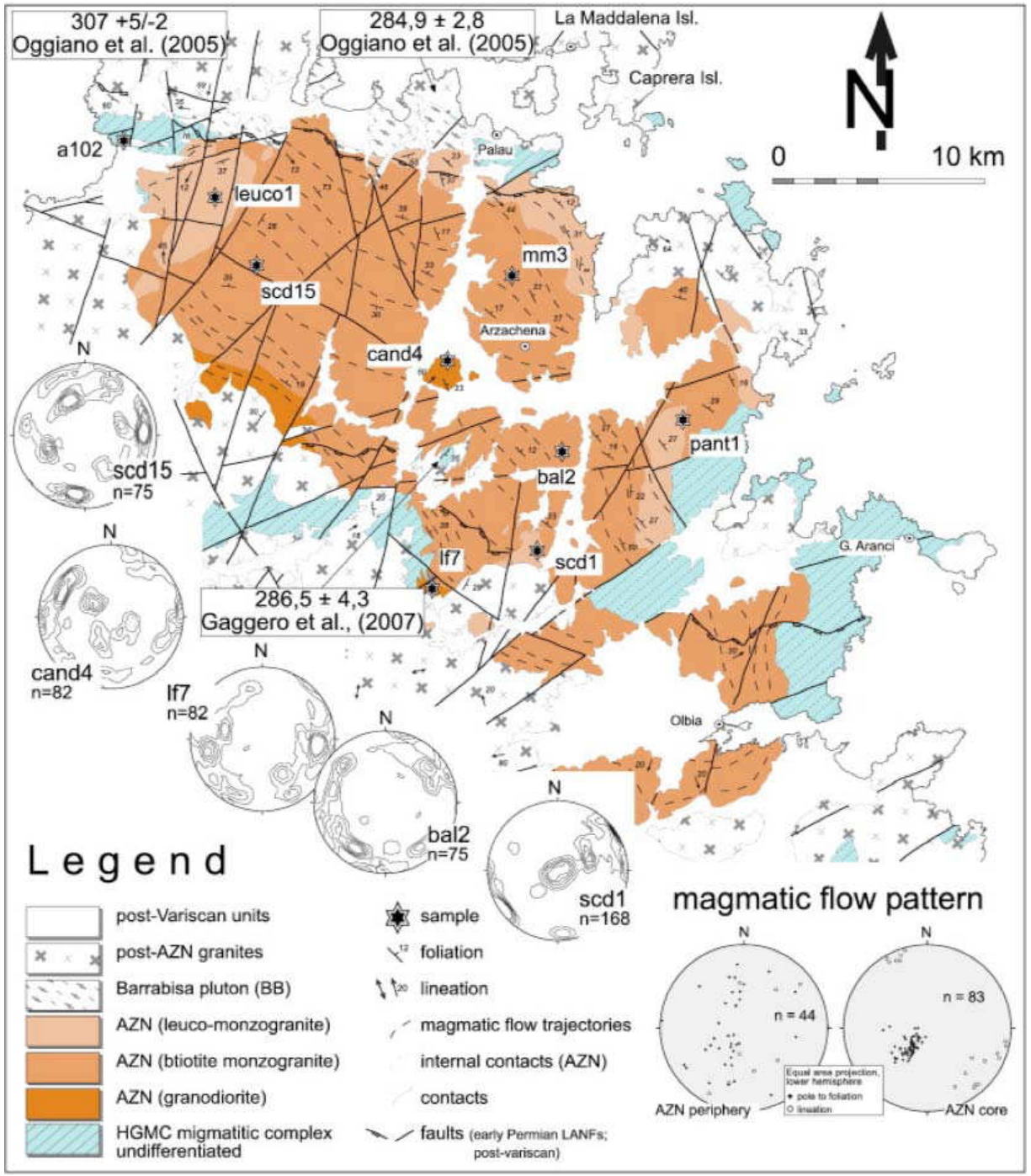

Fig. 4.8 - Tectonic map of the Arzachena pluton in north-eastern Sardinia (from Casini et al., 2012).

DOI: 10.3301/GFT.2015.03

STOP 4.2: Arzachena - Permian magmatism; Nuraghe La Prisgiona (N 41° 02' 52,5; E 9° 21' 43,9").

Return to Arzachena and drive southwest to an archeological site called Nuraghe La Prisgiona where there are outcrops of Permian magmatic rocks.

Stop 4.2a Nuraghe 'La Prisgiona': just below the ruins there are outcrops of quartz-diorite and rare olivine-bearing gabbros; Ar-Ar dating provide a well-constrained Early Permian age of around 286 Ma (Gaggero et al., 2007; Casini et al., 2012).

Fig. 4.9 - Permian quartz-diorite at Nuraghe La Prisgiona.

Stop 4.2b Close to the Paolo Calta church: the southern margin of the Arzachena Pluton is intruded by the P.ta La Ettica mafic complex (Gaggero et al., 2007). The outcrop consists of a thick rim of magmatic breccias formed by contact melting around a small quartz-diorite diaper. Varying degrees of assimilation and mixing between the mafic end-members and the country rocks can be observed. We can visit the beautiful archeological site that dates from nearly 1400 y B.C., with a main tower complex and 40-50 minor constructions. Around the site there are a few outcrops of Permian monzogranite (280 Ma, Casini et al., 2012) that were used to build the nuraghi (Fig. 4.9).

The field trip ends and the participants are taken to the Olbia harbour.

DOI: 10.3301/GFT.2015.03

The Nuraghe "La Prisgiona"

The Nuraghe is a typical Bronze Age tower-shaped edifice, and is very common in Sardinia. The Nuraghe "La Prisgiona" (near Arzachena) currently looks like a pile of rubble, with only a few elements of its supposed former grandeur. The Nuraghe La Prisgiona is located at the top of a granite hill that dominates other nuraghi lying below and commands a view as far as the hills of the Pedres Castle. It was built using large blocks of Permian granite that were roughly squared, in-filled with small stones and clay mortar. The plan of the central building was probably trilobal, but it is difficult to understand the articulation of the interior spaces, which are barely visible. Only an elliptical span highlighted by a clandestine excavation can be observed. The walls were made of medium-sized rough blocks, fixed with clay mortar. The tower vault, called the "tholos" has a typical dome shape. This room led to a corridor characterized by "rectangular light" and a false dome ceiling. The entrance features an architrave made of two large granite slabs, which today are completely replaced by stones. One can still distinguish the imposing defensive walls built on top of a natural rock. The wall includes an entrance that still bears the original architrave, which consists of a large trapezoidal slab. It has never been excavated. The settlement can be placed between the Bronze Age and the Iron Age, because the settlement includes both housing and defensive structures.

Acknowledgements
Research supported by Pisa, Torino Universities (Resp. C. Montomoli and R. Carosi) and by Regione Autonoma della Sardegna, Progetti di Ricerca di base orientata, L.R. 7/2007- annualità 2010 (Resp. M. Franceschelli). We thank Dr. R. Almeida, Prof. A. Indares and Dr. O. Strimpel for their critical reviews that greatly improved the text. Dr. O. Strimpel has been also greatly appreciated for his carefull revision of the english text. We thank L. Casini and S. Cuccuru (University of Sassari) for guiding the Stops of the fourth day during the Workshop (2014).
We also wish to thank F.M. Elter (University of Genova), C. Ghezzo, F. Giacomini, R. Palmeri (University of Siena), G. Oggiano (University of Cagliari), P.C. Pertusati (University of Pisa), C.A. Ricci (University of Siena) for their contributions on the study of Sardinian basement.

DOI: 10.3301/GFT.2015.03

DOI: 10.3301/GFT.2015.03

References

Aubele K., Bachtadse V., Muttoni G. & Ronchi A. (2014) - Paleomagnetic data from Late Paleozoic dykes of Sardinia: Evidence for block rotations and implications for the intra-Pangea megashear system. G3 Geochem. Geophys. Geosyst., 15, 1684-1697.

Baldelli C., Bigazzi G, Elter F.M. & Macera P. (1987) - Description of a Permo-Trias alkaline lamprophyre embedded into the micaschists of garnet-staurolite-kyanite grade of north-eastern Sardinia island. I.G.C.P., N. 5, Newsletter 7, 8-10.

Barca S., Carmignani L., Eltrudis A. & Franceschelli M. (1995) - Origin and evolution of the Permian-Carboniferous basin of Mulargia Lake (South-Central Sardinia, Italy) related to the Late-Hercynian extensional tectonic. C. R. Acad. Sci. Paris, t. 321, series IIa, 171-178.

Barker F. (1979) - Trondhjemite: definition, environment and hypotheses of origin. In: Barker F. (ed.) Trondhjemites, dacites, and related rocks. Developments in petrology, 6, Amsterdam, Elsevier, 1-12.

Berman R.G. (1991) - Thermobarometry using multi-equilibrium calculations: a new technique with petrological applications. Can. Mineral., 29, 833-855.

Cappelli B., Carmignani L., Castorina F., Di Pisa A., Oggiano G. & Petrini R. (1992) - A Variscan suture zone in Sardinia: geological, geochemical evidence. Paleozoic Orogenies in Europe (special issue), Geodin. Acta, 5(1-2), 101-118.

Caredda A.M., Cruciani G., Franceschelli M. & Puxeddu M. (1999) - Genetic link between the tourmaline-bearing pegmatite, leucogranite and migmatized orthogneiss in the Hercynian basement of NE Sardinia (Italy). In: Stanley et al. (eds), Mineral Deposits to Processes to Processing, 1, 328-335. Balkema, Rotterdam, Brookfield.

Carmignani L., Carosi R., Di Pisa A., Gattiglio M., Musumeci G., Oggiano G. & Pertusati P.C. (1994) - The Hercynian Chain in Sardinia (Italy). Geodin. Acta, 7, 31-47.

Carmignani L., Cocozza T., Ghezzo C., Pertusati P.C. & Ricci C.A. (1982) - Lineamenti del basamento sardo. In: Guida alla geologia del Paleozoico sardo. Guide geologiche regionali. Società Geologica Italiana, 11-23.

Carmignani L., Cocozza T., Ghezzo C., Pertusati P.C. & Ricci C.A. (1986) - Guide-book to the escursion on the Paleozoic Basement of Sardinia. I.G.C.P., N. 5, Newsletter, Special Issue, Cagliari, pp 102.

Carmignani L., Franceschelli M., Pertusati P.C, Memmi I. & Ricci C.A. (1979) - Evoluzione tettono-metamorfica del basamento ercinico della Nurra (Sardegna NW). Mem. Soc. Geol. Ital., 20, 57-84.

Carmignani L. & Oggiano G. (1999) - The variscan basement and the post-collisional evolution. Late Palaeozoic continental basins of Sardinia. The continental Permian International Congress, 15-18 Sept. 1999. Field trip guide-volume, 6-13, Pavia University.

Carmignani L., Oggiano G., Barca S., Conti P., Salvadori I., Eltrudis A., Funedda A. & Pasci S. (2001) - Geologia della Sardegna. Note illustrative della Carta Geologica della Sardegna a scala 1:200.000. Mem. descr. Carta Geol. d'It., 60, 283 pp.

Carmignani L. & Pertusati P.C. (1977) - Analisi strutturale di un segmento della catena Ercinica: il Gerrei (Sardegna SE). Boll. Soc. Geol. It., 96, 339-374.

Carmignani L., Pertusati P.C., Barca S., Carosi R., Di Pisa A., Gattiglio M., Musumeci G. & Oggiano G. (1993) - Struttura della catena ercinica in Sardegna. Guida all'escursione. GIGS, pp 177.

Carosi R., Di Pisa A., Iacopini D., Montomoli C. & Oggiano G. (2004a) - The structural evolution of the Asinara Island (NW Sardinia, Italy). Geodin. Acta, 17/5, 309-329.

DOI: 10.3301/GFT.2015.03

Carosi R., Di Pisa A., Iacopini D., Montomoli C., Oggiano G. & Rossi P. (2004b) - Variscan Basement in north Sardinia and Corsica. In: Filed Trip Guide Book P11, Post Congress Field Trip, APAT (Ed.), 32th International Geological Congress, Florence, Italy, pp 20.

Carosi R., Frassi C., Iacopini D. & Montomoli C. (2005) - Post collisional transpressive tectonics in northern Sardinia (Italy). J. Virtual Explorer, 19, Paper 3.

Carosi R., Frassi C., Iacopini D. & Montomoli C. (2006) - Excursion in the Variscan Basement of Northern Sardinia (Italy): Field Guide. In: Köhn D. & De Paor D. (eds.), General Contributions 2006, J. Virtual Explorer, Electronic Edition, ISSN 1441-8142, 22, Paper 3.

Carosi R., Frassi C. & Montomoli C. (2008) - Deformazione traspressiva e metamorfismo Barroviano nelle Baronie (Sardegna settentrionale). GIGS Catania, 26-29 Febbraio 2008, Rend. online Soc. Geol. It. online, 1, 68-70.

Carosi R., Frassi C. & Montomoli C. (2009) - Deformation during exhumation of medium- and high-grade metamorphic rocks in the Variscan chain in northern Sardinia (Italy). Geol. J., 44, 280-305.

Carosi R., Montomoli C., Tiepolo M. & Frassi C. (2012) - Geochronological constraints on post-collisional shear belt in the Variscides of Sardinia, Italy. Terra Nova, 24 (1), 42-51.

Carosi R. & Oggiano G. (2002) - Transpressional deformation in northwestern Sardinia (Italy): insights on the tectonic evolution of the Variscan Belt. C. R. Geoscience, 334, 287-294.

Carosi R. & Palmeri R. (2002) - Orogen-parallel tectonic transport in the Variscan belt of northeastern Sardinia (Italy): implications for the exhumation of medium-pressure metamorphic rocks. Geol. Mag., 139 (5), 497-511.

Carosi R., Palmeri R. & Sabbatini T. (1999) - Ductile transpression and exhumation of greenschists/amphibolite facies metamorphic rocks from NE Sardinia (Italy). Abstract, EUG 10, Strasburgo, 99.

Carosi R., Perillo M., Pertusati P.C. & Gattiglio M. (1995) - Risultati preliminari dello studio strutturale del Complesso del Sulcis meridionale (Sardegna SW). Atti Soc. Tosc. Sc. Nat. mem. Serie A, 102, 105-116.

Carosi R., Perillo M. & Pertusati P.C. (1998) - Structural evolution of the Southern Sulcis Metamorphic Complex (SW Sardinia, Italy). C. R. Acad. Sci. Paris, Sciences de la Terre et des Planètes/Earth & Planetary Sciences, 326, 505-512.

Carosi R. & Pertusati P.C. (1990) - Evoluzione strutturale delle unità tettoniche erciniche nella Sardegna centro- meridionale. Boll. Soc. Geol. It., 109, 325-335.

Casini L., Cuccuru S., Maino M., Oggiano G. & Tiepolo M. (2012) - Emplacement of the Arzachena Pluton (Corsica–Sardinia Batholith) and the geodynamics of incoming Pangea. Tectonophysics, 544–545, 31-49.

Connoly J.A.D., Memmi I., Trommsdorff V., Franceschelli M. & Ricci C.A (1994) - Forward modeling of calc-silicate microinclusions and fluid evolution in a graphitic metapelites, northeast Sardinia. Am. Mineral., 79, 960-972.

Conti P., Carmignani L. & Funedda A. (2001) - Change of nappe transport direction during the Variscan collisional evolution of central-southern Sardinia (Italy). Tectonophysics, 332, 255-273.

Corradini C., Barca S. & Spalletta C. (2003) - Late Devonian-Early Carboniferous conodonts from the "Clymeniae Limestones" of SE Sardinia (Italy). Courier Forschungs-Institut Senckenberg 245, 227-253.

Corsi B. & Elter F.M. (2006) - Eo-Variscan (Devonian?) melting in the High Grade Metamorphic Complex of the NE Sardinia Belt (Italy). Geodin. Acta, 19 (3-4), 155–164.

DOI: 10.3301/GFT.2015.03

Corsini M. & Rolland Y. (2009) - Late evolution of the southern European Variscan belt: Exhumation of the lower crust in a context of oblique convergence. C.R. Geosciences, 341, 214–223.

Cortesogno L., Gaggero L., Oggiano G. & Paquette J.L. (2004) - Different tectono-thermal evolutionary paths in eclogitic rocks from the axial zone of the Variscan chain in Sardinia (Italy) compared with the Ligurian Alps. Ofioliti, 29, 125-144.

Costamagna L.G., Cruciani G., Franceschelli M. & Puxeddu M. (2012) - A volcano-sedimentary sequence with albitite layers in the Variscan basement of NE Sardinia: a petrographical and geochemical study. Per. Mineral., 81, 179-204.

Cruciani G., Dini A., Franceschelli M., Puxeddu M. & Utzeri D. (2010) - Metabasite from the Variscan belt in NE Sardinia, Italy: within plate OIB-like melts with very high Sr and low Nd isotope ratios. Eur. J. Mineral., 22, 509-523.

Cruciani G., Fancello D., Franceschelli M., Scodina M. & Spano M.E. (2014a) - Geothermobarometry of Al-silicate-bearing migmatites from the Variscan chain of NE Sardinia, Italy: a P-T pseudosection approach. Per. Mineral., 83(1), 19-40.

Cruciani G., Franceschelli M., Caredda A.M. & Carcangiu G. (2001) - Anatexis in the Hercynian basement of NE Sardinia, Italy: a case study of the migmatite of Porto Ottiolu. Mineral. Petrol., 71, 195-223.

Cruciani G., Franceschelli M., Elter F.M., Puxeddu M. & Utzeri D. (2008a) - Petrogenesis of Al-silicate-bearing trondhjemitic migmatites from NE Sardinia, Italy. Lithos, 102, 554-574.

Cruciani G., Franceschelli M. & Groppo C. (2011) - P-T evolution of eclogite-facies metabasite from NE Sardinia, Italy: insights into the prograde evolution of Variscan eclogites. Lithos, 121, 135-150.

Cruciani G., Franceschelli M., Groppo C., Brogioni N. & Vaselli O. (2008c) - Formation of clinopyroxene + spinel and amphibole+spinel symplectites in coronitic gabbros from the Sierra de San Luis (Argentina): a key to post-magmatic evolution. J. Metamorph. Geol., 26, 759–774.

Cruciani G., Franceschelli M., Groppo C. & Spano M.E. (2012) - Metamorphic evolution of non-equilibrated granulitized eclogite from Punta de li Tulchi (Variscan Sardinia) determined through texturally controlled thermodynamic modelling. J. Metamorph. Geol., 30, 667-685.

Cruciani G., Franceschelli M., Foley S.F. & Jacob D.E. (2014b) - Anatectic amphibole and restitic garnet in Variscan migmatite from NE Sardinia, Italy: insights into partial melting from mineral trace elements. Eur. J. Mineral., 26, 381-395.

Cruciani G., Franceschelli M., Jung S., Puxeddu M. & Utzeri D. (2008b) - Amphibole- bearing migmatite from Variscan Belt of NE Sardinia, Italy: partial melting of a mid-Ordovician igneous source. Lithos, 102, 208-224.

Cruciani G., Franceschelli M., Marchi M. & Zucca M. (2002) - Geochemistry of metabasite from NE Sardinia, Italy: nature of protoliths, magmatic trend, and geotectonic setting. Mineral. Petrol., 74, 25-47.

Cruciani G., Franceschelli M., Massonne H.-J., Carosi R. & Montomoli C. (2013) - Pressure–temperature and deformational evolution of high-pressure metapelites from Variscan NE Sardinia, Italy. Lithos, 175-176, 272-284.

Del Moro A., Di Pisa A., Oggiano G. & Villa I.M. (1991) - Isotopic ages of two contrasting tectonomorphic episodes in the Variscan chain in N Sardinia. "Geologia del basamento italiano", Siena 21-22 marzo 1991, 33-35.

Del Moro A., Di Simplicio P., Ghezzo C., Guasparri G., Rita F. & Sabatini G. (1975) - Radiometric data and intrusive sequence in the Sardinian batholith. N. Jb. Min. Abh. 126, 28-44.

Di Pisa A., Oggiano G. & Talarico F. (1993) - Post collisional tectono-metamorphic evolution in the axial zone of the hercynian belt in Sardinia: the example from the Asinara Island. Bull. B.R.G.M 219, 216-217, Orleans.

DOI: 10.3301/GFT.2015.03

Di Vincenzo G., Carosi R. & Palmeri R. (2004) - The relationship between tectono-metamorphic evolution and argon isotope records in white mica: constraints from in situ ^{40}Ar-^{39}Ar laser analysis of the Variscan basement of Sardinia. J. Petrol., 45, 1013-1043.

Ellis D.J. & Green D.H. (1979) - An experimental study of the effect of Ca upon garnet-clinopyroxene Fe-Mg exchange equilibria. Contrib. Mineral. Petrol., 71, 13-22.

Elter F.M., Faure M., Ghezzo C. & Corsi B. (1999) - Late Hercynian shear zones in northeastern Sardinia (Italy). Géol. France, 2, 3-16.

Elter F.M., Franceschelli M., Ghezzo C., Memmi I. & Ricci C.A. (1986) - The geology of North Sardinia. In: Guide-book to the excursion on the Paleozoic basement of Sardinia. IGCP N° 5. Final Meeting Sardinia, 1996. Newletter. Special issue. 87-102.

Elter F.M., Musumeci G. & Pertusati P.C. (1990) - Late Hercynian shear zones in Sardinia. Tectonophysics, 176, 387- 404.

Elter, F.M., Padovano, M. & Kraus R.K. (2010) - The Variscan HT metamorphic rocks emplacement linked to the interaction between Gondwana and Laurussia plates: structural constraints in NE Sardinia (Italy). Terra Nova, 22, 369-377.

Elter F.M. & Palmeri R. (1992) - The calc-silicate marbles of Tamarispa (NE Sardinia). In: Contributions to the Geology of Italy with special regard to the Paleozoic basements. A volume dedicated to Tommaso Cocozza. L. Carmignani and F.P. Sassi (Eds.). IGCP N.° 276, Newsletter 5, 117-121.

Ferrandini M., Ginsburg L., Ferrandini M. & Rossi Ph. (2000) - Présence de *Pomelomeryx boulangerii* (Artiodactyla, Mammalia) dans l'Oligocène supérieur de la région d'Ajaccio (Corse): étude paléontologique et conséquences. C. R. Acad. Sci. Paris, 331, 675-681.

Ferrara G., Ricci C.A. & Rita F. (1978) - Isotopic ages and tectono-metamorphic history of the metamorphic basement of north-eastern Sardinia. Contrib. Mineral. Petrol., 68, 99-106.

Fettes D. & Desmons J. (Eds.) (2007) - Metamorphic Rocks: a classification and glossary of terms. Recommendations of the International Union of Geological Science Subcommission on the systematic of metamorphic rocks. Cambridge University Press. Cambridge UK, 244 p.

Franceschelli M., Carcangiu G., Caredda A.M., Cruciani G., Memmi I. & Zucca M. (2002) - Transformation of cumulate mafic rocks to granulite and re-equilibration in amphibolite and greenschist facies in NE Sardinia, Italy. Lithos, 63, 1-18.

Franceschelli M., Eltrudis A., Memmi I., Palmeri R. & Carcangiu G. (1998) - Multi-stage metamorphic re-equilibration in eclogitic rocks from the Hercynian basement of NE Sardinia (Italy). Mineral. Petrol., 62, 167-193.

Franceschelli M., Mellini M., Memmi I. & Ricci C.A. (1986) - Fine-scale chlorite-muscovite association in low-grade metapelites from Nurra (NW Sardinia), and the possible misidentification of metamorphic vermiculite. Contrib. Mineral. Petrol., 93, 137-143.

Franceschelli M., Memmi I., Pannuti F. & Ricci C.A. (1989) - Diachronous metamorphic equilibria in the Hercynian basement of northern Sardinia, Italy. In: Evolution of metamorphic belts (J.S. Daly, R.A. Cliff & BW.D. Yardley Eds.). Geol. Soc. London, Spec. Publ., 43, 371-375.

Franceschelli M., Memmi I. & Ricci C.A. (1982a) - Zoneografia metamorfica della Sardegna settentrionale. Guida alla Geologia del Paleozoico sardo. In: Guide Geologiche Regionali, Società Geologica Italiana, 137-149.

Franceschelli M., Memmi I. & Ricci C.A. (1982b) - Ca distribution between garnet and plagioclase in pelitic and psammitic schists from the metamorphic basement of north eastern Sardinia. Contrib. Mineral. Petrol., 80, 225-295.

Franceschelli M., Pannuti F. & Carcangiu G. (1991) - The formation of fibrolite nodules in a package of melanocratic gneisses from the Hercynian basement of NE Sardinia, Italy. Schweiz. Mineral. Petrog. Mitt., 71, 427-439.

DOI: 10.3301/GFT.2015.03

Franceschelli M., Pannuti F. & Puxeddu M. (1990) - Texture development and PT time path of psammitic schist from the hercynian chain of NW Sardinia (Italy). Eur. J. Mineral., 2, 385-398.
Franceschelli M., Puxeddu M. & Cruciani G. (2005a) - Variscan Metamorphism in Sardinia, Italy: review and discussion. J. Virtual Explorer, 19, paper 2.
Franceschelli M., Puxeddu M., Cruciani G., Dini A. & Loi M. (2005b) - Layered amphibolite sequence in NE Sardinia, Italy: remnant of a pre-Variscan mafic silicic layered intrusion? Contrib. Mineral. Petrol., 149, 164-180.
Franceschelli M., Puxeddu M., Cruciani G. & Utzeri D. (2007) - Metabasites with eclogite facies relics from Variscides in Sardinia, Italy: a review. Int. J. Earth Sci., 96, 795-815.
Frassi C., Carosi R., Montomoli C. & Law R.D. (2009) - Kinematics and vorticity of flow associated with post-collisional oblique transpression in the Variscan Axial Zone of northern Sardinia (Italy). J. Struct. Geol., 31, 1458–1471.
Gaggero L., Oggiano G., Buzzi L., Slejko F. & Cortesogno L. (2007) - Post-Variscan mafic dykes from late orogenic collapse to Tethyan rift: evidences form Sardinia. Ofioliti, 32, 15-37.
Ghezzo C., Memmi I. & Ricci C.A. (1979) - Un evento granulitico nella Sardegna nord-orientale. Mem. Soc. Geol. It., 20, 23-38.
Giacomini F., Bomparola R.M. & Ghezzo C. (2005) - Petrology and geochronology of metabasites with eclogite facies relics from NE Sardinia: constraints for the Palaeozoic evolution of Southern Europe. Lithos, 82, 221-248.
Giacomini F., Bomparola R.M., Ghezzo C. & Guldbransen H. (2006) - The geodynamic evolution of the Southern European Variscides: constraints from the U/Pb geochronology and geochemistry of the lower Paleozoic magmatic-sedimentary sequences of Sardinia (Italy). Contrib. Mineral. Petrol., 152, 19-42.
Giacomini F., Dallai L., Carminati E., Tiepolo M. & Ghezzo C. (2008) - Exhumation of a Variscan orogenic complex: insights into the composite granulitic-amphibolitic metamorphic basement of South-East Corsica (France). J. Metamorph. Geol., 26, 403-436.
Green D.H. & Ringwood A.E. (1967) - An experimental investigation of the gabbro-eclogite transformation. Geochim. Cosmochim. Acta, 31, 767-833.
Helbing H. & Tiepolo M. (2005) - Age determination of Ordovician magmatism in NE Sardinia and its bearing on Variscan basement evolution. J. Geol. Soc. London, 162, 689-700.
Holdaway M.J. (1971) - Stability of andalusite and the aluminium silicate phase diagram. Am. J. Sci., 271, 97-131.
Innocent C., Michard A., Guerrot C. & Hamelin B. (2003) - Datation U-Pb sur zircons à 548 Ma de leptynites des Maures centrales. Signification géodynamique des complexes leptyno-amphibolitiques de l'Europe varisque. Bull. Soc. géol. France, 174, 585-594.
Iacopini D., Carosi R., Montomoli C. & Passchier C.W. (2008) - Strain analysis and vorticity of flow in the Northern Sardinian Variscan Belt: recognition of a partitioned oblique deformation event. Tectonophysics, 446, 77-96.
Iacopini D., Frassi C., Carosi R. & Montomoli C. (2011) - Biases in the three-dimensional vorticity analysis using porphyroclast system: limits and application to natural examples. Geol. Soc. London, Spec. Publ., 360, 301-318.
Ito K. & Kennedy C. (1971) - An experimental study of the basalt-garnet granulite transition. In: Heacock J.G. (Editor), Geophysical Monograph Series 14-The Structural and Physical Properites of the Earth's Crust. Am. Geophys. Union, Washington D.C., pp. 303-314.
Liou J.G., Maruyama S. & Cho M. (1987) - Very low-grade metamorphism of volcanic and volcanoclastic rocks mineral

DOI: 10.3301/GFT.2015.03

assemblages and mineral facies. In: Frey M. (Editor), Low Temperature Metamorphism, Blackie, New York, pp. 59-113.
Massonne H-J., Cruciani G. & Franceschelli M. (2013) - Geothermobarometry on anatectic melts- a high-pressure Variscan migmatite from northeast Sardinia. Int. Geol. Rev., 55, 1490-1505.
Miller L., Sassi F.P. & Armari G. (1976) - On the occurence of altered eclogite rocks in the north-eastern Sardinia and their implications. N. Jb. Miner. Abh. 11, 683-689.
Montomoli C. (2003) - Zone di taglio fragili-duttili nel basamento varisico metamorfico di basso grado della Nurra meridionale (Sardegna nord-occidentale). Atti Soc. Tosc. Sc. Nat. mem., serie A 108 (2002-03), 23-29.
Newton R.C. & Perkins D. (1982) - Thermodynamic calibration of geobarometers based on the assemblages garnet-plagioclase-orthopyroxene-(clinopyroxene)-quartz. Am. Mineral., 67, 203-222.
Oggiano G. & Di Pisa A. (1992) - Geologia della Catena Ercinica in Sardegna La Zona Assiale. in Struttura della Catena ercinica in Sardegna guida all'escursione. GIGS, 147-177, Siena.
Orsini JB. (1980) - Le batholite Corso-sarde: anatomie d'un batholite hercynien. Composition, structure, organisation d'ensemble. Sa place dans la chaîne Varisque française. PhD thesis, Univ. Aix-Marseile.
Padovano M., Dörr W., Elter F.M. & Gerdes A. (2014) - The East Variscan Shear Zone: Geochronological constraints from the Capo Ferro area (NE Sardinia, Italy). Lithos, 196-197, 27-41.
Padovano M., Elter F.M., Pandeli E. & Franceschelli M. (2012) - The East Variscan Shear Zone: new insights into its role in the Late Carboniferous collision in southern Europe. Int. Geol. Rev., 54, (8), 957-970.
Palmeri R. (1992) - Petrography and geochemistry of some migmatites from northeastern Sardinia (Italy). In: L. Carmignani, F.P. Sassi (Eds). Contributions to the Geology of Italy with special regard to the Paleozoic basements. A volume dedicated to Tommaso Cocozza. IGCP No. 276 Newsletter 5, 183-186.
Palmeri R., Fanning M., Franceschelli M., Memmi I. & Ricci C.A. (2004) - SHRIMP dating of zircons in eclogite from the Variscan basement in north-eastern Sardinia (Italy). N. Jb. Miner. Mh., 6, 275-288.
Passchier C.W. & Trouw R.A.J. (2005) - Microtectonics. Springer Verlag, Berlin-Heidelberg–New York, 289 pp.
Patiño-Douce A.E. & Harris N. (1998) - Experimental constraints on Himalayan anatexis. J. Petrol., 39, 4, 689-710.
Pearce J.A. (1982) - Trace element characteristics of lavas from destructive plate boundaries. In: Andesites: orogenic andesites and related rocks. Thorpe R.S. (Ed.), 525-548, Wiley.
Pearce J.A. & Cann J.R. (1973) - Tectonic setting of basic volcanic rocks determined using trace elements analysis. Earth Planet. Sci. Lett., 19, 290-300.
Perugini D. (2003) - The Ordovician gneisses of north-eastern Sardinia (Italy): hypotheses for the petrological evolution of their protoliths. Per. Mineral., 72, 49-67.
Poli T., Ghezzo C. & Conticelli S. (1989) - Geochemistry of granitic rocks from the Hercynian Sardinia-Cosica batolith. Implication for magma gnesis. Lithos, 23, 247-266.
Powell R. (1985) - Regression diagnostic and robust regression in geothermometer/geobarometer calibration: the garnet-clinopyroxene geothermometer revisited. J. Metamorph. Geol., 3, 327-342.
Ricci C.A., Carosi R., Di Vincenzo G., Franceschelli M. & Palmeri R. (2004) - Unravelling the tectono-metamorphic evolution of

DOI: 10.3301/GFT.2015.03

medium-pressure rocks from collision to exhumation of the Variscan basement of NE Sardinia: a review. Special issue 2: A showcase of the Italian research in metamorphic petrology. Per. Mineral., 73, 73-83.

Ringwood A.E. & Green D.H. (1966) - An experimental investigation of the gabbro-eclogite transformation and some geophysical implications. Tectonophysics, 3, 383-427.

Rossi Ph. & Cocherie A. (1991) - Genesis of a Variscan batholith: field mineralogical and geochemical evidence from the Corsica-Sardinia batholith. The European Geotraverse, part 7. Tectonophysics, 195, 319-346.

Rossi Ph. & Faure M. (2012) - The Variscan Corsica. Field trip guide, Geologie de a France. Special meeting of French and Italian Geological Societies 22-23 may 2012 Sassari, Italy.

Schneider J., Corsini M., Reverso-Peila A. & Lardeux J.M. (2014) - Thermal and mechanical evolution of an orogenic wedge during Variscan collision: an example in the Maures-Tanneron massif (SE France). Geol. Soc. London, Special Publ., 405, 313-332.

Simpson G.D. (1989) - Dehydration-related deformation during regional metamorphism, NW Sardinia, Italy. J. Metamorph. Geol., 16, 457-472.

Stampfli G.M., Borel G. & von Raumer J. (2000) - Terrane accretion in the Variscan domain: Basement Tectonics 15, A Coruna, Spain, Program and Abstracts, 167–169.

Stampfli G.M., von Raumer J.F. & Borel G.D. (2002) - Paleozoic evolution of pre-Variscan terranes: from Gondwana to the Variscan collision. Geol. Soc. Am. Special Paper, 364, 263-280.

Tikoff B. & Teyssier C. (1994) - Strain modelling of displacement field partitioning in transpressional orogens. J. Struct. Geol., 16, 1575-1588.

Thompson A.B. & England P.C. (1984) - Pressure-temperature-time paths of regional metamorphism II. Their influence and interpretation using mineral assemblages in metamorphic rocks. J. Petrol., 25, 929–955.

von Raumer J.F. (1998) - The Paleozoic evolution in the Alps - From Gondwana to Pangea. Geol. Rund., 87, 407–435.

von Raumer J.F., Stampfli G.M., Borel G. & Bussy F. (2002) - Organization of pre-Variscan basement areas at the north-Gondwanan margin. Int. J. Earth Sci., 91, 35–52.

von Raumer J.F., Stampfli G.M. & Bussy F. (2003) - Gondwana-derived microcontinents-the constituents of the Variscan and Alpine collisional orogens. Tectonophysics, 365, 7-22.

Wimmenauer W. (1984) - Das praevariszische Kristallin im Schwarzwald. Forscht. Miner. Beih., 62, 69–86.

Winchester J.A. & Floyd P.A. (1977) - Geochemical discrimination of different magma series and their differentiation products using immobile elements. Chem. Geol., 20, 325-343.

DOI: 10.3301/GFT.2015.03